Exhibit A

IN THE UNITED STATES DISTRICT COURT

FOR THE DISTRICT OF DELAWARE

BEST MEDICAL INTERNATIONAL, INC.,	)	
	)	
Plaintiff,	)	
	)	
v.	)	C.A. No. 18-1599-MN
	)	
VARIAN MEDICAL SYSTEMS, INC. and VARIAN MEDICAL SYSTEMS INTERNATIONAL AG,	)	
	)	
Defendants.	)	

REQUEST FOR INTERNATIONAL JUDICIAL ASSISTANCE (LETTERS ROGATORY)

From: The Honorable Maryellen Noreika
United States District Court for the District of Delaware
J. Caleb Boggs Federal Building
844 N. King Street
Wilmington, DE 19801-3555
USA

To: The Appropriate Judicial Authority of Canada

The United States District Court for the District of Delaware presents its compliments to the appropriate judicial authority of Canada, and requests international judicial assistance to obtain evidence to be used in a civil proceeding before this Court in the above-captioned matter. A trial on this matter is scheduled at present for August 23, 2021, in Wilmington, Delaware.

The Court requests the assistance described herein as necessary in the interests of justice. Specifically, this matter is a patent case, and the Court requests that appropriate judicial authority of Canada compel the production of documentary evidence and deposition testimony from CancerCare Manitoba ("CancerCare"), 675 McDermot Avenue, Winnipeg, MB R3E OV9, Canada, regarding a medical treatment system developed at CancerCare that may be prior art to

one or more of the asserted patents. CancerCare is outside this Court's subpoena power, and therefore this Letter of Request is the only way that the requested information can be obtained.

Please return the executed request to this Court and defendants' counsel, with a requested return date of March 13, 2020:

Ryan K. Wong
KEKER, VAN NEST & PETERS LLP
633 Battery Street
San Francisco, CA 94111
USA

1. Summary of the Case

Plaintiff Best Medical, Inc. ("BMI") accuses defendants Varian Medical Systems, Inc. and Varian Medical Systems International AG ("Varian") of infringing four asserted patents: U.S. Patent Nos. 7,266,175, 7,015,490, 6,038,283, and 6,393,096. BMI amended its complaint on September 9, 2019, and Varian has moved to dismiss certain allegations in the amended complaint regarding indirect and willful infringement.

2. Evidence Requested

Varian seeks to obtain the following evidence, which it will use to develop its invalidity defenses for trial. The documents and testimony sought by these requests are directly relevant to the above-captioned litigation. These requests seek information regarding specific features of a medical treatment system developed at CancerCare, which may be prior art to one or more of BMI's asserted patents under 35 U.S.C. § 102. If obtained, Varian would use the documents and

testimony to develop its invalidity defenses for trial, and may rely on the documents and testimony to seek invalidation of one or more asserted patents.

Nothing in this Letter of Request is intended to interfere with any rights of CancerCare to assert privilege or refuse to give evidence under any applicable law of Canada or the United States of America.

a. Documents:

i. Documents sufficient to show the conception, design, and development of the following aspects of the computer optimization program used in IMRT treatment planning systems ("OSCAR"), as disclosed in David A. Viggars, et al., *The Objective Evaluation of Alternative Treatment Plans III: The Quantitative Analysis of Dose Volume Histograms*, 23 Int. J. Radiation Oncology Biol. Phys. 419 (1992), attached hereto as Attachment A-1, before May 27, 1998, and if such documents exist, before October 24, 1996:

cost function computation;

cost function minimization (including, *inter alia*, use of simulated annealing, logic for accepting or rejecting a beam-weight set on a given iteration, and logic for stopping the iteration);

use of partial volume data or dose volume constraints;

use of dose volume histograms;

importance factors; and

user interface(s) for receiving optimization input.

ii. Documents sufficient to identify each version of OSCAR in use before May 27, 1998, and if such documents exist, before October 24, 1996, the release date for each version, and differences between each version with respect to the aspects of OSCAR identified in Request No. i.

iii. Documents sufficient to show the design, operation, and functionality of the aspects of OSCAR identified in Request No. i for each version identified in response to Request No. ii.

iv. Documents sufficient to show that each version of OSCAR identified in response to Request No. ii was publicly available and/or in use anywhere in the world before May 27, 1998, and if such documents

exist, before October 24, 1996, such as academic journal articles, industry publications, press releases, product specifications, manuals, user guides, brochures, and/or web pages describing or identifying such version of OSCAR and its availability.

v. Documents sufficient to identify any apparatus, system, or device using OSCAR before May 27, 1998, and if such documents exist, before October 24, 1996.

vi. Documents and communications sufficient to show the design, function, operation, and availability of each apparatus, system, or device identified in response to Request No. v.

vii. Documents and communications sufficient to show the sale, offer for sale, or importation into the United States of each apparatus, system, or device identified in response to Request No. v before May 27, 1998, and if such documents exist, before October 24, 1996.

b. Deposition Topics:

i. The conception, design, development, operation, and functionality of the aspects of OSCAR set forth in Document Request No. i before the date(s) specified in Document Request No. i.

ii. Each version of OSCAR in use before the date(s) specified in Document Request No. i, and the release date for each version.

iii. The date and circumstances of the first sale, offer for sale, and/or public use in the United States of OSCAR before the date(s) specified in Document Request No. i.

iv. The identity, design, operation, and functionality of any apparatus, system, or device using the aspects of OSCAR set forth in Document Request No. i before the date(s) specified in Document Request No. i.

v. The date and circumstances of the first sale, offer for sale, and/or public use in the United States of any apparatus, system, or device covered by Deposition Topic No. iv.

vi. The authenticity of documents produced in response to this Letter of Request, the public availability and publication dates of documents produced in response to this Letter of Request, the creation and authorship of documents produced in response to this Letter of Request, and whether and how the documents produced in response to this Letter of Request were created and/or stored in the ordinary course of business.

3. Requested Procedures for Deposition Testimony:

The Court requests that CancerCare Manitoba ("CancerCare"), 675 McDermot Avenue, Winnipeg, MB R3E OV9, Canada, designate one or more witnesses who are knowledgeable about the subject matter identified in the deposition topics above. Because the testifying witnesses are outside this Court's subpoena power and cannot be compelled to attend trial, the Court requests that the witnesses' testimony be taken under oath in such manner as provided by the laws of Canada for the formal taking of evidence. The Court further requests that the testimony be taken by oral examination in such manner as provided by the laws of Canada for the formal taking of evidence. To the extent permitted by the laws of Canada, the Court requests that the testimony be recorded by a videographer and transcribed by a stenographer.

Please notify defendants' U.S. legal counsel of the time and place for execution of the requested deposition at the following address:

Ryan K. Wong
KEKER, VAN NEST & PETERS LLP
633 Battery Street
San Francisco, CA 94111
USA

4. Fees, Costs, and Reciprocity

If any reimbursable fees or costs are incurred in executing this Letter of Request, the Court requests that the appropriate judicial authorities of Canada submit a bill of fees and costs to the Court and defendants' U.S. legal counsel:

Ryan K. Wong
KEKER, VAN NEST & PETERS LLP
633 Battery Street
San Francisco, CA 94111
USA

The Court guarantees that defendants' counsel will reimburse the appropriate judicial authorities of Canada for all reimbursable fees and costs incurred in executing this Letter of Request.

This Court expresses its gratitude to the authorities of Canada for assisting with this Letter of Request, and will provide similar assistance to the judicial authorities of Canada when requested.

DATE OF REQUEST: _____

SIGNATURE AND SEAL OF THE REQUESTING AUTHORITY

_____
The Honorable Maryellen Noreika
United States District Judge
U.S. District Court for the District of Delaware
J. Caleb Boggs Federal Building
844 N. King Street
Wilmington, DE 19801-3555
USA

ATTACHMENT A-1

Int. J. Radiation Oncology Biol. Phys., Vol. 23, pp. 419–427
Printed in the U.S.A.

0360-3016/92 $5.00 + .00

● *Technical Innovations and Notes*

THE OBJECTIVE EVALUATION OF ALTERNATIVE TREATMENT PLANS III: THE QUANTITATIVE ANALYSIS OF DOSE VOLUME HISTOGRAMS

DAVID A. VIGGARS, PH.D.,[1,2] SHLOMO SHALEV, PH.D.,[1,2]
MARGARET STEWART, R.T.R. AND PER HAHN, M.D.[1]

Manitoba Cancer Treatment and Research Foundation, 100 Olivia Street, Winnipeg, R3E 0V9, Manitoba, Canada; and Departments of [1]Radiology and [2]Physics, University of Manitoba, Winnipeg, Manitoba, Canada

The computer program OSCAR evaluates dose-volume histograms in a consistent way for use in 3-dimensional treatment planning. Based on a dose prescription specified by a radiation oncologist, the technique provides a quantitative and easily understood visual analysis of a proposed dose distribution. Rapid, reliable, and consistent choices can be made between alternative treatment plans, and if necessary the results of OSCAR calculations can be used to guide the design of a plan that will be closer to the required prescription. The method is well suited to use in the definition of treatment protocols. The use of OSCAR is demonstrated by applying it to the evaluation of alternative volumetric treatment plans for ca lung. The results demonstrate the importance of using corrections for inhomogeneous tissue density in the calculation of 3-dimensional dose distributions.

Radiation treatment planning, Dose volume histograms, Score functions, Density correction, Normalization, Protocol, Dose prescription.

INTRODUCTION

The comparison of alternative treatment plans in three dimensions using only traditional isodose charts is a formidable task. By examining isodose contours superimposed on CT images, the radiation oncologist must decide whether the target will receive an adequate dose throughout its volume, and whether unacceptable volumes of healthy tissue will receive high radiation doses. Since each plan will have many CT slices and there will be several plans to compare, this is clearly a time consuming task and one that is very difficult to perform objectively and consistently.

Dose volume histograms (DVH) are a convenient way of summarizing the information in a 3-dimensional dose distribution. Their convenience is achieved by excluding detailed positional information about the location of dose levels within the region under consideration, and consequently they cannot entirely replace other means of displaying the dose distribution such as isodose charts and images of regret (22) which retain positional information. However, DVH's are extremely useful in the initial stages of comparing and evaluating alternative plans and are increasingly being used in external beam radiotherapy planning (2–6, 14, 20, 24, 26–28, 30). They have also been used to correlate outcome with the treatment dose distribution (1, 9, 18, 19). When calculated on a single CT-slice they are referred to as dose-area histograms (7, 11).

Two forms of the DVH for a volume of tissue are in use. The cumulative dose volume histogram (CDVH) shows V(D) plotted against D, where V(D) is the volume of tissue in which the dose is greater than or equal to D. The differential dose volume histogram (DDVH) shows v(D) plotted against D, where v(D) is the volume of tissue in which the dose is between D and D + ΔD, and ΔD is the "bin width" of the histogram. In constructing such DDVHs care is needed in the choice of bin width. Too large a value will mask details of the dose distribution, while too small a value may cause large fluctuations in the DDVH because of the finite grid used for the dose calculations.

To realize the maximum benefit from the use of DVH's a technique is needed for comparing and evaluating them objectively and consistently. Such a technique would also enable them to be used in defining and ensuring adherence to a treatment protocol. At present most comparisons of DVH's for sensitive organs are made by assuming that smaller volumes at high dose mean better plans. Such a comparison is simple to make when the CDVH for one

Reprint requests to: D. A. Viggars, Manitoba Cancer Treatment and Research Foundation, 100 Olivia St., Winnipeg, Manitoba, R3E 0V9 Canada.

Acknowledgement—This work was supported in part by Theratronics International Ltd.

Accepted for publication 5 December 1991.

plan has smaller cumulative volumes throughout the whole dose range. However, when the CDVH's for alternative plans cross, it is more difficult to decide which is preferable.

An example of this type of difficulty occurred in a treatment for cancer of the uterine cervix that had extended to the pelvic and para-aortic lymph nodes (3). A dynamic conformal technique was compared with treatment using more conventional techniques. The dose distributions in healthy liver tissue generated by the dynamic conformal technique and by one of the conventional plans gave similar average doses, but the CDVH's for the two plans crossed. The conformal plan was judged to be superior on the grounds that it restricted high dose to a smaller volume than in the conventional plan.

In contrast, Austin-Seymour *et al.* (1) evaluated the radiation tolerance of healthy liver tissue during heavy ion treatments of carcinoma of the pancreas and biliary system. They concluded that a plan with a smaller volume of liver above 30–35 GyE would be tolerated better than a plan with a higher volume above 30–35 GyE, even though the former plan might expose larger volumes of liver to doses near 60 GyE than the latter. The criterion used by Chin *et al.* (3) would have led to the opposite conclusion. To resolve such ambiguities it is necessary to characterize DVH's quantitatively, preferably in terms of parameters that can be related to the outcome of treatment.

Several attempts to characterize DVH's objectively have been based on calculations of the risk of complication in a sensitive organ (15–17, 21, 29). These calculations depend on assumptions about how to allow for non-uniformity of dose within the organ and on parameters describing the dose response of the tissue, which are usually very poorly known. They have therefore not been widely used. In this paper we describe a convenient objective technique for characterizing, comparing and evaluating DVH's which uses a simple dose prescription provided by a radiation oncologist based on clinical experience and dose response data. The technique provides visual and quantitative tools for the consistent evaluation and comparison of alternative treatment plans. As an example, conventional and conformal treatment plans for a case of ca lung are compared.

METHODS AND MATERIALS

The scheme for evaluating 3-dimensional treatment plans which we describe here has been developed on a commercial treatment planning system* and has been fully integrated with the conventional software so that it can be used easily on a routine basis. The scheme has a number of components. First, it uses a dose prescription which summarizes the radiation oncologist's perception of the treatment requirements for a patient or group of patients. The dose prescription, which is fully described below, can also be used as part of the definition of a treatment protocol. Once a dose prescription has been prepared the other components of the scheme can be used. They are a) images of regret on multiple CT slices, which are completely analogous to the 2-dimensional images of regret on single slices described in an earlier paper in this series (22), b) a visual display of the prescribed dose-volume limits on the CDVH, c) objective score functions which quantify the deviation of the dose distribution from the dose prescription, d) histograms of regret in either cumulative or differential form, which provide a striking and easily assimilated visual comparison of the CDVH or DDVH with the dose prescription.

The components and programs of the evaluation scheme described here are referred to collectively as OSCAR (Objective Scoring with Colored Areas of Regret).

Dose prescription

We assume that the ideal dose distribution in the target is uniform at 100% of the prescribed dose and zero in all other tissues as shown in Figure 1 by the solid line histograms. Dose distributions which can be achieved in practice are less uniform in the target and are non-zero in normal tissue as shown by the dashed curves in Figure 1. The quality of a proposed plan may therefore be judged by how far its CDVH departs from the ideal histograms, and a dose prescription can be defined by specifying the maximum acceptable deviations from the ideal shape. We refer to such deviations as "regret". A complete description of the acceptable limits of the shape of the CDVH would require a specification of the maximum and minimum permissible cumulative volumes at all doses, but we have found that a much simpler prescription is adequate for practical purposes. A typical prescription is given in Table 1 which is a generalization to three dimensions of the constraints we have used in earlier papers (10, 11, 22, 23). Similar constraints have been used by Langer and Leong (13).

Target overdose limits are defined at two dose levels (optionally only one), each corresponding to a prescribed maximum partial target volume which may exceed the dose limit. They are represented on the CDVH by two triangles, one shaded and one open. The triangles point downward, indicating that the CDVH is constrained to pass below them if the target overdose limits are not to be violated. Accordingly, the solid and dotted histograms in Figure 2a are within the overdose limits, but the dashed histogram violates both of them. For convenience, the lower and higher overdose limits are referred to as the mild and severe limits, respectively.

Similar constraints are placed on underdose in the target by specifying two dose limits and two corresponding

* Theraplan, Theratronics International, Kanata, Canada.

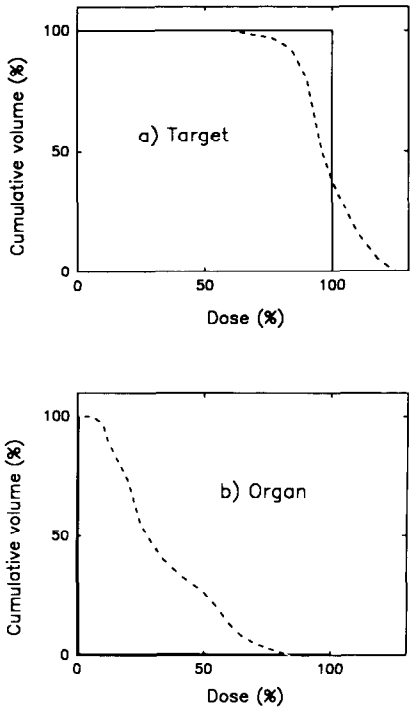

Fig. 1. Cumulative dose volume histograms for ideal (solid line) and realistic (dashed line) dose distributions.

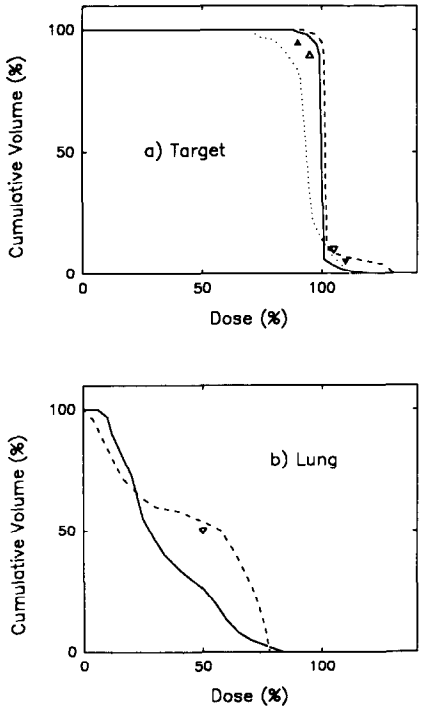

Fig. 2. Cumulative dose volume histograms for target and lung showing dose-volume limits from Table 1.

maximum partial target volumes which may receive a dose less than these limits. In this case the upper underdose limit is referred to as mild, and the lower limit as severe. As in the overdose case a single underdose limit may be used. To represent the target underdose constraints on the CDVH, use is made of the fact that if a volume V% of the tissue is below a certain dose then a volume (100-V)% of the tissue is above that dose. Hence, an underdose limit that permits a maximum of 10% of the target volume to be below 95% dose is equivalent to requiring that at least 90% of the volume be above 95% dose. Therefore, if an underdose limit specifies that no more than V% of the target volume should be below D% dose, an upward pointing triangle is placed at dose D% and volume (100-V)% to indicate that the CDVH should pass above this point. This is illustrated in Figure 2a, where the solid and dashed histograms are within the underdose limits but the dotted histogram is not.

For all non-target tissue and for specific sensitive organs single dose volume limits are specified to limit the volumes above chosen doses. This is illustrated in Figure 2b, where the solid histogram is acceptable but the dashed histogram violates the dose volume limit indicated by the downward pointing triangle.

Table 1. Dose prescription for treatment of ca lung

Type of regret	Dose limit (%)	Maximum volume* (%)
Target overdose (severe)	110	20
Target overdose (mild)	105	50
Target under overdose (severe)	90	5
Target under overdose (mild)	95	50
Non-target overdose	95	100
Left lung	50	30
Right lung	50	30
Spinal cord	75	0

Prescribed dose: 60 Gy at the isocenter.

* Volumes for target and non-target tissue are expressed as a percentage of target volume. Volumes for specific organs are expressed as a percentage of the organ volume.

Histograms of regret

A clear visual representation of how well a dose distribution conforms to a dose prescription can be given by shading areas of the DDVH plot that are in violation of the dose limits. Figure 3a illustrates a DDVH for the target in which any volume above the severe or mild overdose limits are shaded dark or light orange respectively. Similarly, any target volume below the severe or mild underdose limits is shaded dark or light blue, respectively. Purple shading is used to show overdosed volumes of sensitive organs as illustrated in Figure 3b. This representation of the dose distribution is referred to as a "histogram of regret" since the sizes of the shaded areas are proportional to the volumes of tissue in violation of the corresponding dose limits. A similar approach is used for the CDVH as

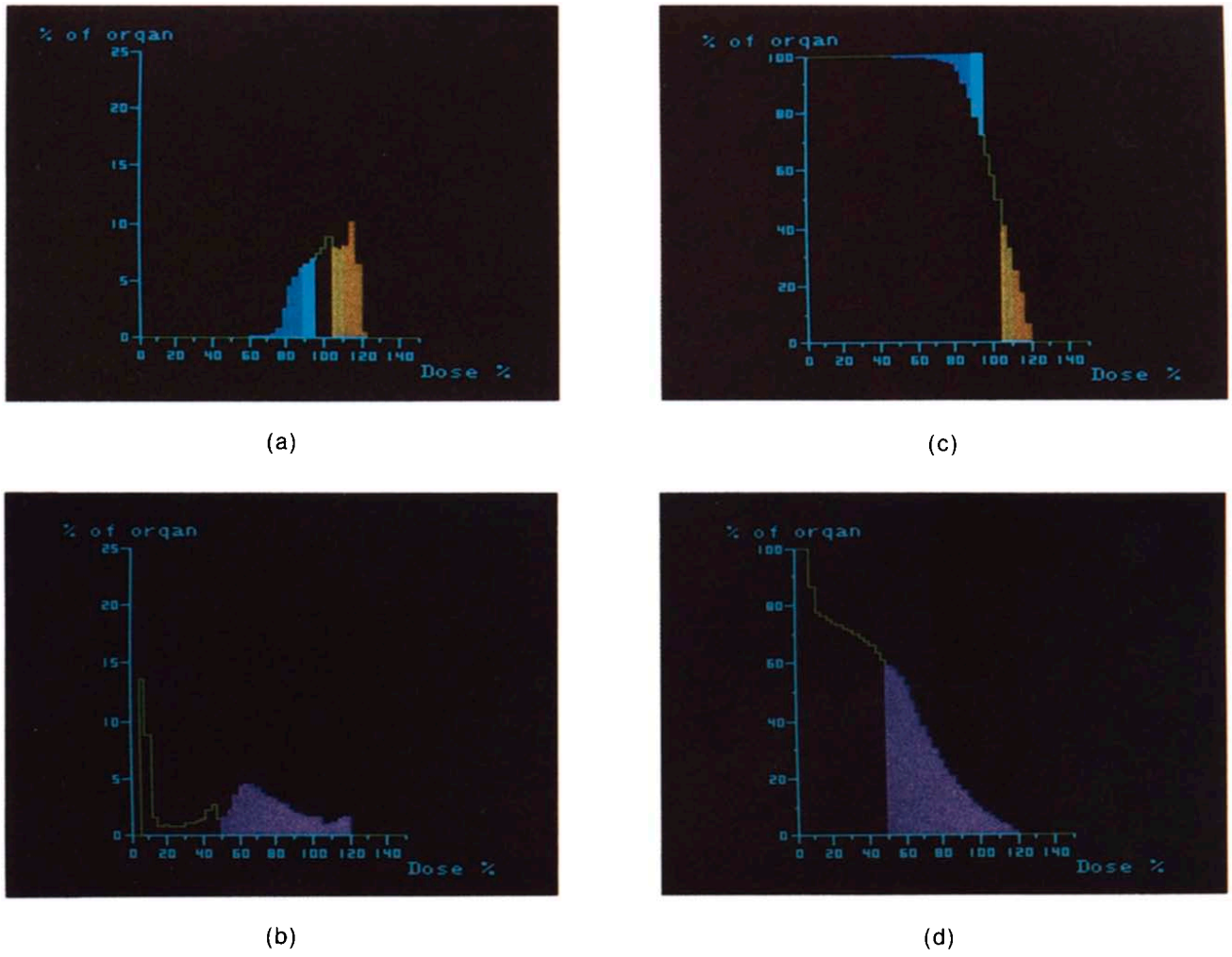

Fig. 3. Histograms of regret for an arbitrary dose distribution. DDVH for (a) the target and (b) a specific organ; and CDVH for (c) the target and (d) the same specific organ.

shown in Figures 3c and 3d, where the regions enclosed by the dose limits, the ideal CDVH and the actual CDVH are shaded. For the CDVH, it is the maximum height rather than the area of the colored regions which has quantitative significance. The colors used and their interpretation correspond to the colors of the areas of regret described in an earlier paper in this series (21).

Score functions

To provide a quantitative measure of how well a proposed treatment plan conforms to the dose prescription, we define a set of score functions which compare the actual deviations of a plan from the ideal CDVH with the maximum deviations allowed by the dose prescription. For each dose volume limit $[D_i, R_i(\max)]$ in the prescription, the score function is derived from a ratio r_i defined as:

$$r_i = R_i(D_i)/R_i(\max).$$

For overdose limits $R_i(D_i)$ is the actual volume of tissue, $V_i(D_i)$, above the dose limit D_i, and $R_i(\max)$ is the maximum permitted or "tolerance" volume, T_i, above the dose limit D_i, as shown in Figure 4a so that:

$$r_i = V_i(D_i)/T_i.$$

For underdose limits $R_i(D_i)$ and $R_i(\max)$ are volumes below the dose limit D_i and therefore, as shown in Figure 4b:

$$r_i = [100 - V_i(D_i)]/[100 - T_i],$$

where $V(D_i)$ is the volume above the dose limit D_i, which can be read directly from the CDVH. For the target and for non-target tissue T_i, $R_i(\max)$, $R_i(D_i)$, and $V_i(D_i)$ are expressed as percentages of the target volume. For specific organs at risk these volumes are expressed as percentages of the volume of the relevant organ. For a particular dose

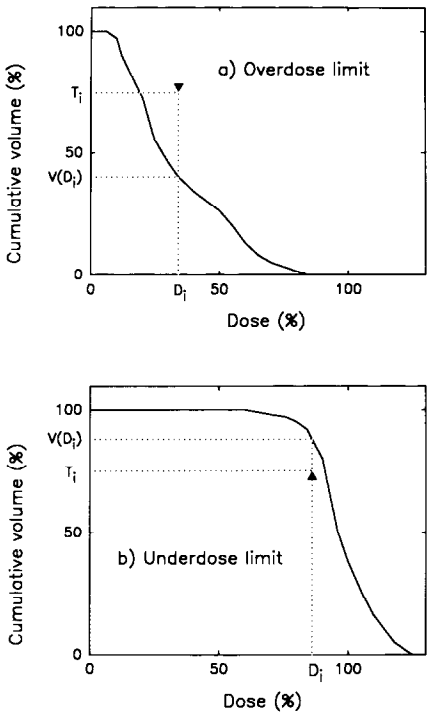

Fig. 4. Definition of quantities used in calculating score functions: (a) for overdose limits, and (b) for underdose limits.

volume limit, the range of r_i is from 0 for an ideal distribution to 1 for a distribution at the limit of acceptability. For a distribution which violates the dose volume limit, r_i is greater than 1.

To obtain a score function with more convenient properties we define

$$S_i = 10[1 - r_i],$$

which is 10 for an ideal distribution, zero at the limit of acceptability, and negative when the dose–volume limit is violated. A single score for target overdose is calculated by averaging the two S_i for the two target overdose limits, and similarly the scores for the two target underdose limits are averaged to give a single target underdose score. This, admittedly somewhat arbitrary, procedure allows some "trading-off" within each pair of constraints. An alternative approach, if only one constraint of the pair is required to be satisfied, would be to concentrate on the larger member of the pair of over- or underdose scores. If the scores for the two constraints in a pair differ by more than 5, the program issues a warning recommending that the two scores be examined individually.

A special case occurs when the dose prescription allows no part of an organ to be above the dose limit, as happens for the spinal cord in Table 1. Then the corresponding score function is set to 10 if this condition is satisfied and is set to zero otherwise.

If the score functions are calculated on a single slice using area instead of volume, they are identical to the score functions defined in an earlier paper (23) on the evaluation of 2-dimensional dose distributions.

RESULTS

Application to planning a case of ca lung

To demonstrate the procedures described above, five alternative plans were compared for a case of squamous cell carcinoma of the left lung. A CT scan of the thoracic region of the patient was acquired from lung apex to diaphragm, using 29 slices 1 cm apart. The tumor was visible on 10 slices and a target region consisting of the tumor plus a 1.5 cm margin was outlined on each of these. The lungs and spinal cord were also outlined on all available slices.

All the plans used two perpendicular equally weighted beams of photons from a 25 MV linear accelerator. The gantry angles were 70° and −20° as shown in Figure 5. The prescription required a dose of 60 Gy at the isocenter. A 55° wedge was used on both beams in plans A, B and C, a 27° wedge on both beams in plan D, and no wedges in plan E. In plan A rectangular beams were used with widths selected so that the 90% isodose covered the target area on the central slice through the tumor. No corrections for inhomogeneous tissue density were used in this calculation. The cumulative histogram of regret for the target in plan A is shown in Figure 6a and indicates that there are substantial regions in the target where the dose is below both the severe (dark blue) and mild (light blue) underdose limits but that there is no violation of the overdose limits. This is confirmed by the scores shown in column 1 of Table 2, which also show that regions of non-target tissue, and in particular the left (ipsilateral) lung, exceed the prescribed dose limits, though in volumes that are within the prescribed limits.

The beam's-eye-views for plan A showed that although the beams cover the target well on the central slice, on other slices large parts of the target volume lie outside the beam, causing the underdosing shown in the DVH's.

In plan B the rectangular beams were enlarged and the

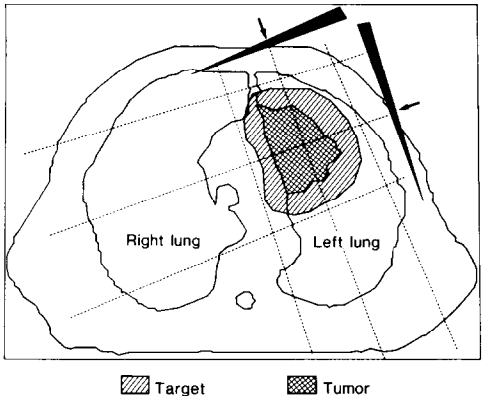

Fig. 5. Beam configuration for plan A defined in the text on a CT-slice through the mid-plane of the tumor.

Table 2. Scores for plans A, B, and C for two different normalizations

	Normalized at isocenter			Renormalized to balance target scores		
Plan scores	A	B	C	A′	B′	C′
% isodose at isocenter	100	100	100	107	104	105
Target overdose	10	10	10	3	8	7
Target underdose	−1	7	4	3	8	7
Non-target tissue	6	3	9	1	−2	9
Left lung	3	4	7	3	4	6
Right lung	10	8	10	9	8	9
Spinal cord	10	10	10	10	10	10

Note: No corrections for inhomogeneous tissue density were included in the calculations. The dose prescription used is shown in Table 1.

isocenter shifted to ensure good coverage of the target on all slices while minimizing the dose to normal tissues. The scores for plan B, shown in column 2 of Table 2, indicate that underdosing of the target has been reduced (i.e., higher scores), but at the expense of increased dose to non-target tissue (score reduced from 6 in plan A to 3 in plan B).

Plan C is a conformal plan in which the shapes of the beams were matched to the target outlines on the corresponding beam's-eye-views. This plan shows improved scores for non-target tissue and for both lungs, but the target underdose score is worse than for plan B because of encroachment of the penumbra on the target volume.

Renormalization

Plans A, B, and C all have scores of less than 10 for target underdose but perfect scores for target overdose, suggesting that they could be improved by increasing the overall dose. This can be done very simply by renormalizing the plans. As the percentage dose at the isocenter (referred to the prescribed 100% dose of 60 Gy) is increased the target underdose score will improve, rising toward 10, while the target overdose score will decrease. A crude optimization of the target dose distribution can therefore be achieved by choosing the normalization so that the overdose and underdose scores for the target are equal. This will, of course, decrease the scores for non-target tissue and for any specific sensitive organs being considered which may make the "target-optimized" normalization less desirable in terms of overall treatment strategy.

The scores following renormalization of plans A, B, and C are shown in under the headings A′, B′, and C′ in Table 2. The low target scores for plan A′ indicate that the target dose is very non-uniform, so that no renormalization can give high scores for both underdose and overdose simultaneously. This difficulty does not occur in plan B′, although the higher dose results in an unacceptable negative score for non-target tissue. Plan C′, the conformal plan, is nearly as good as plan B′ for the target, but is much better at avoiding dose both to non-target tissue and to specific healthy organs.

Effect of inhomogeneities

In many centers it is common practice to neglect tissue density inhomogeneities as we have done in plans A, B, and C. However, a correct calculation requires that the inhomogeneous tissue density be taken into account. We have used two approaches to understanding the implications of heterogeneous tissue density corrections. The first is a prospective recalculation of plans A, B, and C using CT-derived tissue densities and the Equivalent Tissue-Air Ratio (ETAR) method of Sontag and Cunningham (25), and adjusting the beam parameters to optimize the dose distributions.

The corrected plans are referred to as A_{inh}, B_{inh}, and C_{inh} and the scores are shown in Table 3. The histograms of regret for plans A and A_{inh} are shown in Figure 6a and 6b, respectively. The color shading indicates that plan A_{inh} has a more non-uniform target dose than plan A, and this is reflected in the negative target score in column 1 of Table 3. Even the "target-optimized" plan A'_{inh} still produces negative scores for the target. Plan B'_{inh} is somewhat better, though it gives a high dose to non-target tissue which is at the limit of acceptability. Plan C'_{inh} is arguably the best of the three, but still has a very non-uniform target dose with low target scores. It is apparent that the use of inhomogeneity corrections has a significant effect on the scores and therefore on the evaluation of the plans.

The second approach is to examine the "true" dose distribution which would result if the uncorrected plans, A′, B′, and C′ were used. Using the beam parameters and "beam-on times" of plans A′, B′ and C′ retrospective calculations were made including tissue density corrections and yielding plans A_{tr}, B_{tr}, and C_{tr} with scores shown in Table 3. These are the "true" dose distributions and scores which would have been delivered to the patient had plans A′, B′, and C′ been used. The scores for these plans indicate that the target dose is very non-uniform and even for the conformal plan C_{tr} the target overdose score is at the limit of acceptability. It is therefore clear that a proper evaluation of alternative treatment plans for sites near the lungs requires dose distributions to be corrected for the effects of inhomogeneous tissue density.

Effect of wedge modifiers

The effect of the 55° wedge modifiers used in plans A_{inh}, B_{inh}, and C_{inh} is to produce "cold spots" in the left anterior region of the target. Therefore, the corrected conformal plan, C_{inh}, was re-calculated with 27° wedges (D_{inh}) and without any wedges (E_{inh}). The results are shown in Table 4. After renormalization there is little to choose

Table 3. Scores for plans A_{inh}, B_{inh}, and C_{inh} for two different normalizations

	Normalized at isocenter			Renormalized to balance target scores			ETAR calculation for beam parameters of A′, B′, C′		
Plan scores % isodose at isocenter	A_{inh} 100	B_{inh} 100	C_{inh} 100	A'_{inh} 106	B'_{inh} 103	C'_{inh} 104	A_{tr} 109	B_{tr} 106	C_{tr} 107
Target overdose	8	8	8	−1	3	2	−6	−2	0
Target underdose	−9	−1	−4	−1	3	2	3	7	5
Non-target tissue	6	2	10	4	0	9	3	−2	9
Left lung	3	3	6	1	3	6	1	3	6
Right lung	7	6	8	6	5	7	6	4	7
Spinal cord	10	10	10	10	10	10	10	10	10

Note: Corrections for inhomogeneous tissue density were included in the calculations. The dose prescription used is shown in Table 1. The scores designated A_{tr}, B_{tr}, and C_{tr} are from a calculation using the beam parameters and beam-on times of plans A′, B′, and C′, but with inhomogeneity corrections.

between the 55° wedge and the un-wedged plans. However, the 27° wedge is slightly superior to the others because it gives better target homogeneity and less dose to the right lung. Similar conclusions were reached by Glatstein *et al.* (8) and Heukelom *et al.* (12), who found that in planning treatments for breast cancer using tangential opposed fields better dose distributions were obtained with wedge angles in the range 0° to 30° when non-uniform tissue densities, primarily due to the lungs, were taken into account.

DISCUSSION

The OSCAR treatment planning system is based on a dose prescription which represents the radiation oncologist's requirements for target coverage and sparing of normal tissue. These data can then be used to decide, in an objective and systematic way, whether a particular plan is acceptable. Scores are calculated, and an optimal plan could, in principle, be selected by assigning weights to each score to derive an overall objective function. In this work we have given a simple illustration of treatment plan optimization, balancing the target overdose and underdose scores by renormalizing the 100% target dose. We have not attempted to assign relative weights to target and specific organ scores.

Treatment planning using OSCAR follows the path shown in Figure 7, which allows for the renormalization of the dose distribution. If the renormalization fails to provide a good dose distribution, it is necessary to alter the beam parameters. Images of regret (22) displayed on the CT slices greatly facilitate this since they show clearly the location of overdosed and underdosed regions of the target and overdosed regions of healthy tissue.

When OSCAR is used most of the work in selecting and improving a treatment plan can be done without the ongoing intervention of a radiation oncologist, since his or her requirements have been specified in advance in the dose prescription. Although the oncologist may wish to review all plans before giving final approval, his or her active involvement is only necessary when no plan without

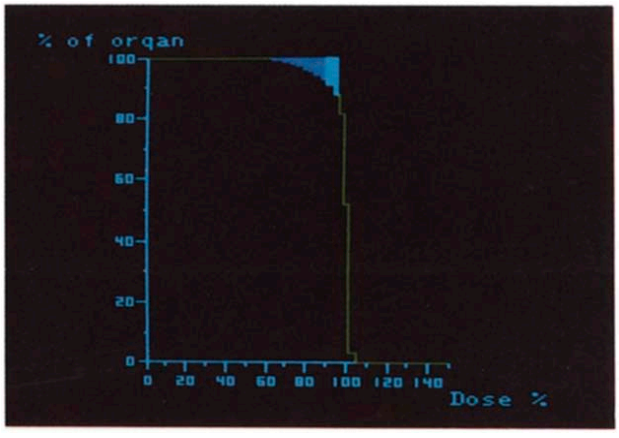

(a)

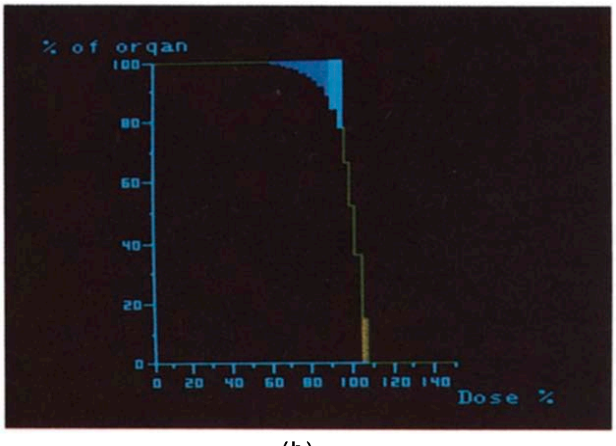

(b)

Fig. 6. CDVH for the target in (a) plan A (without inhomogeneity corrections) and (b) plan A_{inh} (with inhomogeneity corrections). In both cases the dose is normalized to 100% at the isocenter.

Table 4. Scores for conformal plan with different wedge modifiers for two different normalizations

	Plan: wedge (degrees)—% isodose at isocenter					
	Normalized at isocenter			Renormalized to balance target scores		
	C_{inh}	D_{inh}	E_{inh}	C'_{inh}	D'_{inh}	E'_{inh}
Plan: wedge (degrees)	55	27	0	55	27	0
% isodose at isodose	100	100	100	104	105	105
	8	10	9	2	4	3
Target overdose						
Target underdose	−4	−1	−6	2	4	2
Non-target tissue	10	10	10	9	9	9
Left lung	6	6	7	6	6	6
Right lung	8	9	9	7	8	8
Spinal cord	10	10	10	10	10	10

Note: Corrections for inhomogeneous tissue density were included in the calculations. The dose prescription used is shown in Table 1.

negative scores can be found. In such a case it would be necessary to change the prescription or choose a different treatment modality.

It is a simple matter to re-calculate scores using a different dose prescription. This makes it possible to improve dose prescriptions in a systematic way by means of a retrospective survey in which scores for cases where the outcome of treatment is known are calculated using different dose prescriptions. The dose prescription which gives the best correlation between scores and outcome can then be determined. It is our hope that widespread use of 3-dimensional treatment planning will lead to a suitable data base for such studies.

An OSCAR dose prescription provides a convenient means of defining a treatment protocol. Most protocols specify only the dose to the target and the configuration of the beams to be used. A protocol using an OSCAR prescription not only determines dose levels and acceptable inhomogeneity in the target, but also takes into account the dose to non-target tissue and to specific healthy organs. A 2-dimensional example is discussed by Hahn *et al.* (11), where it is shown that a conventional protocol for the treatment of prostate cancer that was effective in ensuring similar target doses nevertheless allowed wide variations in the dose to the rectum.

CONCLUSION

This paper extends the use of the OSCAR method (23) by generalizing the prescription and score functions to three dimensions and introducing techniques for the evaluation of dose volume histograms. The power of the method is derived from the OSCAR prescription which allows a clinician to express the needs of his or her patient in a simple quantitative way taking into account clinical experience as well as any dose response data which may be available. The prescription is used to generate objective score functions as well as colored visual displays which are helpful in evaluating and comparing complex 3-dimensional treatment plans. In particular, they can be used in the interpretation of dose-volume histograms, which hitherto have not been easy to use as evaluation tools.

The choice of numerical values in the OSCAR prescription is not a simple issue. However, by permitting the clinician to define dose-volume limits in accordance with clinical experience, it avoids many of the problems of evaluation techniques based on dose response data and volume effect models. Further investigations are required to produce the most useful prescriptions for various tumor sites.

A single figure of merit for a treatment plan would perhaps be easier to interpret than the full set of scores provided by OSCAR. However, this would require a system of weighting the different scores for the target, non-target tissue and specific dose-limiting organs. It is not clear how such weighting should be carried out, and it seems preferable at present to retain the separate scores, allowing the clinician to make a final decision on their relative importance in accordance with the needs of individual patients. We have suggested simple averaging to combine the pairs of overdose and underdose scores for the target, but, as discussed, this procedure may not always

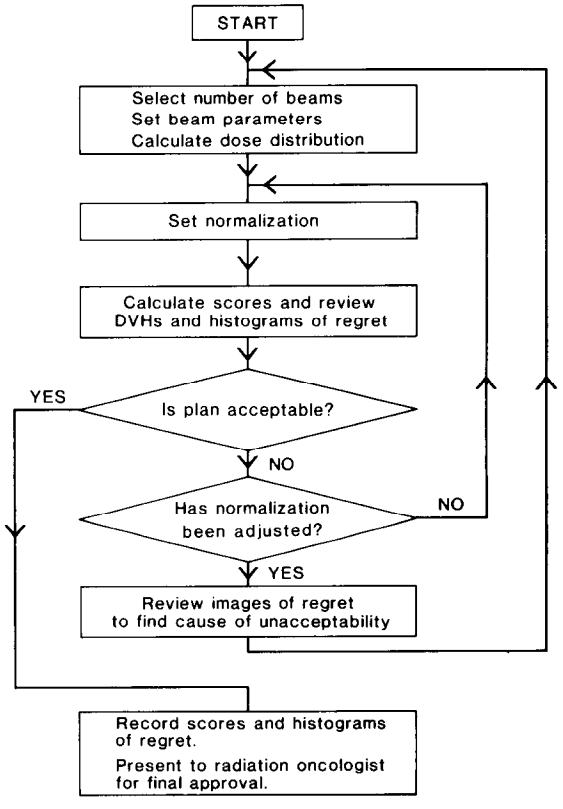

Fig. 7. Flow chart to illustrate the application of OSCAR techniques to treatment planning.

be appropriate and alternative approaches may prove more acceptable.

OSCAR is well adapted for use in the definition of treatment protocols. The quantitative score functions generated by the system provide a useful means of analyzing protocol data and searching for correlations between treatment dose distributions and outcome. Such analyses can also be used to improve the dose prescription used in subsequent treatments.

The application of OSCAR to planning for the treatment of a case of ca lung showed the importance of correcting for inhomogeneities of tissue density when calculating the dose distribution, and showed that such corrections may affect the choice of wedge modifiers.

REFERENCES

1. Austin-Seymour, M. M.; Chen, G. T. Y.; Castro, J. R.; Saunders, W. M.; Pitluck, S.; Woodruff, K. H.; Kessler, M. Dose volume histogram analysis of liver radiation tolerance. Int. J. Radiat. Oncol. Biol. Phys. 12: 31–35; 1986.
2. Chen, G. T. Y.; Pelizzari, C. A.; Spelbring, D. R.; Awan, A. Evaluation of treatment plans using dose volume histograms. Front. Radiat. Ther. Oncol. 21: 44–55; 1987.
3. Chin, L. M.; Kijewski, P. K.; Svensson, G. K.; Chaffey, J. T.; Levene, M. B.; Bjarngard, B. E. A computer-controlled radiotherapy machine for pelvic and para-aortic nodal areas. Int. J. Radiat. Oncol. Biol. Phys. 7: 61–70; 1981.
4. Chin, L. M.; Siddon, R. L.; Svensson, G. K.; Rose, C. Progress in 3-D treatment planning for photon beam radiotherapy. Int. J. Radiat. Oncol. Biol. Phys. 11: 2011–2020; 1985.
5. Chu, J. C. H.; Richter, M. P.; Sontag, M. R.; Larsen, R. D.; Fong, K.; Bloch, P. Practice of three dimensional treatment planning at the Fox Chase Cancer Center, University of Pennsylvania. Radioth. Oncol. 8: 137–143; 1987.
6. Emami, B. N.; Purdy, J. A.; Harms, W. B.; Manolis, J. M.; Wong, J. W.; Dryzmala, R. E.; Simpson, J. R. Scientific report. St. Louis, MO: Radiation Oncology Center, Mallinckrodt Institute of Radiology, Washington University Medical Center; 1987–1988: 129.
7. Fraass, B. A.; Lichter, A. S.; McShan, D. L.; Yanke, B. R.; Diaz, R. F.; Yeakel, K. S.; van de Geijn, J. The influence of lung density corrections on treatment planning for primary breast cancer. Int. J. Radiat. Oncol. Biol. Phys. 14: 179–190; 1988.
8. Glatstein, E.; Lichter, A. S.; Fraass, B. A.; Kelly, R. T.; van der Geijn, J. The imaging revolution and radiation oncology: Use of CT, ultrasound, and NMR for localization, treatment planning and treatment delivery. Int. J. Radiat. Oncol., Biol. Phys. 11: 299–314; 1985.
9. Habrand, J. L.; Austin-Seymour, M.; Birnbaum, S.; Wray, S.; Carroll, R.; Munzenrider, J.; Verhey, L.; Urie, M.; Goitein, M. Neurovisual outcome following proton radiation therapy. Int. J. Radiat. Oncol., Biol. Phys. 16: 1601–1606; 1989.
10. Hahn, P.; Shalev, S.; Therrien, P. Colour visualization as an aid to the comparison of treatment plans for prostatic carcinoma. Acta Oncol. 26: 313–315; 1987.
11. Hahn, P.; Shalev, S.; Viggars, D.; Therrien, P. Treatment planning for protocol-based radiation therapy. Int. J. Radiat. Oncol. Biol. Phys. 18: 937–939; 1990.
12. Heukelom, S.; Lanson, J. H.; van Tienhoven, G.; Mijnheer, B. J. In vivo dosimetry during tangential breast treatment. Radioth. Oncol. 22: 269–279; 1991.
13. Langer, M.; Leong, J. Optimization of beam weights under dose volume restrictions. Int. J. Radiat. Oncol. Biol. Phys. 13: 1255–1260; 1987.
14. Lawrence, T. S.; Tesser, R. J.; Ten Haken, R. K. An application of dose volume histograms to the treatment of intrahepatic malignancies with radiation therapy. Int. J. Radiat. Oncol. Biol. Phys. 19: 1041–1047; 1990.
15. Lyman, J. T. Complication probability as assessed from dose volume histograms. Radiat. Res. 104: S13–S19; 1985.
16. Lyman, J. T.; Wolbarst, A. B. Optimization of radiotherapy III: a method of assessing complication probabilities from dose volume histograms. Int. J. Radiat. Oncol. Biol. Phys. 13: 103–109; 1987.
17. Lyman, J. T.; Wolbarst, A. B. Optimization of radiotherapy IV: a dose volume histogram reduction algorithm. Int. J. Radiat. Oncol. Biol. Phys. 17: 433–436; 1989.
18. McCrae, D.; Rodgers, J.; Dritschilo, A. Dose-volume and complication in interstitial implants for breast carcinoma. Int. J. Radiat. Oncol. Biol. Phys. 13: 525–529; 1987.
19. McNeely, L. K.; Jacobson, G. M.; Leavitt, D. D.; Stewart, J. R. Electron arc therapy: chest wall irradiation of breast cancer patients. Int. J. Radiat. Oncol. Biol. Phys. 14: 1287–1294; 1988.
20. Roberson, P. L.; Lichter, A. S.; Bodner, A.; Fredrickson, H. A.; Padikal, T. N.; Kelly, B. A.; van der Geijn, J. Dose to lung in primary breast irradiation. Int. J. Radiat. Oncol. Biol. Phys. 9: 97–102; 1982.
21. Schultheiss, T. F.; Orton, C. G.; Peck, R. A. Models in radiotherapy: volume effects. Med. Phys. 10: 310–415; 1983.
22. Shalev, S.; Bartel, L.; Therrien, P.; Hahn, P.; Carey, M. The objective evaluation of alternative treatment plans: I. Images of regret. Int. J. Radiat. Oncol. Biol. Phys. 15: 763–767; 1988.
23. Shalev, S.; Viggars, D. A.; Carey, M.; Hahn, P. The objective evaluation of alternative treatment plans: II. Score functions. Int. J. Radiat. Oncol. Biol. Phys. 20: 1067–1073; 1991.
24. Simpson, J. R.; Purdy, J. A.; Harms, W. B.; Manolis, J. M.; Wong, J. W.; Dryzmala, R. E.; Emami, B. N.; Pilcpich, M. V. Three dimensional treatment planning considerations for prostate cancer. In: Scientific report. St. Louis, MO: Radiation Oncology Center, Mallinckrodt Institute of Radiology, Washington University Medical Center; 1987–88: 155.
25. Sontag, M. R.; Cunningham, J. R. The equivalent tissue air ratio method for making absorbed dose calculations in a heterogeneous medium. Radiology 104: 787–795; 1978.
26. Tait, D.; Nahum, A.; Southall, M.; Chow, M.; Yarnold, J. R. Benefits expected from simple conformal radiotherapy in the treatment of pelvic tumors. Radioth. Oncol. 13: 23–30; 1988.
27. Ten Haken, R. K.; Perez-Tamayo, C.; Tesser, R. T. T.; McShan, D. L.; Fraass, B. A.; Lichter, A. S. Boost treatment for prostate using shaped fixed fields. Int. J. Radiat. Oncol. Biol. Phys. 16: 193–200; 1989.
28. Ulso, N.; Christenson, J. J. Performance evaluation of an algorithm for optimization with compensating filters. In: Proc. 8th Conf. on Use of Computers in Radiation Therapy. IEEE Computer Society (ISBN 0-8186-0559-6). 1984: 83–87.
29. Wolbarst, A. B.; Sternick, E. S.; Curran, B. H.; Dritschilo, A. Optimized radiotherapy treatment planning using the complication probability factor (CPF). Int. J. Radiat. Oncol. Biol. Phys. 6: 723–728; 1980.
30. Zink, S. R.; Lyman, J. T.; Castro, J. R.; Chen, G. T. Y.; Collier, J. M.; Saunders, W. M. Treatment planning study for carcinoma of the esophagus: helium ions versus photons. Int. J. Radiat. Oncol. Biol. Phys. 14: 993–1000; 1988.

Exhibit B

IN THE UNITED STATES DISTRICT COURT

FOR THE DISTRICT OF DELAWARE

BEST MEDICAL INTERNATIONAL, INC.,	)	
	)	
Plaintiff,	)	
	)	
v.	)	C.A. No. 18-1599-MN
	)	
VARIAN MEDICAL SYSTEMS, INC. and VARIAN MEDICAL SYSTEMS INTERNATIONAL AG,	)	
	)	
Defendants.	)	

LETTER OF REQUEST FOR INTERNATIONAL JUDICIAL ASSISTANCE PURSUANT TO THE HAGUE CONVENTION OF 18 MARCH 1970 ON THE TAKING OF EVIDENCE ABROAD IN CIVIL OR COMMERCIAL MATTERS

The United States District Court for the District of Delaware presents its compliments to the appropriate judicial authority of France, and requests international judicial assistance to obtain evidence to be used in a civil proceeding before this Court in the above-captioned matter. A trial on this matter is scheduled at present for August 23, 2021, in Wilmington, Delaware. This request is made pursuant to Article 1 of the Hague Convention of 18 March 1970 on the Taking of Evidence Abroad in Civil or Commercial Matters (the "Hague Evidence Convention").

The Court requests the assistance described herein as necessary in the interests of justice. Specifically, this matter is a patent case, and the Court requests that appropriate judicial authority of France compel the production of documentary evidence and deposition testimony from L'Institut Curie, 26 rue d'Ulm, 75248 Paris cedex 05, regarding a medical treatment system developed at L'Institut Curie that may be prior art to one or more of the asserted patents.

1. Sender

The Honorable Maryellen Noreika
United States District Court for the District of Delaware
J. Caleb Boggs Federal Building
844 N. King Street
Wilmington, DE 19801-3555
USA

2. Central Authority of the requested state

Ministère de la Justice
Direction des Affaires Civiles et du Sceau
Bureau du droit de l'Union, du droit international privé et de l'entraide civile (BDIP)
13, Place Vendôme
75042 Paris Cedex 01
France

3. Person to whom the executed request is to be returned

Defendants' counsel:

Ryan K. Wong
KEKER, VAN NEST & PETERS LLP
633 Battery Street
San Francisco, CA 94111
USA

4. Specification of the date by which the requesting authority requires receipt of the response to the Letter of Request: **March 13, 2020**.

IN CONFORMITY WITH ARTICLE 3 OF THE HAGUE EVIDENCE CONVENTION, THE UNDERSIGNED APPLICANT HAS THE HONOR TO SUBMIT THE FOLLOWING REQUEST:

5. a. Requesting judicial authority (Article 3, *a*):

The Honorable Maryellen Noreika
United States District Court for the District of Delaware
J. Caleb Boggs Federal Building
844 N. King Street
Wilmington, DE 19801-3555
USA

b. To the competent authority of (Article 3, *a*):

Ministère de la Justice
Direction des Affaires Civiles et du Sceau
Bureau du droit de l'Union, du droit international privé et de l'entraide civile (BDIP)
13, Place Vendôme
75042 Paris Cedex 01
France

c. Names of the case and any identifying number:

Best Medical International, Inc. v. Varian Medical Systems, Inc. and Varian Medical Systems International AG
Civil Action Number 18-1599-MN
United States District Court for the District of Delaware

6. Names and addresses of the parties and their representatives (Article 3, *b*)

Plaintiff:

Best Medical International, Inc.
7643 Fullerton Road
Springfield, Virginia 22153
USA

Plaintiff's U.S. legal representative:

Philip Hirschhorn
BUCHANAN INGERSOLL & ROONEY PC
640 5th Avenue, 9th Floor
New York, NY 10019-6102
USA

Defendants:

Varian Medical Systems, Inc.
3100 Hansen Way
Palo Alto, CA 94304
USA

Varian Medical Systems International AG
Hinterbergstrasse 14
6312 Steinhausen
Switzerland

Defendants' U.S. legal representative:

Ryan K. Wong
KEKER, VAN NEST & PETERS LLP
633 Battery Street
San Francisco, CA 94111
USA

Other parties: None

7. Nature of the proceedings, summary of complaint, and summary of defenses (Article 3, *c*):

Plaintiff Best Medical, Inc. ("BMI") accuses defendants Varian Medical Systems, Inc. and Varian Medical Systems International AG ("Varian") of infringing four asserted patents: U.S. Patent Nos. 7,266,175, 7,015,490, 6,038,283, and 6,393,096. BMI amended its complaint on September 9, 2019, and Varian has moved to dismiss certain allegations in the amended complaint regarding indirect and willful infringement.

8. Evidence to be obtained and purpose of the evidence sought (Article 3, *d*):

a. Evidence to be obtained

i. Documents sufficient to show the conception, design, and development of the following aspects of the intensity-modulated radiation therapy system, integrated with the KONRAD inverse treatment planning system developed at L'Institut Curie, as referenced in Papatheodorou, et al., *Integration of the KONRAD Inverse Planning Tool into the iSis3D Treatment Planning System*, Proc. 13th Int. Conf. on the Use of Computers in Radiation Therapy (Heidelberg), pp. 54–6 (May 2000) (the "ISis3D Treatment Planning System") before the stated date:

(a) Before August 11, 2003:

cost function computation for determining, selecting, or optimizing a collimator angle of a multi-leaf collimator;

cost function minimization relating to the determination, selection, or optimization of a collimator angle (including, *inter alia*, use of simulated annealing, logic for accepting or rejecting a beam-weight set on a given iteration, and logic for stopping the iteration);

consideration of target conformity and/or treatment plan delivery efficiency as cost terms in a cost function to determine, select, or optimize a collimator angle; and

user interface(s) for receiving optimization input relating to the determination of a collimator angle.

(b) Before July 11, 2003:

cost function computation;

cost function minimization (including, *inter alia*, use of simulated annealing, logic for accepting or rejecting a beam-weight set on a given iteration, and logic for stopping the iteration);

use of treatment plan delivery efficiency;

treatment delivery time;

total beam segments and/or total monitor units as part of treatment plan optimization;

use of dosimetric fitness as part of treatment plan optimization; and

user interface(s) for receiving optimization inputs and/or controlling tradeoffs between treatment plan delivery efficiency and dosimetric fitness.

ii. Documents sufficient to identify each version of the ISis3D Treatment Planning System in use before August 11, 2003, the release date for each version, and differences between each version with respect to the aspects of the ISis3D Treatment Planning System identified in Request No. i.

iii. Documents sufficient to show the design, operation, and functionality of the aspects of the ISis3D Treatment Planning System identified in Request No. i for each version identified in response to Request No. ii.

iv. Documents sufficient to show that each version of the ISis3D Treatment Planning System identified in response to Request No. ii was publicly available and/or in use anywhere in the world before August 11, 2003, such as academic journal articles, industry publications, press releases, product specifications, manuals, user guides, brochures, and/or web pages describing or identifying that version of the ISis3D Treatment Planning System and its availability.

v. Documents sufficient to identify any apparatus, system, or device using the ISis3D Treatment Planning System before August 11, 2003. This request

includes intensity-modulated radiation therapy systems that comprise linear accelerators, treatment planning programs, and multi-leaf collimators.

vi. Documents and communications sufficient to show the design, structure, function, operation, and availability of each apparatus, system, or device identified in response to Request No. v.

vii. Documents and communications sufficient to show the sale, offer for sale, or importation into the United States of each apparatus, system, or device identified in response to Request No. v before August 11, 2003, and if such documents exist, before July 11, 2003.

b. Purpose of the evidence sought

The documents sought by these requests are directly relevant to the above-captioned litigation. These requests seek documents regarding specific features of a medical treatment system developed at L'Institut Curie, which may be prior art to one or more of BMI's asserted patents under 35 U.S.C. § 102. If obtained, Varian would use these documents to develop its invalidity defenses for trial, and may rely on the documents to seek invalidation of one or more asserted patents.

9. Identity and address of any person to be examined (Article 3, *e*):

The Court requests that L'Institut Curie, 26 rue d'Ulm, 75248 Paris cedex 05, designate one or more witnesses who are knowledgeable about the subject matter identified in section 10 below.

10. Statement of the subject matter about which the persons are to be examined (Article 3, *f*):

i. The conception, design, development, operation, and functionality of the aspects of the ISis3D Treatment Planning System at L'Institut Curie set forth in Document Request No. i before the date(s) specified in Document Request No. i.

ii. Each version of the ISis3D Treatment Planning System in use before the date(s) specified in Document Request No. i, and the release date for each version.

iii. The date and circumstances of the first sale, offer for sale, and/or public use in the United States of the ISis3D Treatment Planning System before the date(s) specified in Document Request No. i.

iv. The identity, design, operation, and functionality of any apparatus, system, or device using the aspects of the ISis3D Treatment Planning System set forth in Document Request No. i before the date(s) specified in Document Request No. i.

v. The date and circumstances of the first sale, offer for sale, and/or public use in the United States of any apparatus, system, or device covered by Deposition Topic No. iv.

vi. The authenticity of documents produced in response to this Letter of Request, the public availability and publication dates of documents produced in response to this Letter of Request, the creation and authorship of documents produced in response to this Letter of Request, and whether and how the documents produced in response to this Letter of Request were created and/or stored in the ordinary course of business.

11. Any requirement that the evidence be given on oath or affirmation and any special form to be used (Article 3, *h*):

Because the testifying witnesses are outside this Court's subpoena power and cannot be compelled to attend trial, the Court requests that the witnesses' testimony be taken under oath in such manner as provided by the laws of France for the formal taking of evidence.

12. Special methods or procedure to be followed (Articles 3, *i* and 9):

The Court requests that the testimony be taken by oral examination in such manner as provided by the laws of France for the formal taking of evidence. To the extent permitted by the laws of France, the Court requests that the testimony be recorded by a videographer and transcribed by a stenographer.

13. Request for notification of the time and place for the execution of the Request and identity and address of any person to be notified (Article 7):

Please notify defendants' U.S. legal counsel at the following address:

Ryan K. Wong
KEKER, VAN NEST & PETERS LLP
633 Battery Street
San Francisco, CA 94111
USA

14. Specification of privilege or duty to refuse to give evidence under the law of the State of origin (Article 11, *b*):

Nothing in this Letter of Request is intended to interfere with any rights of L'Institut Curie to assert privilege or refuse to give evidence under any applicable law of France or the United States of America.

15. Fees and costs

If the Ministère de la Justice incurs fees or costs in executing this Letter of Request that are reimbursable under the second paragraph of Article 14 or Article 26 of the Hague Evidence Convention, the Court requests that the Ministère de la Justice submit a bill of fees and costs to the Court and defendants' U.S. legal counsel:

Ryan K. Wong
KEKER, VAN NEST & PETERS LLP
633 Battery Street
San Francisco, CA 94111
USA

The Court guarantees that defendants' counsel will reimburse the Ministère de la Justice for all reimbursable fees and costs incurred in executing this Letter of Request.

This Court expresses its gratitude to the authorities of France for assisting with this Letter of Request, and will provide similar assistance to the judicial authorities of France when requested.

DATE OF REQUEST: _____

SIGNATURE AND SEAL OF THE REQUESTING AUTHORITY

_____
The Honorable Maryellen Noreika
United States District Judge

Exhibit C

IN THE UNITED STATES DISTRICT COURT

FOR THE DISTRICT OF DELAWARE

BEST MEDICAL INTERNATIONAL, INC.,	)	
	)	
Plaintiff,	)	
	)	
v.	)	C.A. No. 18-1599-MN
	)	
VARIAN MEDICAL SYSTEMS, INC. and VARIAN MEDICAL SYSTEMS INTERNATIONAL AG,	)	
	)	
Defendants.	)	

LETTER OF REQUEST FOR INTERNATIONAL JUDICIAL ASSISTANCE PURSUANT TO THE HAGUE CONVENTION OF 18 MARCH 1970 ON THE TAKING OF EVIDENCE ABROAD IN CIVIL OR COMMERCIAL MATTERS

The United States District Court for the District of Delaware presents its compliments to the appropriate judicial authority of Germany, and requests international judicial assistance to obtain evidence to be used in a civil proceeding before this Court in the above-captioned matter. A trial on this matter is scheduled at present for August 23, 2021, in Wilmington, Delaware. This request is made pursuant to Article 1 of the Hague Convention of 18 March 1970 on the Taking of Evidence Abroad in Civil or Commercial Matters (the "Hague Evidence Convention").

The Court requests the assistance described herein as necessary in the interests of justice. Specifically, this matter is a patent case, and the Court requests that appropriate judicial authority of Germany compel the production of documentary evidence and deposition testimony from Deutsches Krebsforschungszentrum ("DKFZ"), Im Neuenheimer Feld 280, 69120 Heidelberg, Germany, regarding a medical treatment system developed at DKFZ that may be prior art to one or more of the asserted patents.

1. Sender

The Honorable Maryellen Noreika
United States District Court for the District of Delaware
J. Caleb Boggs Federal Building
844 N. King Street
Wilmington, DE 19801-3555
USA

2. Central Authority of the requested state

Präsident des Amtsgerichts Freiburg
Holzmarkt 2
D-79098 Freiburg
Germany

3. Person to whom the executed request is to be returned

Defendants' counsel:

Ryan K. Wong
KEKER, VAN NEST & PETERS LLP
633 Battery Street
San Francisco, CA 94111
USA

4. Specification of the date by which the requesting authority requires receipt of the response to the Letter of Request: **March 13, 2020**.

IN CONFORMITY WITH ARTICLE 3 OF THE HAGUE EVIDENCE CONVENTION, THE UNDERSIGNED APPLICANT HAS THE HONOR TO SUBMIT THE FOLLOWING REQUEST:

5. a. Requesting judicial authority (Article 3, *a*):

The Honorable Maryellen Noreika
United States District Court for the District of Delaware
J. Caleb Boggs Federal Building
844 N. King Street
Wilmington, DE 19801-3555
USA

b. To the competent authority of (Article 3, *a*):

Präsident des Amtsgerichts Freiburg
Holzmarkt 2
D-79098 Freiburg
Germany

c. Names of the case and any identifying number:

Best Medical International, Inc. v. Varian Medical Systems, Inc. and Varian Medical Systems International AG
Civil Action Number 18-1599-MN
United States District Court for the District of Delaware

6. Names and addresses of the parties and their representatives (Article 3, *b*)

Plaintiff:

Best Medical International, Inc.
7643 Fullerton Road
Springfield, Virginia 22153
USA

Plaintiff's U.S. legal representative:

Philip Hirschhorn
BUCHANAN INGERSOLL & ROONEY PC
640 5th Avenue, 9th Floor
New York, NY 10019-6102
USA

Defendants:

Varian Medical Systems, Inc.
3100 Hansen Way
Palo Alto, CA 94304
USA

Varian Medical Systems International AG
Hinterbergstrasse 14
6312 Steinhausen
Switzerland

Defendants' U.S. legal representative:

Ryan K. Wong
KEKER, VAN NEST & PETERS LLP
633 Battery Street
San Francisco, CA 94111
USA

Other parties: None

7. Nature of the proceedings, summary of complaint, and summary of defenses (Article 3, *c*):

Plaintiff Best Medical, Inc. ("BMI") accuses defendants Varian Medical Systems, Inc. and Varian Medical Systems International AG ("Varian") of infringing four asserted patents: U.S. Patent Nos. 7,266,175, 7,015,490, 6,038,283, and 6,393,096. BMI amended its complaint on September 9, 2019, and Varian has moved to dismiss certain allegations in the amended complaint regarding indirect and willful infringement.

8. Evidence to be obtained and purpose of the evidence sought (Article 3, *d*):

a. Evidence to be obtained

i. Documents sufficient to show the conception, design, and development of the following aspects of the computer optimization program developed under Computer Vision in Radiology (COVIRA), project A2003 of the AIM (Advanced Informatics in Medicine) program of the European Union, of which DKFZ was a participant (the "COVIRA Algorithm"), as more fully described in Mark Oldham, Anthony Neal, Steve Webb, *A Comparison of Conventional 'Forward Planning' With Inverse Planning for 3D Conformal Radiotherapy of the Prostate*, 35 Radiotherapy & Oncology 248 (1995), attached hereto as Attachment A-1, before May 27, 1998, and if such documents exist, before October 24, 1996:

cost function computation;

cost function minimization (including, *inter alia*, use of simulated annealing, logic for accepting or rejecting a beam-weight set on a given iteration, and logic for stopping the iteration);

use of partial volume data or dose volume constraints;

use of dose volume histograms;

importance factors; and

user interface(s) for receiving optimization input.

ii. Documents sufficient to identify each version of the COVIRA Algorithm in use before May 27, 1998, and if such documents exist, before October 24, 1996, the release date for each version, and differences between each version with respect to the aspects of the COVIRA Algorithm identified in Request No. i.

iii. Documents sufficient to show the design, operation, and functionality of the aspects of the COVIRA Algorithm identified in Request No. i for each version identified in response to Request No. ii.

iv. Documents sufficient to show that each version of the COVIRA Algorithm identified in response to Request No. ii was publicly available and/or in use anywhere in the world before May 27, 1998, and if such documents exist, before October 24, 1996, such as academic journal articles, industry publications, press releases, product specifications, manuals, user guides, brochures, and/or web pages describing or identifying that version of the COVIRA Algorithm and its availability.

v. Documents sufficient to identify any apparatus, system, or device using the COVIRA Algorithm before May 27, 1998, and if such documents exist, before October 24, 1996. This request may include the VIRTUOS System.

vi. Documents and communications sufficient to show the design, function, operation, and availability of each apparatus, system, or device identified in response to Request No. v.

vii. Documents and communications sufficient to show the sale, offer for sale, or importation into the United States of each apparatus, system, or device identified in response to Request No. v before May 27, 1998, and if such documents exist, before October 24, 1996.

viii. Documents sufficient to show the conception, design, and development of the following aspects of the simulated annealing technique developed and implemented at DKFZ (the "Simulated Annealing Implementation"), as disclosed in S. Webb, *Optimizing Radiation Therapy Inverse Treatment Planning Using the Simulated Annealing Technique*, 6 Int'l J. Imaging Sys. & Tech. 71 (1995), p. 77, attached hereto as Attachment A-2, in the three-dimensional treatment planning program used in IMRT treatment planning systems at DKFZ and incorporated into the VIRTUOS treatment planning package ("VOXELPLAN"), a version of which is described in the document referenced at https://www.ncbi.nlm.nih.gov/pubmed/8588040, before May 27, 1998, and if such documents exist, before October 24, 1996:

cost function computation;

cost function minimization (including, *inter alia*, use of simulated annealing, logic for accepting or rejecting a beam-weight set on a given iteration, and logic for stopping the iteration);

use of partial volume data or dose volume constraints;

use of dose volume histograms;

importance factors; and

user interface(s) for receiving optimization input.

ix. Documents sufficient to identify each version of the Simulated Annealing Implementation in VOXELPLAN in use before May 27, 1998, and if such documents exist, before October 24, 1996, the release date for each version, and differences between each version with respect to the aspects of the Simulated Annealing Implementation identified in Request No. viii.

x. Documents sufficient to show the design, operation, and functionality of the aspects of the Simulated Annealing Implementation in VOXELPLAN identified in Request No. viii for each version identified in response to Request No. ix.

xi. Documents sufficient to show that each version of the Simulated Annealing Implementation in VOXELPLAN identified in response to Request No. ix was publicly available and/or in use anywhere in the world before May 27, 1998, and if such documents exist, before October 24, 1996, such as academic journal articles, industry publications, press releases, product specifications, manuals, user guides, brochures, and/or web pages describing or identifying that version of the Simulated Annealing Implementation and its availability.

xii. Documents sufficient to identify any apparatus, system, or device using the Simulated Annealing Implementation in VOXELPLAN before May 27, 1998, and if such documents exist, before October 24, 1996. This request may include the VIRTUOS System.

xiii. Documents and communications sufficient to show the design, function, operation, and availability of each apparatus, system, or device identified in response to Request No. xii.

xiv. Documents and communications sufficient to show the sale, offer for sale, or importation into the United States of each apparatus, system, or device identified in response to Request No. xii before May 27, 1998, and if such documents exist, before October 24, 1996.

xv. Documents sufficient to show the conception, design, and development of the following aspects of the inverse treatment planning system developed at DKFZ and commercialized by MRC Systems GmbH ("KONRAD"), as described in the documents available at https://www.accessdata.fda.gov/cdrh_docs/pdf2/K022307.pdf and https://www.dkfz.de/TechTrans/patentsearch_pdf/93809_DKFZ_P-854%20local%20dose%20shaping.pdf, at DKFZ before the stated date:

(a) Before August 11, 2003:

cost function computation for determining, selecting, or optimizing a collimator angle of a multi-leaf collimator;

cost function minimization relating to the determination, selection, or optimization of a collimator angle (including, *inter alia*, use of simulated annealing, logic for accepting or rejecting a beam-weight set on a given iteration, and logic for stopping the iteration);

consideration of target conformity and/or treatment plan delivery efficiency as cost terms in a cost function to determine, select, or optimize a collimator angle; and

user interface(s) for receiving optimization input relating to the determination of a collimator angle.

(b) Before July 11, 2003:

cost function computation;

cost function minimization (including, *inter alia*, use of simulated annealing, logic for accepting or rejecting a beam-weight set on a given iteration, and logic for stopping the iteration);

use of treatment plan delivery efficiency;

treatment delivery time;

total beam segments and/or total monitor units as part of treatment plan optimization;

use of dosimetric fitness as part of treatment plan optimization; and

user interface(s) for receiving optimization inputs and/or controlling tradeoffs between treatment plan delivery efficiency and dosimetric fitness.

xvi. Documents sufficient to identify each version of KONRAD in use before August 11, 2003, the release date for each version, and differences between each version with respect to aspects of KONRAD at DKFZ identified in Request No. xv.

xvii. Documents sufficient to show the design, operation, and functionality of the aspects of KONRAD identified in Request No. xv for each version identified in response to Request No. xvi.

xviii. Documents sufficient to show that each version of KONRAD identified in response to Request No. xvi was publicly available and/or in use anywhere in the world before August 11, 2003, such as academic journal articles, industry publications, press releases, product specifications, manuals, user guides, brochures, and/or web pages describing or identifying that version of KONRAD and its availability.

xix. Documents sufficient to identify any apparatus, system, or device using KONRAD before August 11, 2003, and if such documents exist, before July 11, 2003. This request includes intensity-modulated radiation therapy systems that comprise linear accelerators, treatment planning programs, and multi-leaf collimators.

xx. Documents and communications sufficient to show the design, structure, function, operation, and availability of each apparatus, system, or device identified in response to Request No. xix.

xxi. Documents and communications sufficient to show the sale, offer for sale, or importation into the United States of each apparatus, system, or device identified in response to Request No. xix before August 11, 2003, and if such documents exist, before July 11, 2003.

b. Purpose of the evidence sought

The documents sought by these requests are directly relevant to the above-captioned litigation. These requests seek documents regarding specific features of a medical treatment system developed at DKFZ, which may be prior art to one or more of BMI's asserted patents under 35 U.S.C. § 102. If obtained, Varian would use these documents to develop its invalidity defenses for trial, and may rely on the documents to seek invalidation of one or more asserted patents.

9. Identity and address of any person to be examined (Article 3, *e*):

The Court requests that Deutsches Krebsforschungszentrum, Im Neuenheimer Feld 280, 69120 Heidelberg, Germany, designate one or more witnesses who are knowledgeable about the subject matter identified in section 10 below.

10. Statement of the subject matter about which the persons are to be examined (Article 3, *f*):

i. The conception, design, development, operation, and functionality of the aspects of the COVIRA Algorithm, the Simulated Annealing Implementation in VOXELPLAN, and KONRAD set forth in Document Request Nos. i, viii, and xv, before the date(s) specified in Document Request Nos. i, viii, and xv.

ii. Each version of the COVIRA Algorithm, the Simulated Annealing Implementation in VOXELPLAN, and KONRAD in use before the date(s) specified in Document Request Nos. i, viii, and xv, and the release date for each version.

iii. The date and circumstances of the first sale, offer for sale, and/or public use in the United States of the COVIRA Algorithm, the Simulated Annealing Implementation in VOXELPLAN, and KONRAD before the date(s) specified in Document Request Nos. i, viii, and xv.

iv. The identity, design, operation, and functionality of any apparatus, system, or device using the aspects of the COVIRA Algorithm, the Simulated Annealing Implementation in VOXELPLAN, and KONRAD before the date(s) specified in Document Request Nos. i, viii, and xv.

v. The date and circumstances of the first sale, offer for sale, and/or public use in the United States of any apparatus, system, or device covered by Deposition Topic No. iv.

vi. The authenticity of documents produced in response to this Letter of Request, the public availability and publication dates of documents produced in response to this Letter of Request, the creation and authorship of documents produced in response to this Letter of Request, and whether and how the documents produced in response to this Letter of Request were created and/or stored in the ordinary course of business.

11. Any requirement that the evidence be given on oath or affirmation and any special form to be used (Article 3, *h*):

Because the testifying witnesses are outside this Court's subpoena power and cannot be compelled to attend trial, the Court requests that the witnesses' testimony be taken under oath in such manner as provided by the laws of Germany for the formal taking of evidence.

12. Special methods or procedure to be followed (Articles 3, *i* and 9):

The Court requests that the testimony be taken by oral examination in such manner as provided by the laws of Germany for the formal taking of evidence. To the extent permitted by the laws of Germany, the Court requests that the testimony be recorded by a videographer and transcribed by a stenographer.

13. Request for notification of the time and place for the execution of the Request and identity and address of any person to be notified (Article 7):

Please notify defendants' U.S. legal counsel at the following address:

Ryan K. Wong
KEKER, VAN NEST & PETERS LLP
633 Battery Street
San Francisco, CA 94111
USA

14. Specification of privilege or duty to refuse to give evidence under the law of the State of origin (Article 11, *b*):

Nothing in this Letter of Request is intended to interfere with any rights of DFKZ to assert privilege or refuse to give evidence under any applicable law of Germany or the United States of America.

15. Fees and costs

If the Präsident des Amtsgerichts Freiburg incurs fees or costs in executing this Letter of Request that are reimbursable under the second paragraph of Article 14 or Article 26 of the

Hague Evidence Convention, the Court requests that the Präsident des Amtsgerichts Freiburg submit a bill of fees and costs to the Court and defendants' U.S. legal counsel:

Ryan K. Wong
KEKER, VAN NEST & PETERS LLP
633 Battery Street
San Francisco, CA 94111
USA

The Court guarantees that defendants' counsel will reimburse the Präsident des Amtsgerichts Freiburg for all reimbursable fees and costs incurred in executing this Letter of Request.

This Court expresses its gratitude to the authorities of Germany for assisting with this Letter of Request, and will provide similar assistance to the judicial authorities of Germany when requested.

DATE OF REQUEST: _____

SIGNATURE AND SEAL OF THE REQUESTING AUTHORITY

_____
The Honorable Maryellen Noreika
United States District Judge

ATTACHMENT A-1

VOL. 35, NO. 3 JUNE 1995 ISSN 0167-8140
RAONDT (35) 177–274 (1995)

RADIOTHERAPY & ONCOLOGY

Journal of the European Society for Therapeutic Radiology and Oncology

ELSEVIER

Radiotherapy and Oncology, 1995, Volume 35, Number 3, June, pp. 177–274

CONTENTS

Cited in: Chemical Abstracts, Excerpta Medica (EMBASE), Current Contents (Clinical Medicine; Life Sciences), Index Medicus (MEDLINE), Current Awareness in Biological Sciences (CABS)

Original Papers

Epidermoid carcinomas of the floor of mouth treated by exclusive irradiation: statistical study of a series of 207 cases
M. Pernot, S. Hoffstetter, D. Peiffert, E. Luporsi, C. Marchal, P. Kozminski, D. Dartois, P. Bey (France) 177

Indications, techniques and results of postoperative brachytherapy in cancer of the oral cavity
M. Pernot, P. Aletti, J.M. Carolus, I. Marquis, S. Hoffstetter, F. Maaloul, D. Peiffert, M. Lapeyre, E. Luporsi, C. Marchal, A. Noël, P. Bey (France) 186

Low dose rate versus high dose rate intraluminal brachytherapy for malignant endobronchial tumors
T.C.M. Lo, L. Girshovich, G.A. Healey, J.F. Beamis, Jr., D.C. Webb-Johnson, A.G. Villanueva, A.W. Gray, Jr., T.R. Wu (USA) 193

Postoperative radiotherapy in carcinoma of the cervix: treatment results and prognostic factors
G. Atkovar, Ö. Uzel, M. Özşahin, S. Koca, İ. Şahinler, S. Okkan, R. Uzel (Turkey) 198

Radiation treatment of cervical lymph node metastases from an unknown primary: an analysis of outcome by treatment volume and other prognostic factors
L. Weir, T. Keane, B. Cummings, P. Goodman, B. O'Sullivan, D. Payne, P. Warde (Canada) 206

Intrarectal formalin application, an effective treatment for grade III haemorrhagic radiation proctitis
B.M. Biswal, P. Lal, G.K. Rath, N.K. Shukla, B.K. Mohanti, S. Deo (India) 212

Toxicity, biodistribution and radioprotective capacity of L-homocysteine thiolactone in CNS tissues and tumors in rodents: comparison with prior results with phosphorothioates
A.M. Spence, J.S. Rasey, L. Dwyer-Hansen, Z. Grunbaum, J. Livesey, L. Chin, N. Nelson, D. Stein, K.A. Krohn, F. Ali-Osman (USA) 216

A mathematical model of the volume effect which postulates cell migration from unirradiated tissues
H. Shirato, M. Mizuta, K. Miyasaka (Japan) 227

Clinical implementation of an objective computer-aided protocol for intervention in intra-treatment correction using electronic portal imaging
F. Van den Heuvel, W. De Neve, D. Verellen, M. Coghe, V. Coen, G. Storme (Belgium) 232

A diagnostic-quality electronic portal imaging system
R. Sephton, J. Hagekyriakou (Australia) 240

A comparison of conventional 'forward planning' with inverse planning for 3D conformal radiotherapy of the prostate
M. Oldham, A. Neal, S. Webb (UK) 248

ESTRO Meetings 263
ESTRO Courses 264
Calendar of Events 265

Volume contents 268
Author index 271
Subject index 273

0167-8140(199506)35:3;1-7

ELSEVIER

Radiotherapy and Oncology 35 (1995) 248–262

RADIOTHERAPY & ONCOLOGY

A comparison of conventional 'forward planning' with inverse planning for 3D conformal radiotherapy of the prostate

Mark Oldham*, Anthony Neal, Steve Webb

Joint Department of Physics, Institute of Cancer Research and the Royal Marsden Hospital, Downs Road, Sutton, Surrey, SM2 5PT, UK

Received 6 October 1994; revision received 20 March 1995; accepted 27 March 1995

Abstract

A radiotherapy treatment plan optimisation algorithm has been applied to 48 prostate plans and the results compared with those of an experienced human planner. Twelve patients were used in the study, and 3-, 4-, 6- and 8-field plans (with standard coplanar beam angles for each plan type) were optimised by both the human planner and the optimisation algorithm. The human planner 'optimised' the plan by conventional forward planning techniques. The optimisation algorithm was based on fast simulated annealing using a cost-function designed to achieve a homogenous dose in the 'planning-target-volume' and to minimise the integral dose to the organs at risk. 'Importance factors' assigned to different regions of the patient provide a method for controlling the algorithm, and it was found that the same values gave good results for almost all plans. A study of the convergence of the algorithm is presented and optimal convergence parameters are determined. The plans were compared on the basis of *both* dose statistics and 'normal-tissue-complication-probability' (NTCP) and 'tumour-control-probability' (TCP). The results of the comparison study show that the optimisation algorithm yielded results that were at least as good as the human planner for all plan types, and on the whole slightly better. A study of the beam-weights chosen by the optimisation algorithm and the planner revealed differences that increased with the number of beams in the plan. The planner was found to make small perturbations about a conceived optimal beam-weight set. The optimisation algorithm showed much greater variation, in response to individual patient geometry, frequently deselecting certain beams altogether from the plan. The algorithm is shown to be a useful tool for radiotherapy treatment planning. For simple (e.g., three-field) plans it was found to consistently achieve slightly higher TCP and lower NTCP values. For more complicated (e.g., eight-field) plans the optimisation also achieved slightly better results with generally less numbers of beams, unfavourable beams being deselected from the plan. Probably the greatest benefit is the reduced time taken by the optimisation to compute optimised beam-weights. This time was always ≤ 5 min; a factor of up to 20-times faster than the human planner.

Keywords: Conformal therapy; Treatment planning; Optimisation; Biological modelling; Simulated annealing

1. Introduction

The aim of conformal radiotherapy is to achieve tumour control with as low normal tissue morbidity as possible. In terms of radiation-dose, and making the assumption of uniform clonogenic cell density within the PTV, this goal translates to achieving a high uniform dose throughout the planning target volume (PTV) and as low a dose as possible elsewhere, specifically in organs at risk (OAR). With the advent of computer controlled multileaf collimators attached to computer controlled linacs, conformal radiotherapy is entering a new era with the possibility of significant improvement in treatment delivery. It is now becoming feasible to deliver plans with large numbers of beams, each shaped to the beam's eye view of the PTV, in reasonable times under computer control [8].

The technical ability to implement more complicated plans presents a new challenge to the treatment planner who traditionally has used 'forward planning' (manual trial-and-error based on informed experience) to calculate the best field arrangements and beam-weights. Whilst forward planning is acceptable for plans with only a few fields, the process becomes impossibly

* Corresponding author.

0167-8140/95/$09.50
SSDI 0167-8140(95)01556-V

tedious for plans with larger numbers of fields [23]. Much effort has been devoted recently to the challenge of designing algorithms to compute optimised beam-weights for such complicated plans [2,4,6,7,9,10, 13–22,24,27–30].

To date, the majority of these new algorithms and planning techniques have illustrated their potential with the application to just one or two sample cases. Our own developments have been no exception [20,21,27–30]. This paper presents a detailed study comparing the performance of an inverse optimisation algorithm with conventional planning techniques over a wide range of patient cases. The aim of the study was to investigate the effectiveness, reliability, and time saving potential of an optimisation algorithm which has been under development at the Royal Marsden Hospital over the past 4 years. The algorithm is inverse in the sense that a dose prescription is specified a priori, and an algorithm used to work backwards to find the dose distribution (and corresponding beam-weights) that match as closely as possible the prescription. Details of the algorithm (COVIRAOPT) have already been published [20] and it remains the same except for some minor modifications which are discussed in the text. COVIRAOPT has been developed under the European COVIRA programme (see Acknowledgements).

The optimisation algorithm we have developed currently only has the facility to optimise beam-weights and wedge angles. Ideally it would also optimise the orientation and energy of the beams, and even the number of beams in the plan. These last facilities are the subject of current research but are not simple problems to solve. In this paper we have used the algorithm solely to optimise the beam-weights of plans that have been pre-defined by a human planner. The planner used standard beam arrangements on which to base his plans but was free to individually customise the wedge angle and the beam orientation for each patient as required. This procedure is the same as that used in the clinic. The inclusion of wedge angle optimisation will be the subject of later work. This paper is primarily concerned with evaluating the likely benefits associated with optimising the beam-weights of predefined, standard plans.

2. Method

2.1. The optimisation algorithm

To optimise the beam-weights of an arbitrary treatment plan, a numerical method is employed to find the set of beam-weights that corresponds to the minimum of a cost function. The cost function is a measure of fit between a dose distribution and some ideal, user-specified, dose distribution. In this paper the numerical method used is fast simulated annealing (FSA) with zero temperature [25,13] and the cost function is based on attaining a uniformly homogenous dose in the planning target volume (PTV) and minimising the integral doses to the organs at risk (OAR). Full details of both the numerical method and the cost function are given in [20], and here only a brief overview is included highlighting some modifications that have been made.

2.1.1. Fast simulated annealing with zero temperature

The numerical method used to find the cost-function minimum was fast simulated annealing. In this iterative method, at each iteration all beam-weights are independently perturbed by adding a 'grain' of beam-weight which is selected randomly from a Cauchy distribution. (The grains are randomly positive or negative and hence individual beam-weights can independently increase or decrease, the only restriction being that the beam-weight must remain zero or positive.) A cost function is evaluated for the current beam-weight set and compared to the running cost-function value (i.e., the lowest cost-function value found from previous iterations). If the new cost function is lower than the running value, then the running value is set equal to the new value and the new beam-weight set is stored. If the new cost-function value is greater than the running value then no change is made to the running value and the algorithm moves to the next iteration.

In this manner the algorithm finds beam-weight sets that successively converge to that set which corresponds to the minimum of the cost function. There are two differences between the method outlined above and that of our previous paper [20]. The first is that all beam-weights are now perturbed at each iteration (or cost-function evaluation) instead of just one beam-weight per iteration. This change was made in accordance with the approach of [13] and allows for more efficient convergence. The second change is that no beam-weight sets that make the cost function greater are ever accepted. This is equivalent to setting the temperature to zero in FSA, thereby disallowing all up-hill changes. For the linear-quadratic cost function used in this paper (Section 2.1.2), there is only a single minimum, and therefore the acceptance of up-hill changes to escape from local minima is not required. This approach applied to a biological cost function has previously been investigated [13] and it was found that even if local minima are present there is no need to accept up-hill changes with FSA because of an alternative 'tunnelling' mechanism. Tunnelling arises because of the broad wings of the Cauchy distribution which allow occasional large grains to be selected.

In this scenario (FSA with zero temperature) the efficiency of the optimisation depends only on the Cauchy probability distribution from which the grains of beam-weight are selected. This distribution gradually collapses as the iterations increase so as to more finely probe the cost-function structure near the minimum. The collapse

of the distribution is controlled by the parameter $W(n)$, the full-width at half-maximum of the distribution, which varies according to Eq. 1 [20].

$$W(n) = \frac{W(0)}{(1 + n/R)} \quad (1)$$

In Eq. 1, $W(0)$ is the full-width at half-maximum at the start of the optimisation, n is the iteration number and R is a constant that controls the speed with which the distribution collapses. Appropriate values of R to produce efficient convergence are determined in Section 2.3.1.

2.1.2. Cost-function structure

The minimum of the cost function defines the theoretical ideal dose distribution (and beam-weight set) which the optimisation algorithm attempts to achieve. It is therefore critical that the cost function should reflect what is clinically desired in each different region of the patient. In accord with our previous paper [20], the cost function was segmented into component terms from each of the regions PTV, OAR and BODY (i.e., all tissue that is not in the PTV or in an OAR). The following mathematical formulae were used, reflecting the desired clinical dose to each region.

$$C_{PTV} = \Sigma_{i \text{ in PTV}} (D_i - 100)^2 \quad (2)$$

$$C_{OAR} = \Sigma_{i \text{ in OAR}} (D_i) \quad (3)$$

$$C_{BODY} = \Sigma_{i \text{ in BODY}} (D_i) \quad (4)$$

where D_i is the dose to the ith cubic voxel of each segmented region. The figure 100 appearing in Eq. 2 represents the desired 100% uniform dose to the PTV. The quadratic cost function is used in Eq. 2, as opposed to the modulus for example, because it is inherently better at controlling the dose in extreme regions (either very hot or cold).

A useful feature of the linear OAR and BODY cost function terms is that the voxel summation need only be done once, for each beam, at the start of the optimisation. All future changes in the C_{OAR} and C_{BODY} terms due to the addition of a grain of beam-weight can simply be calculated by multiplying the 'global' contribution of that beam, for unit weight, by the grain size. This shortcut leads to a reduction of about a factor 30 in the computation time necessary to evaluate the cost function. For plans with ≥ 4 beams, almost all the computer time taken to optimise the plan comes from evaluating the cost function over many iterations and therefore this is a significant time saving.

The component terms (2)–(4) were merged linearly to form the total cost function (Eq. 5). Each term was weighted by an 'importance factor' to define its relative importance at the start of the optimisation. In Eq. (5), n is the iteration number, the subscript ST denotes the starting value of the term (i.e., at $n = 1$), and m is the number of OARs. (Note, the value of the WEIGHT_{OAR} factor can be arbitrarily set for each OAR.)

$$C_{TOTAL}(n) = \text{WEIGHT}_{PTV} \times C_{PTV}(n)/C_{PTVST}(1) + \sum_{j=1}^{m} (\text{WEIGHT}_{OAR_j} \times C_{OAR_j}(n)/C_{OARST_j}(1)) + \text{WEIGHT}_{BODY} \times C_{BODY}(n)/C_{BODYST}(1) \quad (5)$$

Minimising the cost function C_{TOTAL} thus corresponds to minimising the integral dose in the OAR and BODY regions, while attempting to achieve a uniform dose of 100% in the PTV. Although of simple design, without the sophistication to model complicated volume effects, the cost function is designed to be effective at differentially reducing the dose received by segmented regions. The algorithm and cost function should therefore be effective for tumours at locations other than the prostate via judicious choice of importance factors.

2.2. The patient data set

The 12 patients in the study were all diagnosed with early prostate cancer (either stage T1 or T2), and underwent a pelvic CT scan as part of their routine treatment planning. The CT data sets consisted of 5-mm contiguous axial images, acquired when the patient had a full bladder. The only difference with standard CT imaging protocol was that the number of CT slices per patient was extended so that the complete bladder was contained in the 3D data set. This was done for the purposes of calculating meaningful dose-volume histograms (DVH) and normal tissue-complication probabilities (NTCP) for the bladder. For each patient, the PTV was segmented in 3D by first outlining the gross tumour volume (macroscopic disease spread), then adding a margin of 5 mm to create the clinical target volume (including microscopic tumour spread), and finally adding a further 5 mm to create the PTV (this extra margin accounting for random and systematic treatment delivery and set-up errors). The rectum, bladder, and left and right femoral heads were also segmented in 3D. In most patients there was a small region which was classified as both PTV and rectum. In the optimisation algorithm, this overlap region was considered as being PTV only. The consequences of this overlap region have been explored in [20].

2.2.1. Conventional 'forward' treatment planning

For each patient, four plans were created by a human planner (A.J. Neal) using the fully 3D VIRTUOS (VIRTUal radiOtherapy Simulator) treatment planning system [1]. The plans consisted of a 3-, 4-, 6- and an 8-field plan (Fig. 1a–d). Beam configurations were adhered to whenever possible but gantry angles and

ANTERIOR

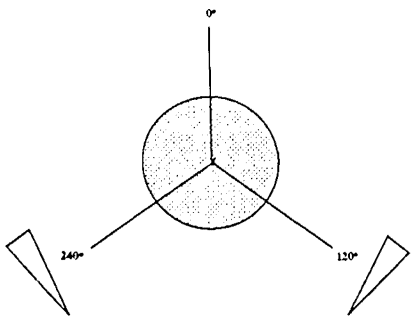

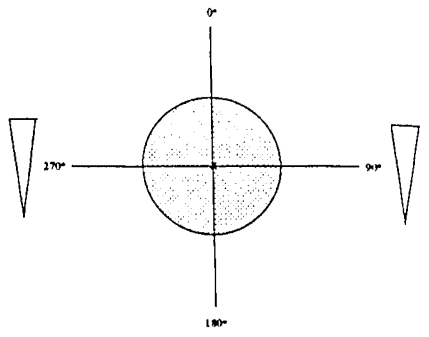

POSTERIOR

Fig 1a

Fig 1b

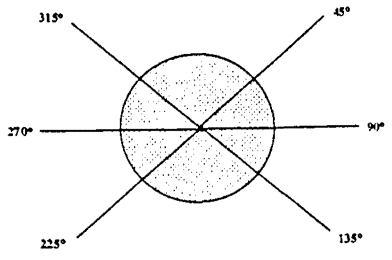

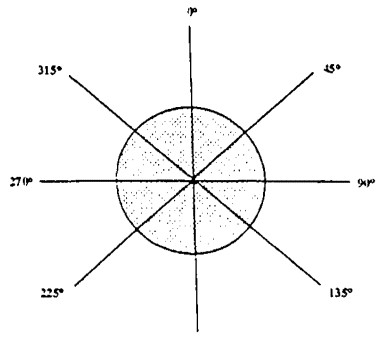

Fig 1c

Fig 1d

Fig. 1. (a) the 3-field arrangement of an anterior field and two posterior wedged oblique fields; (b) the 4-field arrangement of opposed anterior/posterior and right lateral/left lateral wedged fields; (c) the 6-field arrangement of opposed left anterior oblique/right posterior oblique fields, opposed right anterior oblique/left posterior oblique fields and opposed right lateral/left lateral fields; and (d) the 8-field arrangement as 6-field arrangement but with the addition of opposed anterior and posterior fields.

wedge compensators were adjusted individually to optimise the plan for that particular patient's anatomy. In all cases where the plan was adjusted, it was the adjusted plan that was also optimised by the algorithm. All fields were coplanar and shaped to the beam's eye view of the PTV. A margin of 6 mm around the PTV was added to allow for beam penumbra. This study was retrospective in that all the patients had been previously treated with 3-field wedged plans. The delivery plans were not necessarily exactly the same as the 3-field plans reproduced here because they were created using a different planning system, by a different planner.

Beam weights were iteratively adjusted, in the conventional forward planning manner, from an initial 'best guess' to give a satisfactory dose distribution. The acceptability of the plan was determined from isodoses overlaid upon the CT data in transverse, sagittal and coronal views. Priority was given to treating the PTV to a homogeneous dose, using the isocentre as a reference point. A PTV dose homogeneity of ±5% was aimed for. Once attained, consideration was given to reducing irradiation of the adjacent OARs. In practice, the bladder and rectum were considered to be the OARs which determined the acceptance or rejection of a particular plan. The femoral heads were considered in the comparison of plans but was not a major factor in the human optimisation of individual plans.

The dose calculation algorithm was of the Bentley-

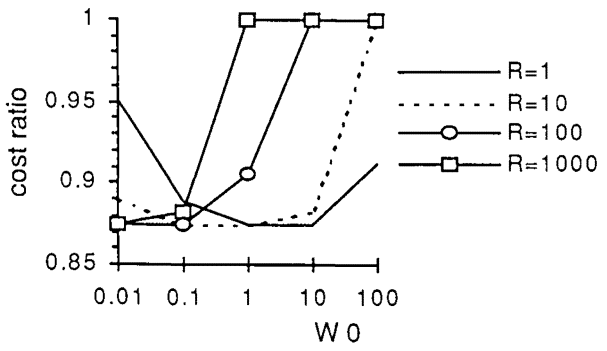

Fig. 2. Plot of the dependence of the cost ratio (the ratio of the final cost-function value to the starting cost-function value) on the annealing parameters $W(0)$ (the starting full-width–half-maximum of the Cauchy distribution), and R which is a constant that controls the speed of collapse of the distribution (Eq. 1).

Milan ray-tracing type which took into account tissue inhomogeneity for the primary beam, and equivalent field-size scatter effects. The effects of tissue inhomogeneity on the scatter was not modelled. The beam data used was that of 15-MV photons from a Siemens Mevatron 77 linear accelerator.

2.3. Optimised treatment planning

Before the optimisation algorithm was applied to the patient data set, suitable optimisation parameters needed to be found. These parameters fall into two categories; annealing parameters, and importance factors. The annealing parameters, $W(0)$ and R in Eq. 1, control the convergence of the optimisation and, if badly set, the algorithm may converge to a value that is not the minimum of the cost function in the allowed space, or converge ineffectively. The importance factors, $\text{WEIGHT}_{\text{PTV}}$, $\text{WEIGHT}_{\text{OAR}_i}$, and $\text{WEIGHT}_{\text{BODY}}$ (Eq. 5) determine the minimum of the cost function and thus the final beam-weights.

2.3.1. Finding suitable annealing parameters

A series of optimisation runs on the 3-field plan of an arbitrary patient were performed where the parameters $W(0)$ and R were varied over several orders of magnitude. These runs represented a coarse sampling to estimate $W(0)$, R combinations that produced fast convergence. Each run was allowed to progress for a 1000

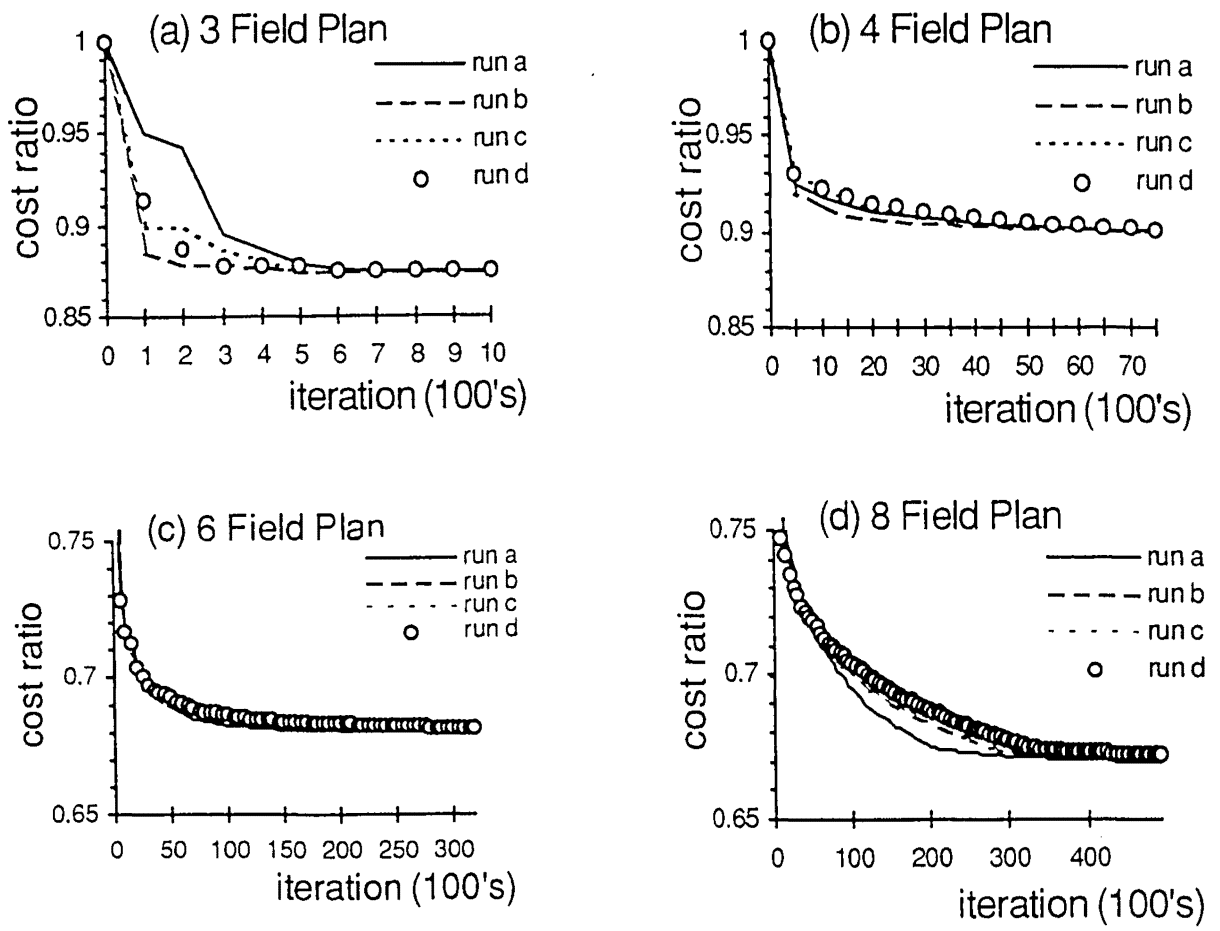

Fig. 3. Plots of the cost ratio (the ratio of the final cost-function value to the starting cost-function value), vs. iteration number, for four $W(0)$, R combinations. Runs a, b, c and d correspond to $W(0)$,R combinations of 0.01,1000; 0.05,100; 0.5,10; 5.0,1.

iterations and the efficiency of convergence was then quantified by evaluating the 'cost ratio', i.e., the ratio of the final cost function to the starting cost function. The plot of the value of the cost ratio after a 1000 iterations for different $W(0)$, R combinations is shown in Fig. 2. The cost function minimum in allowed space corresponds to the smallest value of the cost ratio which, for the 3-field plan of this patient is about 0.875. For some runs (i.e., $W(0)$, R combinations) it is clear that the algorithm has not found the minimum, indicating false convergence.

Four ($W(0)$, R) combinations were selected from Fig. 2 that all produced convergence to the minimum within the 1000 iterations. These four combinations (which were $W(0) = 0.01$, $R = 1000$ (run a); $W(0) = 0.05$, $R = 100$ (run b); $W(0) = 0.5$, $R = 10$ (run c); and $W(0) = 5.0$, $R = 1$ (run d)) were then studied further by plotting the cost ratio against iteration number for all four plan types (Fig. 3a–d). The aim was to find a parameter set that guaranteed fast convergence for all plan types. Fig. 3a–c shows that for the 3-, 4- and 6-field plans, despite initial differences in the rate of convergence, all four runs arrived at the minimum in roughly the same number of iterations. This indicates that for these few-beam plans, rapid collapse of the Cauchy distribution from an initially large $W(0)$ is equivalent to slow collapse from an initially small $W(0)$. In Fig. 3d a trend is seen that we have observed in all plans with more than eight fields, that of the fastest convergence being achieved by the runs with the slower collapse schedules (and correspondingly smaller $W(0)$ value). Fig. 3a–d indicates that all runs truly converged (given enough time) and therefore the algorithm is robust concerning the exact settings of the annealing parameters in this range.

Although the results shown here are for a single patient (this patient actually needed more iterations to converge than any others studied), a similar series of runs was also performed on the physically largest and smallest prostate patients, respectively. These runs confirmed the trends found in Fig. 3a–d, although there were slight inter-patient variations ($\leq 10\%$) in the number of iterations needed to reach the minimum. On the basis of Fig. 3a–d, the parameter values of run a ($W(0) = 0.01$, $R = 1000$) were selected as producing true convergence for all patients, for all plan types, in close to the minimum number of iterations possible. The final beam-weights produced by the optimisation algorithm thus correspond to the minimum of the cost function in allowed space and are independent of small variations in the parameter settings.

2.3.2. Finding suitable importance factors

In this paper we are interested in evaluating the performance of a practical and usable optimisation algorithm. The practicality of the algorithm would be severely reduced if it was necessary to individually adjust the importance factors (Eq. 5) for each patient and each plan type. The difficulty here is that in reality each patient may have a slightly different importance factor set that is 'optimal', depending on inter-patient variables like patient size, organ positioning, target size, etc. Furthermore the optimal set might be expected to vary between plan types with very different geometries (the 3- and 8-field plans for example). This section details work undertaken to identify a 'practical' importance factor set; practical in the sense of consistently giving good dose distributions over the 48 plans. (In the rest of the paper this importance factor set is referred to as the 'practical' set, and was used for all patients.)

An exhaustive study comparing the resulting dose distributions arising from all possible sets of importance factors, each set evaluated over 48 plans, is clearly not feasible. Instead, informed importance factor set 'guesses' were made and these then evaluated on the physically largest and smallest patients, hopefully ensuring the set would yield good results over as wide a range of patient geometry as possible. In practice it was found surprisingly easy to find a practical set that gave good dose distributions for both patients, for all four plan types. This set was arrived at after three 'guesses' shown in Table 1. (The first guess was loosely based on the perceived clinical importance of structures. Although the contour region obviously does not have zero importance, it was set to zero in order to give the algorithm a high degree of freedom. In subsequent tests we did not find it necessary to increase this value. The second and third guesses were refinements of the first guess, attempting to get a better dose distribution. All subsequent refinements after the third guess showed no benefit.)

Table 1
Three 'guesses' were necessary to identify a practical importance factor set that gave good results for all patients and all plan types in the patient data set

Guess	PTV	Rectum	Bladder	Femorals	Contour
1	2	20	5	1	0
2	10	10	5	1	0
3 (practical set)	18	20	5	1	0

The numbers refer to the importance factors guessed for that region of the patient.

Table 2
NTCP and TCP values for three importance factor set guesses for an arbitrary patient

Guess	B-NTCP	R-NTCP	LFH-NTCP	TCP	RFH-NTCP
1 (64 Gy)	<0.1	3.6	<0.1	86.1	<0.1
2 (64 Gy)	<0.1	3.4	<0.1	86.0	<0.1
3 (64 Gy)	<0.1	3.4	<0.1	86.0	<0.1
1	<0.1	5.0	<0.1	87.2	<0.1
2	<0.1	5.0	<0.1	87.4	<0.1
3	<0.1	5.0	<0.1	87.4	<0.1

The column heading notation (B-, R-, LFH- and RFH-) corresponds to the bladder, rectum, and left and right femoral heads, respectively. The first three rows correspond to when a dose of 64 Gy is prescribed to the isocentre. In the last three rows, the prescribed dose was scaled until a rectal NTCP of 5% was obtained.

The dose distribution corresponding to each guess was analysed primarily on the basis of TCP and NTCP values and also careful study of the DVH. (The calculation of TCP and NTCP is discussed in Section 2.4.). The greater reliance on NTCP and TCP numbers simply reflects the great time saving incurred over studying DVHs for a large patient data set. The NTCP and TCP values for the three guesses as applied to the largest patient are given in Table 2. Although the values are the same for guesses 2 and 3, and in all patients studied these two guesses gave very similar results, the latter was judged to be marginally superior on investigation of the DVH. The NTCP and TCP values of guess 1 are similar to those of guesses 2 and 3 because, even with a relatively low importance factor, the quadratic nature of the cost function in the PTV ensures a quite uniform dose. Further investigations into modifications of the practical importance factor set showed no improvement in the NTCP or TCP values for any of the plan types of the two patients selected for this evaluation. It was thus assumed that this set could be applied to all the patients in the data set.

2.4. Normal tissue-complication probability (NTCP) and tumour-control probability (TCP) computation

NTCP values were calculated using the Lyman model [12] combined with the DVH reduction scheme of Kutcher and Burman [11] and the biological parameters given in Burman et al. [5] (full details can be found in Oldham and Webb [20]). TCP was computed using the model of Webb and Nahum [31] (Eq. 6), with the values $\alpha = 0.547$, $\sigma_\alpha = 0.19$, clonogenic cell density = 10^7 per cm^3, and the number of patients averaged over to account for inter-patient variation in radio-sensitivity was 40 000 (guaranteeing a precision of $\leq 0.1\%$). It is stressed that these biological models are at an early stage of development. In the absence of good quality data, the parameters used in the model have been derived from a mixture of very sparse data and clinician's estimates [5]. The errors in absolute values of NTCP may be quite large. However, the models embody the general principles that are believed to approximate the response of organs to radiation. In this respect we have relied upon the models to rank dose distributions according to clinical benefit. The uncertainties in model parameters, we believe, will not affect the central conclusions of this paper which are based on comparative 'average rankings'.

$$\mathrm{TCP_{TOT}} = \frac{1}{K} \sum_{n=1}^{k} \left(\Pi_{i \text{ in PTV}} \, e^{-N_i e^{-\alpha_n D_i}} \right) \tag{6}$$

In Eq. 6, i is an index looping over voxels in the PTV, D_i and N_i are the dose and number of clonogenic cells of the ith voxel, respectively, and K is a number of the order 10^4 which represents averaging over a patient population. A discussion of the fitting of Eq. 6 to clinical data, and its use in predicting TCP is given in [20].

3. Results

Each of the four plan types for all patients were optimised according to the algorithm outlined above with the importance factors set to the practical set of Table 1 and with the appropriate annealing parameters R and $W(0)$ (Section 2.3.1). The optimised dose distributions were then compared with those obtained by the human planner on the basis of dose statistics in the PTV, dose-volume histograms for the OARs, and NTCP and TCP calculations. To determine any consistent, significant difference between the results obtained from the optimisation algorithm and those of the human planner, the mean of the individual patient differences, the 95% confidence interval of this mean, and a two-tailed paired Student's t-test were computed. The 95% confidence interval describes the magnitude of any effect and the t-test quantifies the statistical significance of the mean difference. For each plan the mean dose in the PTV (D), and standard deviation (σ_D) of the dose in the PTV about this mean was computed. σ_D represents the uniformity of dose in the PTV. The average standard deviation ($\bar{\sigma}_D$) over the 12 patients was computed as

Table 3
Comparison of the dose homogeneity in the PTV achieved by the human planner and the optimisation algorithm

	Average S.D. $\overline{\sigma_D}$	Average S.D. $\sigma_{\overline{\sigma D}}$	Mean Diff $\overline{\delta}$	95% C.I. for Mean diff.	P value of Mean diff.
3-F Human	0.012	(0.001)			
3-F Optimised	0.011	(0.002)	−0.002	−0.002 to −0.001	0.004
4-F Human	0.015	(0.005)			
4-F Optimised	0.011	(0.003)	−0.004	−0.006 to −0.001	0.022
6-F Human	0.014	(0.007)			
6-F Optimised	0.010	(0.004)	−0.004	−0.006 to −0.002	0.002
8-F Human	0.012	(0.003)			
8-F Optimised	0.008	(0.003)	−0.004	−0.005 to −0.003	>0.001

The first column 'Average S.D.' is the average of the standard deviations in the PTV over the 12-patient sample. The 'Mean diff.' column is the average of the individual patient differences of the S.D. in the PTV achieved by the optimisation and the human planner. The P value was computed from a two-tailed paired Student's t-test. C.I. is the confidence interval.

well as the standard deviation of this average ($\sigma_{\overline{\sigma}D}$), the latter representing the variability over the sample. Next, the mean difference ($\overline{\delta}$) in the PTV dose homogeneity achieved by the optimisation and the human planner was computed (i.e., $\overline{\delta} = \overline{\sigma_{D,\text{opt}} - \sigma_{D,\text{human}}}$). The more negative this quantity is, the better the optimisation is in terms of uniformity of dose in the PTV.

The quantities $\overline{\sigma_D}$, $\sigma_{\overline{\sigma D}}$ and $\overline{\delta}$ for each plan type are shown in Table 3, and the individual δ values for each patient and each plan type are given in Fig. 4. (In order to make the standard deviations of the dose in the PTV for different plans directly comparable, dose distributions were scaled so that the mean in the PTV was the same for all plans: an arbitrary value of unity was selected. In Table 3 it is shown that $0.008 \leq \overline{\sigma_D} \leq 0.015$ for the different plan types (i.e., the average standard deviation of dose in the PTV ranges between 0.8 and 1.5%.) DVH comparisons were made by noting down the percentage volume of the OAR in each of the four dose bins <20, 20–50, 50–80 and >80%, and

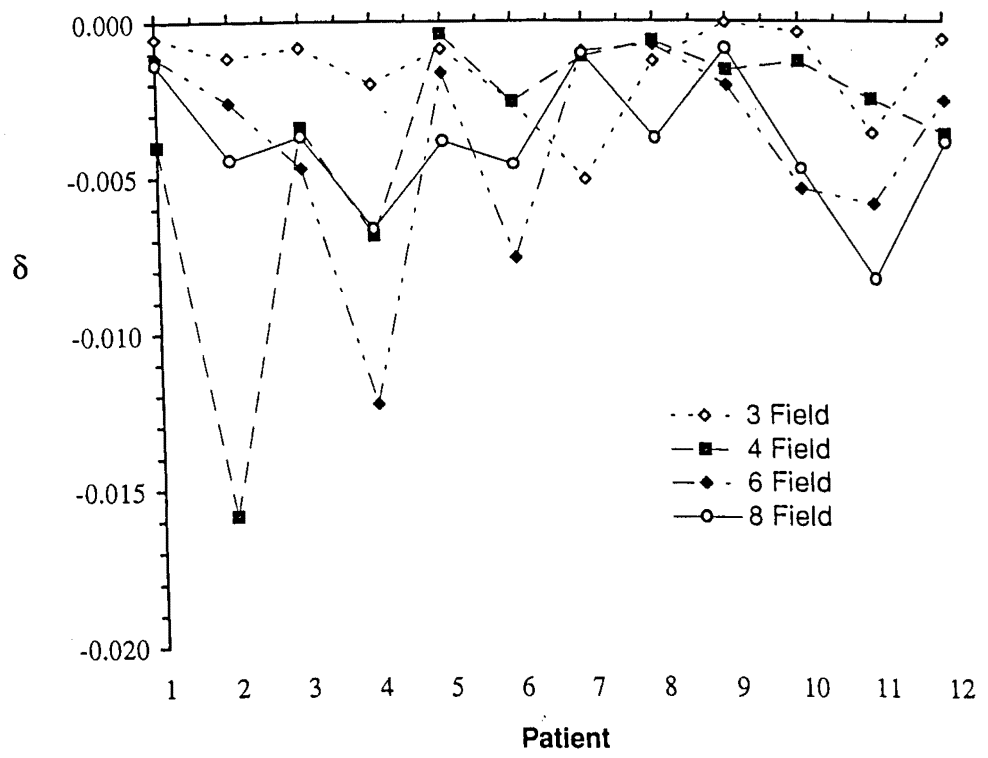

Fig. 4. Graph showing the δ values (i.e., the difference in the standard deviation of the dose in the PTV achieved by the optimisation algorithm and the human planner) for all 12 patients, and for each plan type.

averaging over the 12 patients (Fig. 5a–p). For all plans the DVHs were normalised to the dose at the isocentre. In Fig. 5a–p, the one standard deviation limit of the 12 patient sample is indicated by the upper and lower curves. In Tables 4 and 5, average TCP and NTCP values are shown after the dose to the isocentre was scaled to give a rectal NTCP of 5%. The average beam-weights selected by the human planner are compared to those computed by the optimisation algorithm in Fig. 6, and the average planning times (i.e., the time taken to determine optimal beam-weights once the beam orientations and field shape have been defined and implemented) are compared in Table 6. The optimisation times are real-times, recorded on an IBM RS6000 530H mainframe under conditions of light usage by other users.

4. Discussion

Both Fig. 4 and the '$\overline{\sigma_D}$' column of Table 3 show that the optimisation algorithm has achieved a more homogenous PTV dose for all plan types. The standard deviation of the average ('$\sigma_{\overline{\sigma D}}$' column in Table 3) are similar for the 3-, 4- and 8-field plan types, indicating a similar level of inter-patient consistency. For the 6-field plans there is greater inter-patient consistency in the optimised plans. A more revealing analysis comes from studying the mean of the individual differences (optimised — human) given in the '$\overline{\delta}$' column. A statistically significant effect was observed for all plan types, particularly for 3-, 6- and 8-field plans. The magnitude of the improvement, as indicated by the 95% confidence interval, is greatest for the 8-field plans and least for the 3-field plans (as expected, because the optimisation algorithm has more degrees of freedom in the 8-field plan). However, there is no obvious trend towards greater improvement with larger numbers of beams. In studying the individual results of the human planner it was observed that occasionally a plan was accepted that, although acceptable, was noticeably sub-optimal with regards to PTV dose homogeneity. The optimisation algorithm provides an effective method of reducing these anomalies. The increased dose inhomogeneity in the planner's plans was found to be largely due to patient-specific tumour shapes (odd bulges, etc.) rather than to any systematic under or overdosing.

The dose distributions in the OARs are summarised in Fig. 5a–p. By and large, the distribution of dose between the four bins (<20, 20–50, 50–80 and >80%), for the bladder and rectum, are similar for the human planner and the optimisation, for all plan types. The optimisation does, however, produce about 1–2% more rectal volume in the >80% bin for the 3-, 4- and 8-field plans, and 1–2% less for the 6-field plans. For the left and right femoral heads there is a significant difference in distribution of dose for the 4-, 6- and 8-field plans. In the 4-field plans, the optimisation produces a higher volume in the 20–50% bin, and a lower volume in the 50–80% bin. This trend is reversed for the 6-field plans, and in the 8-field plans the optimisation produces less volume in both bins. The precise cause of these trends is difficult to ascertain but an important feature is certainly that in trying to achieve a homogenous PTV dose the optimisation consistently favours beam orientations differently from the human planner.

The salient point from the PTV homogeneity data of Table 3 and the OAR DVH data of Fig. 5, is that compared with the human planner the optimisation algorithm achieves a more homogenous PTV dose by slight re-distribution of dose in the bladder and rectum, and significant re-distribution in the femoral heads. Of particular importance to NTCP is the amount of OAR volume in the >80% dose bin. From Fig. 5 we expect that the optimisation has slightly worsened the rectal dose for the 3-, 4- and 8-field plans, and slightly improved it for the 6-field plans. The femoral head dose also appears worse for the 3-, 4- and 6-field plans, but better for the 8-field plans. The TCP and NTCP values in Table 4 can be used to assess the relative merit of a more homogenous PTV dose against the worsening of the rectal and femoral heads dose. By scaling the dose so that the rectal NTCP is 5% for all plans, the best plans can be judged as those having the highest TCP, providing that the NTCP of other organs are acceptable.

From Table 4, the optimisation has achieved a slightly higher average TCP for all plan types than the human planner. The internal consistency (indicated by the S.D. column) is similar for the 3-, 4- and 8-field plans, and better for the 6-field plans. Surprisingly, the optimisation does not appear to attain relatively better results for the more complicated 6- and 8-field plans. In fact the opposite is observed where the largest benefit is obtained for the 3-field plans. In the 4-field plans, the optimisation achieved a significantly worse NTCP in both femoral heads (first row). Analysis of the NTCP values for both right and left femoral heads revealed that they were less than 5% for all except three patients who had extremely high values (up to 20%). It was obvious that the practical parameter set was inappropriate for these few patients and so they were recalculated with the 'importance factor' for the femoral head increased from 1 to 3. An increase of more than this resulted in the anterior-posterior beams being too strongly favoured. The corrected average NTCP and TCP values are shown as the lower italicised row in the Table. (All other relevant Tables and figures incorporate the results of these three corrected runs.) A marked decrease in NTCP values for the femoral heads was thus achieved for the 3- and 4-field plans.

A more revealing analysis is again obtained by studying the individual patient TCP and NTCP differences (Table 5). (The 'Bladder' data has been omitted from

this table because the mean differences as indicated in Table 4 were always too small to be significant.) One may see from the 'TCP' column that the optimisation algorithm achieved a statistically significant improvement of about 0.5% for the 3- and 4-field plans. It must be stressed here that statistical significance is not the same as clinical significance. Although a 0.5% improvement in TCP is not of great importance clinically, the implication is that the optimisation performs at least as well as the human planner. The real benefit of the optimisation algorithm comes in the planning time saved (see below). There is also a suggestion of a benefit for the 6- and 8-field plans although the effect is not proved significant at the 95% level. The femoral head NTCP values in Table 5 suggest the optimisation achieves a small (<1.0%) improvement in all cases except for the right femoral head in the 6-field plan.

Tables 3–5 and Fig. 5a–p indicate that the optimisation algorithm produced dose distributions that were as good as the human planner and often slightly better. For

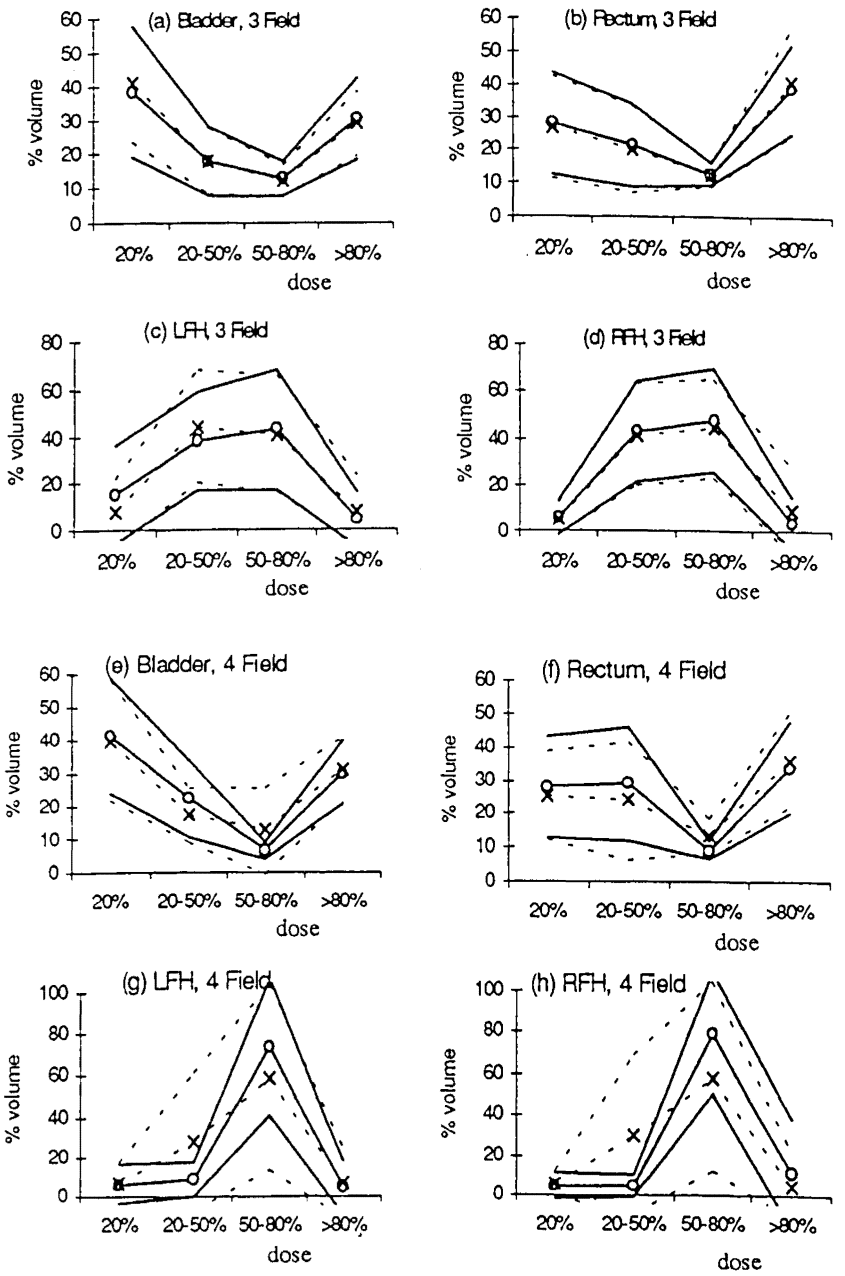

Fig. 5 (a)–(h). Each plot surnmarises average extracted dose-volume histogram statistics over the 12 patients. The central solid line with circle marker is the average achieved by the human planner; the upper and lower solid lines are one standard deviation bounds. Similarly, the central dashed line with cross marker is the average achieved by the optimisation algorithm, with the one standard deviation bound shown as the upper and lower dashed lines.

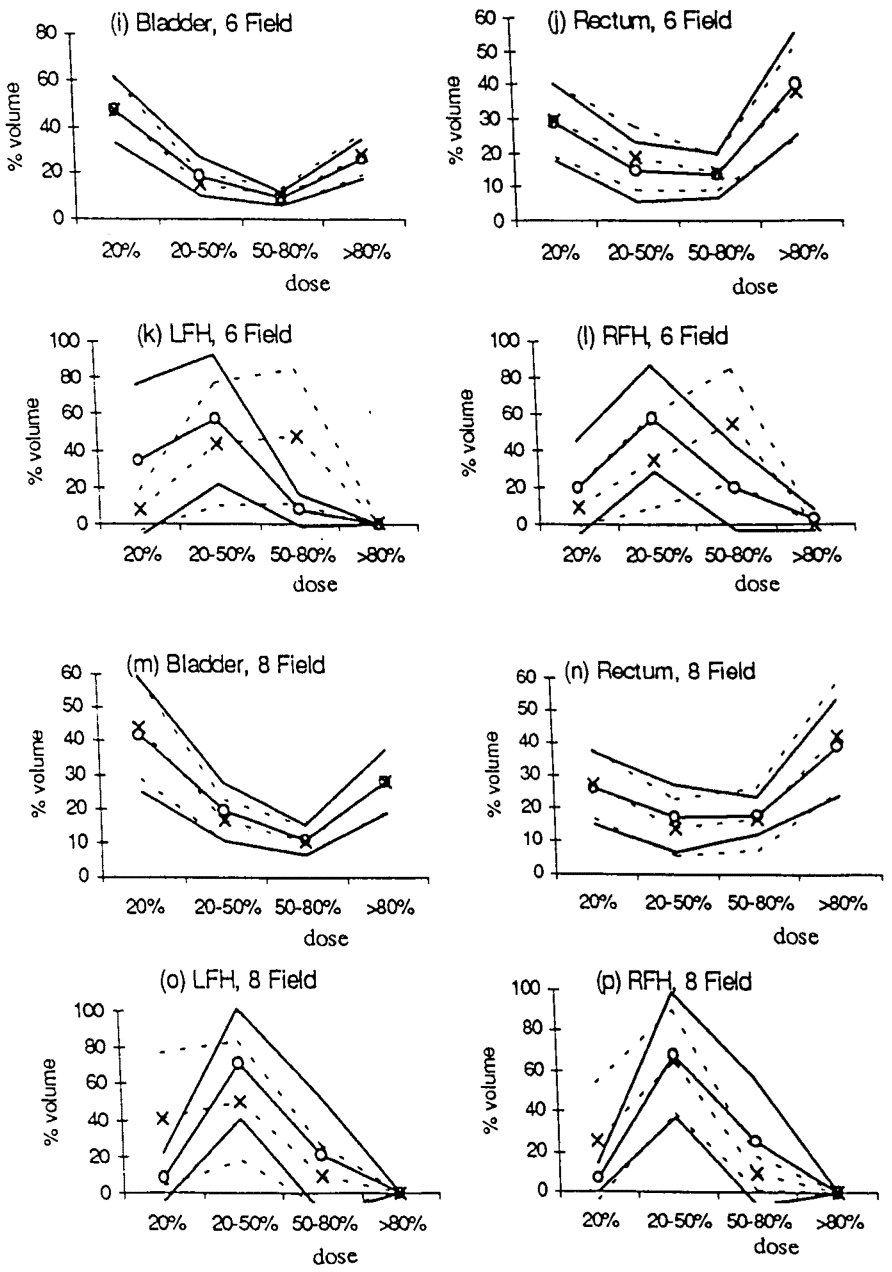

Fig. 5 (i)–(p).

the four plan types studied, the optimisation achieved a more homogenous PTV dose whilst keeping the NTCPs acceptable (i.e., <5%). From the statistical data alone (Table 3 and Fig. 5) one might have expected a more significant benefit to have translated into the TCP and NTCP values. We believe that this is not observed because of the 'overlap factor' which has been shown to limit the therapeutic advantage for radiotherapy of the prostate [20]. The overlap factor is the phenomenon where part of the rectum is inside (or overlaps with) the PTV. Achieving a homogenous PTV dose thus raises the overlap part of the rectum to a high dose and this high dose region is almost entirely responsible for the NTCP.

A comparison study of the beam-weights selected by the human planner and the optimisation algorithm is presented in Fig. 6. It is clear that as the number of beams in the plan increases, there is increasing divergence between the human and the optimisation algorithm. For the 4-, 6- and 8-field plans, the low standard deviations on the beam-weights selected by the human

Table 4
Comparison of the average TCP and NTCP values achieved by the human planner (using conventional forward planning) and the optimisation algorithm over 12 prostate patients, and the corresponding standard deviations

	TCP		NTCP					
	Mean (%)	S.D.	Bladder		Left femoral head		Right femoral head	
			Mean (%)	S.D.	Mean (%)	S.D.	Mean (%)	S.D.
3-F Human	87.9	1.5	<0.1	0.0	1.1	3.4	1.5	4.1
3-F Optimised	88.5	1.4	<0.1	0.0	0.6	1.5	0.7	1.8
4-F Human	88.1	1.6	<0.1	0.0	2.9	2.8	2.7	2.6
4-F Optimised	88.7	1.7	<0.1	0.0	5.0	7.1	5.0	7.2
	88.7	*1.7*	*<0.1*	*0.0*	*1.7*	*1.8*	*1.8*	*1.8*
6-F Human	87.8	1.7	<0.1	0.0	0.0	0.1	0.1	0.1
6-F Optimised	88.1	1.5	<0.1	0.0	0.0	0.0	0.2	0.6
8-F Human	87.9	1.6	<0.1	0.0	0.0	0.0	0.0	0.0
8-F Optimised	88.1	1.5	<0.1	0.0	0.0	0.0	0.0	0.0

Values are shown for 3-, 4-, 6- and 8-field (F) plans. The dose for each plan was normalized so that the rectal NTCP was 5%. The results in the italicised row are for the patient sample after three patients were re-optimised with the femoral head importance factor increased to 3 (see main text Section 4).

planner suggest that small perturbations were made about a perceived 'optimal' beam-weight set. For the 4-field plans the optimisation algorithm found a moderately similar ($\leq 10\%$) optimal set, but had significantly greater variation about these values. For the 6- and 8-field plans the optimal sets of the human and the optimisation show almost no correlation at all. In fact, for the 6-field plan, the beam-weight pattern is almost opposite. The fact that acceptable plans can be produced by such differences in beam-weight patterns indicates that there exists a remarkable degree of flexibility in the planning process. Our results support the idea that many different beam-weight sets can give a similar dose distribution, and particularly, similar TCP and NTCP values.

It is of interest to note that for the 6- and 8-field plans the optimisation algorithm sometimes set certain beam-weights to zero. Three out of the twelve 6-field plans had at least one beam-weight set to zero and were thus actually 5-field plans (in one case, two beam-weights were set to zero). For the 8-field plans the effect was more pronounced with only one actual 8-field plan, six 7-field plans, three 6-field plans and a 5-field plan. This, together with the inter-patient beam-weight variability discussed above, is evidence that the optimum number of beams and their beam-weights for complicated standard plan arrangements are significantly dependent on the patients geometry. It also suggests that significant gains might be had in optimising beam orientations. The implications for clinical practice are a significant reduc-

Table 5
An analysis of the difference in TCP and NTCP values achieved by the optimisation and the human planner over the 12 patient sample

	TCP		NTCP			
	Mean diff. (%) (95% C.I.)	*P* value	Left femoral head		Right femoral head	
			Mean diff. (%) (95% C.I.)	*P* value	Mean diff. (%) (95% C.I.)	*P* value
3-Field	0.56 (0.43 to 0.69)	<0.01	−0.53 (−1.69 to 0.64)	0.39	−0.89 (−2.14 to 0.55)	0.27
4-Field	0.57 (0.34 to 0.79)	<0.01	−1.12 (−2.11 to −0.13)	0.05	−0.84 (−1.77 to 0.08)	0.10
6-Field	0.29 (−0.01 to 0.60)	0.09	−0.13 (−0.08 to 0.02)	0.22	0.13 (−0.20 to 0.45)	0.46
8-Field	0.13 (−0.08 to 0.34)	0.24	0.0	—	0.0	

The 'Mean diff.' columns are the average of the differences between the results obtained by the optimisation algorithm and by the human planner. The *P* value was computed from a two-tailed paired Student's *t*-test, and the dose was scaled for all plans so that the rectal NTCP was 5%. C.I. is the confidence interval.

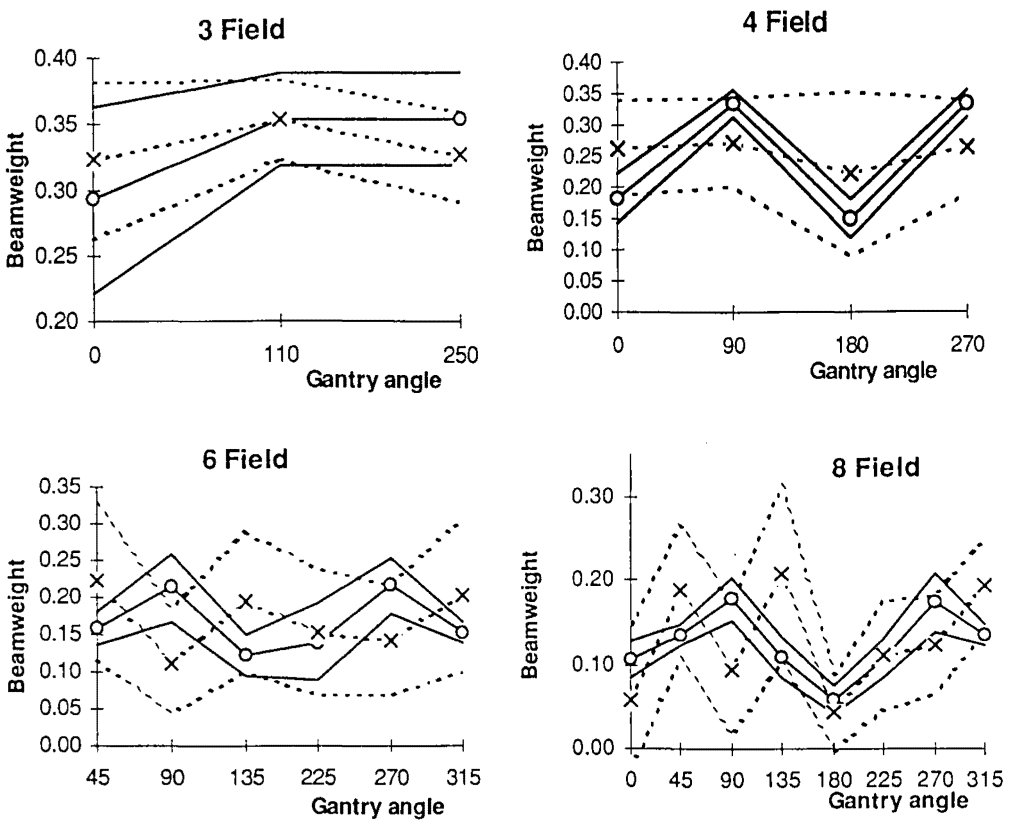

Fig. 6. Average beam-weight statistics over the 12 patient sample. As with Fig. 5, the central solid line with circle marker is the average achieved by the human planner; the upper and lower solid lines are one standard deviation bounds. The central dashed line with cross marker is the average achieved by the optimisation algorithm, with the one standard deviation bound shown as the upper and lower dashed lines.

tion in the delivery time and a general simplification of the delivery process. The deselection of beams seems to be dependent on the shape of the tumour. An irregular tumour with, for example, a large protuberance, is more likely to have a beam deselected from the plan than a spherically shaped tumour. This is due to the inherently strong (Section 2.1.2) quadratic nature of the cost function in the PTV which is sensitive to beams that cause inhomogeneity.

Table 6
Average values over five patients of the time taken (min) to determine optimal beam-weights by a human planner and the optimisation algorithm

	Planner		Optimisation (a)		Optimisation (b)	
	Mean	S.D.	Mean	S.D.	Mean	S.D.
3-Field	21.6	4.4	1.4	0.1	0.5	0.0
4-Field	28.4	8.0	1.6	0.2	1.0	0.1
6-Field	20.2	3.9	2.7	0.3	2.0	0.2
8-Field	22.0	2.4	5.0	0.5	4.1	0.4

The optimisation column (a) includes the time taken by the dose calculation algorithm, and is therefore the total time taken to plan a patient for the first time. The optimisation column (b) is the time for subsequent optimisations of the patient for which the dose calculation does not need to be called again.

The results of the timing study (Table 6) show the most significant advantage of the optimisation algorithm. The times shown are average values over the last five patients in the study, when the planner was fully familiar with the planning system and was therefore working with high efficiency. For all plan types the optimisation was much faster at computing optimised beam-weights (by a factor of 4 for the 8-field plans to 20 for the 3-field plans). Furthermore, whilst the optimisation is computing the beam-weights, the human planner is free to perform other tasks (e.g., further inspection of patient anatomy displayed on the screen). For the three patients where it was necessary to increase the importance factor for the femoral heads, the total time taken to optimise the beam-weights is estimated by adding the mean 'optimisation (a)' time and the mean 'optimisation (b)' time in Table 6. Significant time savings are still observed.

5. Conclusions

The dose distributions produced by the optimisation algorithm were compared with those of the human plan-

ner by studying both dose statistics and biological NTCP and TCP values. The more descriptive dose statistics study broadly supported the more quantitative biological modelling study. The studies have shown two advantages of the optimisation algorithm. Firstly the optimisation consistently achieved a more homogenous PTV dose (Table 3) while maintaining the dose to the OAR at acceptable levels (Figs. 5a–p). This translated into a small but statistically significant increase in TCP (about 0.5%) for the 3- and 4-field plans and there was also the suggestion of a benefit for the 6- and 8-field plans (Table 5). The predicted improvement in treatment outcome associated with the optimisation algorithm, applied to the plan types studied, is thus quite small (0.5%). The second and probably more significant advantage is in the time saving incurred by the optimisation algorithm (a factor of between 20 and 4 for 3- and 8-field plans, respectively).

The clinical implications of the benefits that the optimisation algorithm could bring to routine treatment planning are significant. A reduction in planning time would increase the efficiency of the planning process allowing more patients to be planned and a reduction in costs. The consistency of the algorithm has been demonstrated to be high, which could result in more reliable plan production. From the clinician's viewpoint the algorithm can be used to quickly generate optimised beam-weights for a range of plan types, and for different organ weightings (via the importance factors). The relative merits of these rival plans can then be assessed and the best plan selected for treatment. Finally, the quality of the optimised plans were found to be slightly better on average than the planners plans indicating a potential therapeutic benefit.

Acknowledgements

This work is part of COVIRA (Computer Vision in Radiology), project A2003 of the AIM (Advanced Informatics in Medicine) programme of the European Union.

Participants in the COVIRA consortium are:

Philips Medical Systems. Best (NL) (prime contractor) and Madrid (E); Philips Corporate Research, Hamburg (D); Siemens AG, Eriangen (D) and Munich (D); IBM UK Scientific Centre, Winchester (UK); Gregorio Maranon General Hospital, Madrid (E); University of Tübingen, Neuroradiology and Theoretical Astrophysics (D); German Cancer Research Centre, Heidelberg (D); University of Leuven, Neurosurgery, Radiology and Electrical Engineering (B); University of Utrecht, Neurosurgery and Computer Vision (NL); Royal Marsden Hospital and Institute of Cancer Research, Sutton (UK); National Hospital for Neurology and Neurosurgery, London (UK) Foundation of Research and Technology, Crete (GR); University of Sheffield (UK); University of Genoa (I); University of Aachen (D); University of Hamburg (D); Federal Institute of Technology, Zurich (CH).

We would especially like to thank Ms A. Hoess, Dr R. Bendl, Mr C. Schulze, Dr J. Pross and Prof Schlegel, at DKFZ, for their support, stimulating discussion and providing VIRTUOS; also to Dr P. Evans, Dr P. Mayles, Mrs V. Hansen, Professor W. Swindell, and Dr A.Nahum for discussions at RMH/ICR; Dr P. Elliot, Dr K. Goodson, Dr R. Riste-Smith, Dr G. Sivewright at IBMUKSC. Dr R. Bentley and Mr S. Bashford have provided invaluable help with computing and networking support.

References

[1] Bendl, R., Pross, J., Hoess, A., Keller, M.A., Preiser, K. and Schlegel, W. "VIRTUOS — A Program for Virtual Radiotherapy Simulation and Verification". In: Proc. of the 11th Int. Conf. on the Use of Computers in Radiation Therapy, p. 226. Editors: A.R. Hounsell, J.M. Wilkinson and P.C. Williams. Manchester, 1994.

[2] Boyer, A.L., Desobry, G.E. and Wells, N.H. Potential and limitations of invariant kernel conformal therapy. Med. Phys. 18: (4) 703–712, 1991.

[3] Bortfeld, T.R., Kahler, D.L., Waldron, T.J. and Boyer, A.L. X-ray field compensation with a multi-leaf collimators. Int. J. Radiat. Oncol. Biol. Phys. 28: 3, 1993.

[4] Brahme, A. Treatment optimisation using physical and radiobiological objective functions. In: Radiation Therapy Physics. Editor: A. Smith. Springer, Berlin, 1992.

[5] Burman, C., Kutcher G.J., Emami, D. and Goitein, M., Fitting of normal tissue tolerance data to an analytic function. Int. J. Radiat. Oncol. Biol. Phys. 21: 123–135, 1991.

[6] Censor, Y., Altschuler, M.D. and Powlis, W.D. On the use of Cimmino's simultaneous projections method for computing a solution of the inverse problem in radiation therapy treatment planning. Invest. Prob. 4: 607–623, 1988.

[7] Censor, Y., Powlis, W.D. and Altschuler, M.D. On the fully discretised model for the inverse problem of radiation therapy treatment planning. Proc 13th Annual Northeast Bioengineering Conference. Editor: K.R. Foster. IEEE 87-CH2436-4 Library of Congress catalog card number 87-80502: 211–214, 1987.

[8] Galvin, J.M., Smith, R.M. and Chen, X.-G. Modulation of photon beam intensity with a multileaf collimator. Proc. 1st Biennial ESTRO Meeting on Physics in Clinical Radiotherapy. Budapest, 14–17 October, 1991.

[9] Holmes, T. A model for the physical optimisation of external beam radiotherapy. PhD thesis, University of Winsconsin, Madison, 1993.

[10] Holmes, T. and Mackie, T.R. Simulation studies to characterise the search space of a radiotherapy optimisation algorithm. Proc AAPM Conference, August, 1992.

[11] Kutcher, G.J. and Burman, C. Calculation of complication probability factors for non-uniform normal tissue irradiation: the effective volume method. Int. J. Radiat. Oncol. Biol. Phys. 16: 1623–1630, 1989.

[12] Lyman, J.T. Complication probability as assessed from dose volume histograms. Radiat. Res. 104: S-13–S-19, 1985.

[13] Mageras, G.S. and Mohan, R. Application of fast simulated annealing to optimisation of conformal radiation treatments. Med. Phys. 20: 639–647, 1992.

[14] Mohan, R., Mageras, G.S., Baldwin, B., Brewster, L.J., Kutcher, G.J., Leibel, S, Burman, C.M., Ling, C.C. and Fuks, Z. Clinically relevant optimisation of 3D conformal treatments. Med. Phys. 19 (4): 933–944, 1992.

[15] Mohan, R., Mageras, G. and Podmaniczky, K.C. A model for computer-controlled delivery of 3D conformal treatments. Med. Phys. 18: 612, 1991.

[16] Morrill, S.M., Lane, R.G., Jacobson, G. and Rosen, I. Treatment planning optimization using constrained simulated annealing. Phys. Med. Biol. 36: 1341–1361, 1991.

[17] Niemierko, A. Random search algorithm (RONSC) for optimisation of radiation therapy with both physical and biological endpoints and constraints. Int. J. Radiat. Oncol. Biol. Phys. 23: 89–98, 1992.

[18] Niemierko, A., Urie, M. and Goitein, M. Optimisation of 3D radiation therapy with both physical and biological endpoints and constraints. Int. J. Radiat. Oncol. Biol. Phys. 23: 99–108, 1992.

[19] Oldham, M. and Webb, S. Clinical implementation of Inverse Treatment Planning. Br. J. Radiol. 66: 162.

[20] Oldham, M. and Webb, S. The optimisation and inherent limitations of 3D conformal radiotherapy treatment plans of the prostate. Br. J. Radiat. 1994a (in press).

[21] Oldham, M. and Webb, S. Inverse planning and the optimisation of radiotherapy plans by simulated annealing incorporating dual weighting p. 60. Proc. of the 11th Int Conf. on the Use of Computers in Radiation Therapy. Editors: A.R. Hounsell, J.M. Wilkinson and P.C. Williams. Manchester, 1994b.

[22] Rosen, I.I., Lane, R.G., Morrill, S.M. and Belli, J.A. Treatment plan optimisation using linear programming. Med. Phys. 18: 141–152, 1991.

[23] Smith, R.M., Galvin, J.M. and Chen, X.G. The use of a multileaf collimator to optimise dose distributions. Med. Phys. 18: 613, 1991.

[24] Starkschall, G. and Eifel, P.J. An interactive beam-weight optimisation tool for three-dimensional radiotherapy treatment planning. Med. Phys. 19: 155–163, 1992.

[25] Szu, H. and Hartley, R. Fast simulated annealing. Phys. Lett. A122: 157–162, 1987.

[26] Vance, R., Sandham, W.A. and Durrani, T.S. Optimisation of beam profiles in conformal radiotherapy using genetic algorithms. Phys. Med. Biol., 39a, Abstracts of the World Congress on Medical Physics and Biomedical Engineering. Editors: L.N. Rodrigues and J. Nadal. Rio de Janeiro, 1994.

[27] Webb, S. Optimisation by simulated annealing of three-dimensional conformal treatment planning for radiation fields defined by a multileaf collimator. Phys. Med. Biol. 36: 1201–1226, 1991.

[28] Webb, S. Optimisation by simulated annealing of three-dimensional conformal treatment planning for radiation fields defined by a multileaf collimator: 2. Inclusion of two-dimensional modulation of the X-ray intensity. Phys. Med. Biol. 37: 1689–1704, 1992a.

[29] Webb, S. Techniques for optimisation of dose with a multileaf collimator for conformal radiotherapy of target volumes with concave outlines. In: Three-Dimensional Treatment Planning. Editor: P. Minet. (Proceedings of the E.A.R Conference in Geneva at W.H.O., October, 1992) 163–172, 1992b.

[30] Webb, S. Optimised three dimensional treatment planning for volumes with concave outlines, using a multileaf collimator. Proc. ART91 Munich, April 1991 (Abstract book p. 66). In: Advanced Radiation Therapy: Tumour Response and Treatment Planning, pp. 495–502. Editor: A. Breit. Springer, Berlin, 1992c.

[31] Webb, S. and Nahum, A.E. A model for calculating tumour control probability including the effects of inhomogenous distributions of dose and clonogenic cell density. Phys. Med. Biol. 38: 653–666, 1993.

ATTACHMENT A-2

Optimizing Radiation Therapy Inverse Treatment Planning Using the Simulated Annealing Technique

Steve Webb

Joint Department of Physics, Institute of Cancer Research and Royal Marsden Hospital, Downs Road, Sutton, Surrey SM2 5PT, London, United Kingdom

ABSTRACT

The role of simulated annealing in therapy planning is discussed from a historical, theoretical and practical viewpoint. The properties of the method are discussed in detail together with available options and specific implementations. © 1995 John Wiley & Sons, Inc.

I. WHAT IS TREATMENT PLAN OPTIMIZATION?

The aim of radiotherapy of local disease is to achieve a high dose to the planning target volume (PTV), simultaneously keeping the dose to organs at risk (OAR) as low as possible. When a small number of rectangular fields with or without wedges and blocking is intended for use, the treatment planning technique is to try a number of different beam weightings, compute the dose distribution, evaluate the plan, and then repeat the task until the plan meets prescribed criteria satisfactorily. This is known as forward treatment planning. It is the traditional method and is still in widespread use. It might be called "human optimization," but in fact the resulting plan has no more status than "acceptable."

As we move toward an era of increased automation and precision in three-dimensional radiotherapy, a number of desirable treatment options will increasingly be called upon, including:

1. the use of a larger number (than simply two or three) of fields;
2. the use of noncoplanar fields;
3. the use of fields shaped to the beam's-eye-view (BEV) of the PTV by a multileaf collimator (MLC);
4. the introduction of intensity-modulated beams (IMBs) (Figure 1) via:
   a. multiple exposures with different static MLC settings;
   b. dynamic sweeping of MLC leaves;
   c. apparatus for tomotherapy;
   d. electronically steered, time-modulated pencil beams.

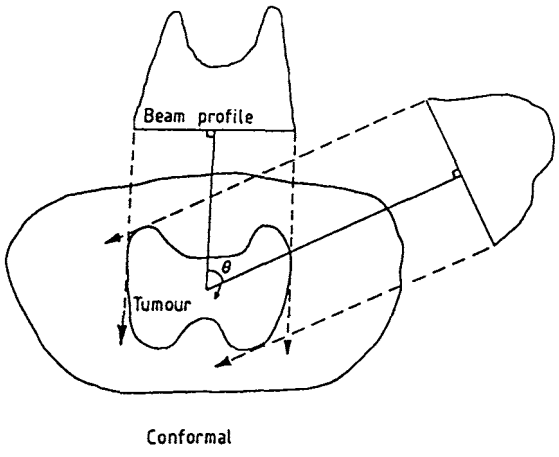

Figure 1. The concept of intensity-modulated beams. Two (of a large set of) such beams with one-dimensional intensity modulation are shown irradiating a two-dimensional slice. The beams combine to create a high-dose treatment volume spanning the PTV, which has a concave outline in which might lie OARs. Such uniform high-dose treatment volumes cannot be achieved using beams without intensity modulation. Planning such treatments relies on tools, such as simulated annealing, for solving the inverse problem.

As these quite technologies become increasingly more common, it becomes impossible to create treatment plans by forward treatment planning, because there are just too many possibilities to explore and not enough human time to do this task; there is little chance of arriving at the optimum treatment plan by trial and error; and if an acceptable plan could be found, there is no guarantee it would be the best, nor any criteria to specify its precision in relation to an optimum plan.

For this reason, the treatment planning process has to be radically changed to solve the problem, "Given a prescription of desired outcomes, compute the best beam arrangement." Stated this way, the problem is solved by inverse treatment planning. The task has to be solved by a computer with human guidance rather than by human experience alone.

II. CLASSES OF INVERSE TREATMENT PLANNING TECHNIQUES

Inverse treatment planning was first discussed by Brahme in the early 1980s. Since then, several groups of workers have developed inverse treatment planning tools. They fall into two broad classes:

1. Analytic techniques. These involve deconvolving a dose-kernel from a desired dose distribution to obtain the distribution of photon fluence and forward projecting this fluence with attenuation factors to create profiles of beam intensity. Because of the formal similarity

International Journal of Imaging Systems and Technology, Vol. 6, 71–79 (1995)

CCC 0899-9457/95/010071-09

with X-ray slice imaging, these methods have sometimes been called inverse computed tomography. The first tools were used for two-dimensional planning, later extended to three dimensions.

2. Iterative techniques. Both linear-programming algorithms (Simplex) and the Cimmino algorithm have been exploited, together with simulated annealing.

Some optimization tools combine a mixture of analytic and iterative-refinement stages. In particular, negative beam weights, created by analytic inversions, have to be removed in some way.

Optimization is a vast field, not further reviewed here. The reference list in this review is restricted to papers on simulated annealing, since other articles in this Special Issue and the references in Webb [1] point to this vast field.

III. SIMULATED ANNEALING: GENERAL CONCEPTS AND PROPERTIES

Simulated annealing is an iterative optimization technique. It is a method of finding the global minimum of some function when the state-space of this function may possess multiple local minima. Because of this property it may have advantages compared to other iterative methods which may become trapped in a local minimum. Simulated annealing has been used in a variety of different fields with many applications [e.g., 2–9]. It was first introduced into the field of medical physics (coded aperture reconstruction of images of radioactive distributions) by Professor Harry Barrett and colleagues in Tucson, Arizona, who applied the method to minimizing a quadratic cost function [10–12]. The present author continued this application into SPECT [13] and then into radiotherapy treatment planning (see Section VII) [14–22]. Recently, Mageras and Mohan [31] have further extended the method and application with other cost functions and techniques to accelerate convergence (see Section VIII).

To give the discussion substance in the radiotherapy context, let us imagine that a number of beam orientations have been selected and the problem is to determine the optimum set of beam weights for beams with intensity modulation [i.e., it is required to compute the beam weight sinogram (Figure 2)]. The analogy with medical imaging is shown in Figure 3.

A large number of combinations of beam weights are explored in some iterative manner (see Section IV). Define a quadratic cost function V_n at the nth iteration (i.e., nth choice of such beam weights) to be:

$$V_n = \left[\left(\frac{1}{M} \right) \sum_{\underline{r}} I(\underline{r}) (D_p(\underline{r}) - D_n(\underline{r}))^2 \right]^{0.5} \qquad (1)$$

where $D_p(\underline{r})$ means the prescribed dose value at some point $\underline{r}$ in the patient and $D_n(\underline{r})$ denotes the actual dose at the same point at the nth iteration, and the mean is taken over a large number M of specified dose points. $I(\underline{r})$ is a term which allows the user to weight the importance of contributions to the cost from different parts of the body. For example, it may be more important to have the dose conform in the PTV than in the OAR, or conversely, protection of the OAR may be the desired goal at the expense of some dose inhomogeneity in the PTV. The choice of the parameters $I(\underline{r})$ greatly influences

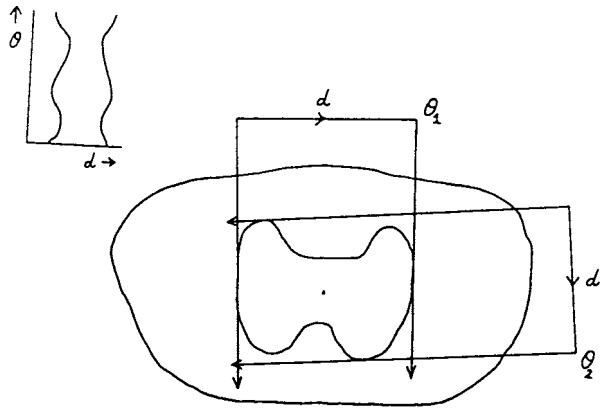

Figure 2. The concept of the beam weight sinogram. The butterfly-shaped region is the PTV, and a number of beams with intensity modulation are arranged to span the PTV. The angle θ labels each beam and the parameter d labels each element of each beam. If the beamweights are stacked as shown in the upper left, then the resulting image is a beamweight sinogram by analogy with medical imaging (see Figure 3).

the outcome of the optimization. The aim of the optimization is to compute the lowest value of V_n, since this corresponds to the calculated dose distribution best matching the prescription in a least-squares sense (Figures 4 and 5).

This suffices for the purpose of discussion, although this is only one of many possible functions to minimize and the quadratic cost function does not actually have any local minima when optimising beam weights. Bortfeld has shown that the same dose quadratic cost function does have local minima when optimizing beam directions. We return later (see Section IV) to discuss other cost functions, including those

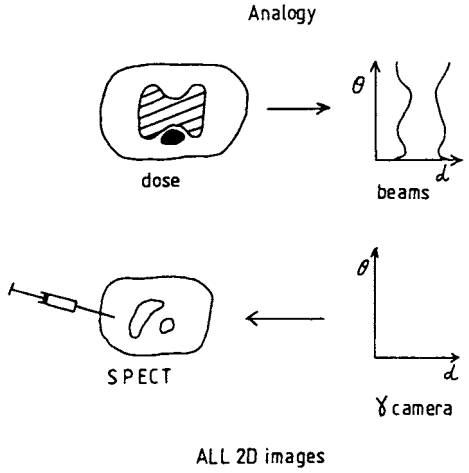

Figure 3. The analogy of inverse treatment planning when the one-dimensional beams are intensity modulated, and emission tomography imaging. In the former, the dose prescription is known on a two-dimensional matrix (top left), and it is required to compute the beam weight sinogram (top right). In the latter, a γ camera makes a measurement of the projection sinogram (bottom right) of the distribution of activity; this is reconstructed (bottom left) from these data. Simulated annealing has been used to solve *both* problems, the latter problem providing the stimulus and motivation for introducing simulated annealing into radiotherapy treatment planning.

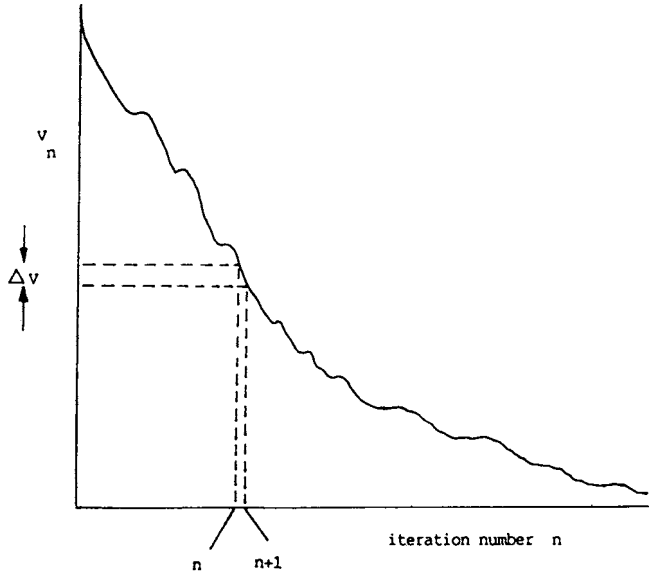

Figure 4. In one dimension, a general cost function V_n which may have local minima as shown as well as a global minimum.

embodying biological end points, which almost certainly do have local minima.

For some general cost function it is not possible to know ahead of time the form of the multidimensional surface in state space of the function for all possible beam arrangements. As different beam arrangements are tested, the cost function will change (Figure 6). The problem is to compute a very large number of elemental beam weights which combine to give a dose distribution evaluated on all the pixels contributing to the cost function.

Sometimes the cost function will be larger than at the previous iteration, and sometimes smaller. At first sight it

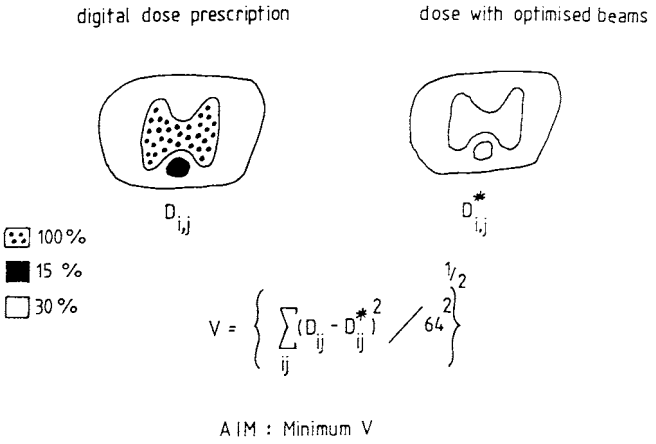

Figure 5. The left part shows a possible dose prescription (D is $D_p(r)$ in the text). The aim is to have a high dose in the PTV (dots) and a low dose in the OAR (black). The right part shows the "running estimate" of the dose on a two-dimensional grid specified by i, j (D^* is $D_n(r)$ in the text) and this example illustrates the computation of a dose quadratic cost function on a 64^2 grid. For simplicity the importance of all regions is considered to be the same (unity). In practice (see Section VII) tuning the importance changes the outcome. The aim of simulated annealing is to minimize the cost function V.

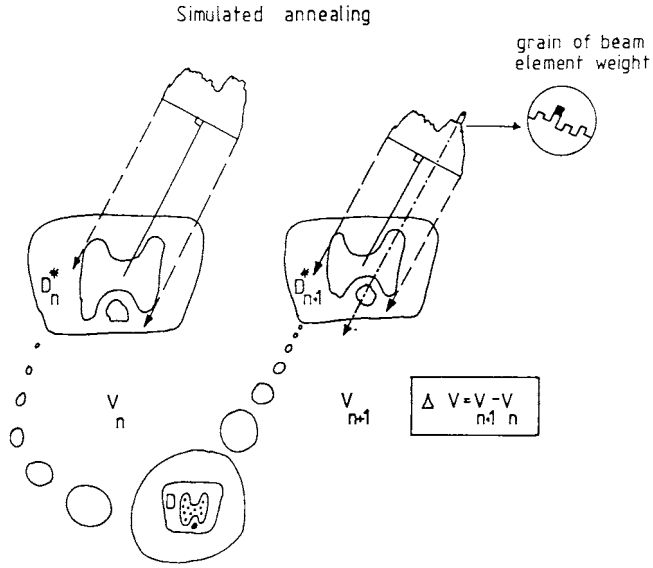

Figure 6. The way the addition of a grain changes the cost function. On the left at the nth iteration the current estimate of the dose distribution is D_n^* and the cost function is V_n, computed by comparing the running estimate of the dose distribution with the prescription D (shown as bubbles). Then (right) one particular element of beam weight has a grain added (black), the new dose distribution becomes D_{n+1}^*, and the new cost function is V_{n+1}. The change of the cost function ΔV_n controls what happens next.

would seem obvious to accept only each new beam weight set that *lowers* the cost function, and those that achieve this reduction are indeed substituted for the previous best estimate. However, in simulated annealing a mechanism for accepting changes which lead to an *increase* in the cost function is also built in. This mechanism allows the system to climb out of local minima in the cost function, should there be any, and eventually reach the global minimum. If the cost function changes by ΔV_n in progressing from the nth to the $(n+1)$th iteration and if ΔV_n is positive, then this change is accepted with a small probability

$$\exp(-\Delta V_n/kT) \tag{2}$$

where k is the Boltzmann constant and T is the temperature (Figure 7).

In practice, kT is simply a quantity ascribed the same dimensions as ΔV_n. Initially in the iterative process, the temperature is large allowing many "wrong-way" changes of the cost function (and thus a wide exploration of state space). In so-called classical simulated annealing provided the temperature in equation 2 is reduced slower than, or as $(1/\ln(n))$ this guarantees progression toward the global minimum as iterations proceed [6].

The method gets its name from the process by which metals are annealed. If the temperature falls too fast, then amorphous states can arise, whereas annealed metals form from slow cooling. Consider also the analogy with a skier descending a slope (Figure 8). Imagine the slope is the graph of the cost function. The skier starts at the top (large value of the cost function) and wishes to reach the hotel at the bottom (global minimum of cost function).

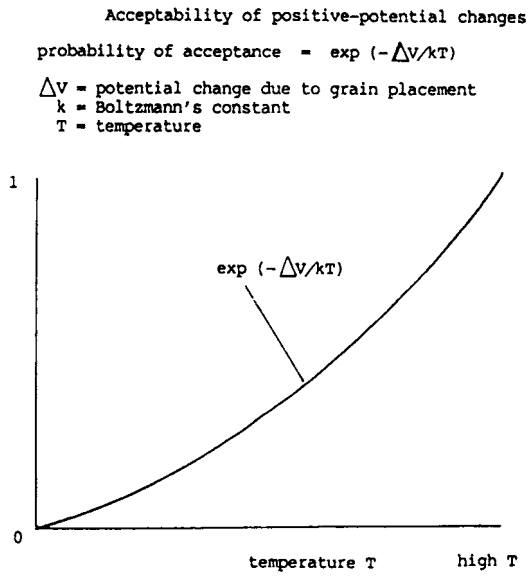

Figure 7. The graph controlling the acceptability or otherwise of wrong-way (uphill) changes in the cost function. When ΔV_n is positive, Equation (2) gives the probability with which such changes should be accepted. At high temperatures the probability will be high, and vice-versa.

In general, the skier must aim to go downhill, of course. But if our skier is overprincipled and refuses ever to suffer a potential energy rise (i.e., go uphill), then that skier will be trapped behind any snow bump blocking his path (see Figure 8) and will not reach the bottom. Just as a skier requires some momentum to rise over the snow bump, so the optimization requires the described mathematical step for overcoming local minima. However, in multidimensional problems, simultaneous minima in many directions are rare.

IV. THE POWER OF SIMULATED ANNEALING: COST FUNCTIONS

The great power of simulated annealing lies in its flexibility. The cost function can be as simple or as complicated as one likes. The quadratic cost function in dose [Eq. (1)] is a popular choice because it has an intuitive meaning. The outcome can be tuned via the importance parameters $I(\underline{r})$. As the name "cost function" suggests, what is achieved depends on what the user is prepared to pay for. A pure quadratic cost function in dose for beam weight optimisation has no local minima, and the matrix linking three-dimensional dose to a set of beam weights could, in principle, be analytically inverted. However, such inversions would be lengthy and ill conditioned. The enormous matrices would be hard to compute and would require huge computer storage. The analytic inversion may well be impossible, would almost certainly lead to the inclusion of negative beam weights; simulated annealing still provides a convenient way to solve the problem and build in the constraint of positivity and flexible tuning. In the case of beam weight optimization with the dose quadratic cost function, simulated annealing at zero temperature reduces to constrained iterative least-squares optimization. If beam orientation is optimized with the quadratic cost function in

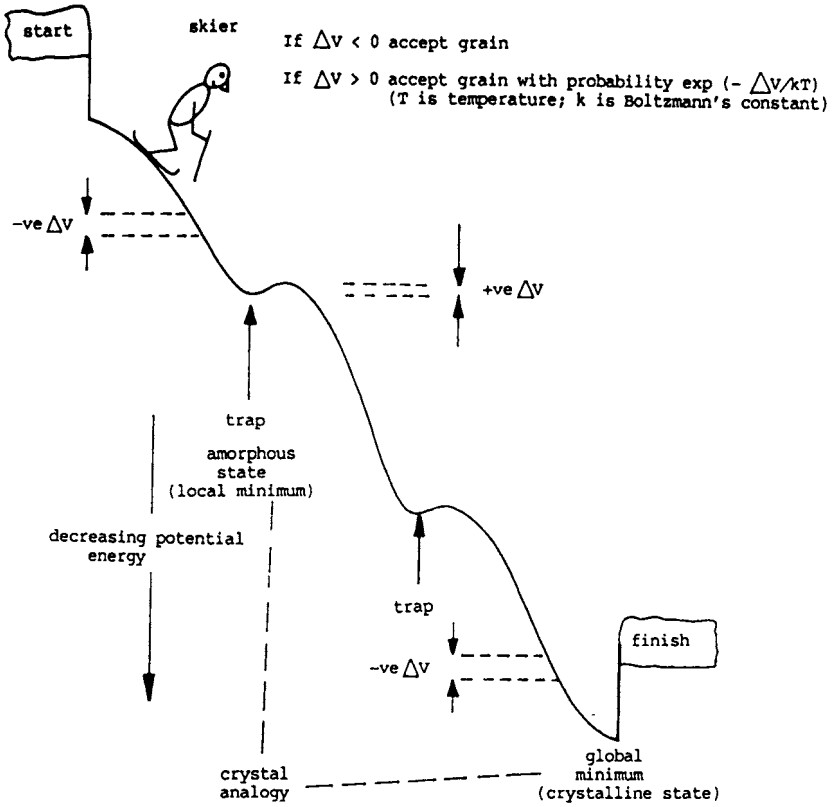

Figure 8. The analogy of minimizing a cost function by simulated annealing and the technique of a skier descending a slope (see text for discussion).

dose, nonzero–temperature simulated annealing must be implemented.

An alternative cost function still based on dose is to use a quadratic term in the PTV and a linear term in the OAR, representing integral dose to the OAR and the rest of the body B. Oldham and Webb [24] used

$$V_n = a_1 \frac{C_{\mathrm{PTV}}}{C_{\mathrm{PTV}_{st}}} + a_2 \frac{C_{\mathrm{OAR}}}{C_{\mathrm{OAR}_{st}}} + a_3 \frac{C_B}{C_{B_{st}}} \tag{3}$$

where C_{PTV} has the same form as in Equation (1) and

$$C_{\mathrm{OAR}} = \sum_{\underline{r}} D_n(\underline{r}) \quad \text{with } \underline{r} \text{ in OAR} \tag{4}$$

and

$$C_B = \sum_{\underline{r}} D_n(\underline{r}) \quad \text{with } \underline{r} \text{ in } B \tag{5}$$

and the subscript $_{st}$ indicates the starting value when all beam weights are uniform. a_1, a_2, and a_3 are constants which control the optimization allowing different initial importance to be ascribed to each region of interest in the fit.

Since dose is only a surrogate for biological outcome, some workers have argued that instead of trying to match a dose prescription, it is better to optimize biological outcome. The argument applies equally to analytic and iterative techniques. Using models supported by observational data, tumor control probability (TCP) and normal tissue complication probability (NTCP) can both be computed knowing the three-dimensional dose distribution in the PTV and OAR. Formally, the TCP at the nth iteration is

$$\mathrm{TCP}_n = f_1[D_n(\underline{r})] \quad \text{with } \underline{r} \text{ in PTV} \tag{6}$$

where f_1 represents the function linking inhomogeneous dose and TCP. Similarly, the NTCP at the nth iteration is

$$\mathrm{NTCP}_n = f_2[D_n(\underline{r})] \quad \text{with } \underline{r} \text{ in OAR} \tag{7}$$

where f_2 represents the function linking inhomogeneous dose and NTCP.

It is then possible to specify different cost functions for optimization involving biological outcome—e.g., maximize TCP subject to some maximum-allowed NTCP; minimize NTCP subject to some minimum-allowed TCP; and maximize the probability of uncomplicated tumor control TCP × (1 − NTCP).

Not all of these objectives are endorsed. For example, the third option might correspond to too-high NTCP. Clinicians usually regard an upper NTCP as a constraint and the first option is often the preferred clinical rationale in determining a treatment.

It would even be possible to construct cost functions involving both dose and biological outcome. Cost functions based on TCP and NTCP almost certainly have local minima. Note, however, that a physical parameter cannot both be a constraint and a goal for optimization simultaneously.

The argument in favor of optimizing biological outcome is that this is, of course, the aim of radiotherapy, dose being a traditional surrogate. The argument against it is that the biological models are relatively new and not universally accepted. To an extent there exists a difference in philosophy between some workers in the United Kingdom who have preferred to optimize dose and compute TCP and NTCP *a posteriori* and some in the United States who have taken a bolder approach and bypass dose (see Section VIII). There is plenty of scope for debate on the issue, which has received some attention already [17].

V. CLASSICAL AND FAST SIMULATED ANNEALING

Imagine that the system of beam weights are changed at each iteration by the addition of a "grain" g of beam weight to one particular beam element (see Figure 6). In classical simulated annealing the system is perturbed only slightly at each iteration, sometimes with a Gaussian generating function for g

$$\exp(-g^2/T_n) \tag{8}$$

where T_n is the temperature at iteration n. The author's early work had a generating function, which was simplified to a delta-function choice of either a positive or negative grain g, initially constant and then reduced in size toward the closing stages of iteration. The cooling proceeds as, or slower than,

$$\frac{T_0}{\ln(1+n)}. \tag{9}$$

In fast simulated annealing [25, 26], the grains are generated by a Cauchy distribution

$$\frac{T_n}{(T_n^2 + g^2)}. \tag{10}$$

The cooling proceeds as

$$\frac{T_0}{(1+n)}. \tag{11}$$

The faster cooling (and hence quicker computational times) is allowed because the form of the Cauchy distribution generates occasional large grains which allow the system to tunnel out of a local minimum. Depending on the cost function there may be no need for classical hill climbing (see Section VIII).

VI. PRACTICALITIES OF IMPLEMENTING SIMULATED ANNEALING FOR INVERSE TREATMENT PLANNING

First, it should be made clear that simulated annealing substitutes for only one part of the planning process, the calculation of beam weights by otherwise traditional forward planning. Thus, it requires to be fed exactly the same data as the forward planning problem, including:

1. specification of the PTV and OAR contours, derived from high-quality three-dimensional imaging data (e.g., X-ray CT, MRI, SPECT, and PET);
2. specification of the dose to each dose-space voxel per unit beam weight;
3. relevant biological models and data if a biological cost function is used; and
4. prescription/constraints on the treatment plan and/or on the beam weights themselves.

Similarly, the results of the calculation (three-dimensional dose maps) must be evaluated by the same tools as would be used to evaluate the outcome of forward treatment planning [i.e., DVHs, display of isodoses, three-dimensional shaded-surface display of dose, dose ribbons, display of dose super-

posed on anatomical sections, *a posteriori* TCP, and NTCP calculations (if simulated annealing was dose-based), etc.].

Hence, simulated annealing should properly form part of an integrated three-dimensional treatment planning system. When first introduced into the armamentarium of planning tools [14], this was not possible. A stand-alone implementation demanded that all these tasks be worked up independently for the application. How this was done is not central to understanding simulated annealing, but is described at length in a suite of papers [14–20, 27, 28].

The following features must be included:

1. Both positive and negative grains must be sampled so that there is a mechanism to "undo" structures which may be created early in the optimization but which may need to be removed once a wide search of state space has been made.
2. In classical simulated annealing the grain size should be reduced at the later stages of iteration to fine-tune the solution. In fast simulated annealing the Cauchy distribution should become increasingly more narrow.
3. Beam weights must be constrained positive. Any candidate change which passes the acceptance criterion for annealing is nevertheless rejected if it would lead to a beam weight going negative. This is an important step. Analytic inversion techniques on the other hand generally generate negative beam weights and then artificially, these have to be set to zero *a posteriori*, somewhat massaging the status of the result. Constrained iterative solution never gets into this difficulty.
4. Attention must be paid to the computational aspects of the calculation of the cost function, because this is at the heart of each iteration. This part must be computer-optimized. For example, there are tricks whereby the change in a quadratic cost function can be computed without evaluating the full function for each of two successive iterations [13, 14]. Also, when large three-dimensional arrays are being manipulated, care must be exercised in handling the order of sequencing through the dimensions of the array.
5. Other constraints can be applied to beam weights (e.g., requirement for smoothness in intensity-modulated beam profiles). The application of constraints leads to its being impossible to reach a zero of the cost function (which would require disallowed negative beam weights). The optimization will achieve some finite global minimum, which in turn will depend on the constraints.

Although simulated annealing appeals because of its wide flexibility, this very same ability to be tailored in many ways has a drawback. In the author's experience it is necessary to experiment somewhat in choice of grain sizes, number of iterations, and the importance weighting in the cost function, which in turn depends on the desired clinical outcome. If the cost function is expected to have local minima and uphill moves are to be included, then attention must be paid to the cooling scheme and the initial temperature (which determines both the initial and the total number of "wrong-way" changes accepted). The early papers by Barrett et al. [10] did not address these points, and in discussion with Professor Barrett he was of the opinion that the choices depended to some extent on the nature of the cost function in parameter space. Yet, this function is not well known *a priori*, hence the need to experiment [29].

Barrett (private communication, 1994) commented that problems such as the one used here for illustration may have cost functions with a very broad region with shallow curvature in the vicinity of the global minimum, and that consequently, different schemes for optimization can arrive at different parts of this "floor," with the global minimum being hard to reach. Put another way, there can be a large number of possible beam arrangements which correspond to much the same final dose distribution, the inversion from three-dimensional dose to beam weights being ill conditioned. Simulated annealing and least-squares iterative optimization provide a tool to control the optimization via the tuning features.

VII. IMPLEMENTATIONS AT ICR/RMH, LONDON

The work at ICR/RMH has proceeded in several stages:

The first application was to compute the one-dimensional intensity-modulated beam profiles which would create a two-dimensional dose distribution for a PTV with a concave outline in which might lie OARs. A series of model problems and clinical cases from the literature was solved, first with a simple beam model [14] and then with a model including scattered radiation [28]. This work occupied the period July 1988 to March 1990, and at that time there was a lot of interest in the potential uses of intensity-modulated radiation even though it was almost impossible to deliver radiation with this feature at the time (Figures 9 and 10).

The second application was to compute the beam weights for fields defined by an MLC [27]. The main advance was to recognize that each field could be divided into two, with one part seeing only PTV and the other seeing both PTV and OAR. The application was for those problems where it was not possible to create beams whose primary radiation only intersected PTV. For example, when irradiating the prostate, the rectum is in the field of view and indeed often overlaps the PTV. Simulated annealing was used to find the optimum set of pairs of beam weights. A number of "difficult" geometric model problems were studied where the PTV wrapped around the OAR (Figure 11).

The third application was to compute the two-dimensional

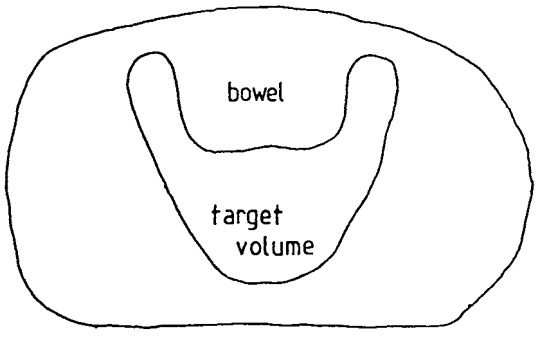

Figure 9. A two-dimensional planning problem where the aim is to obtain a high-dose treatment volume within the irregular PTV shown, while simultaneously sparing the dose to the bowel (OAR). This is a clinical planning problem first presented by Chin.

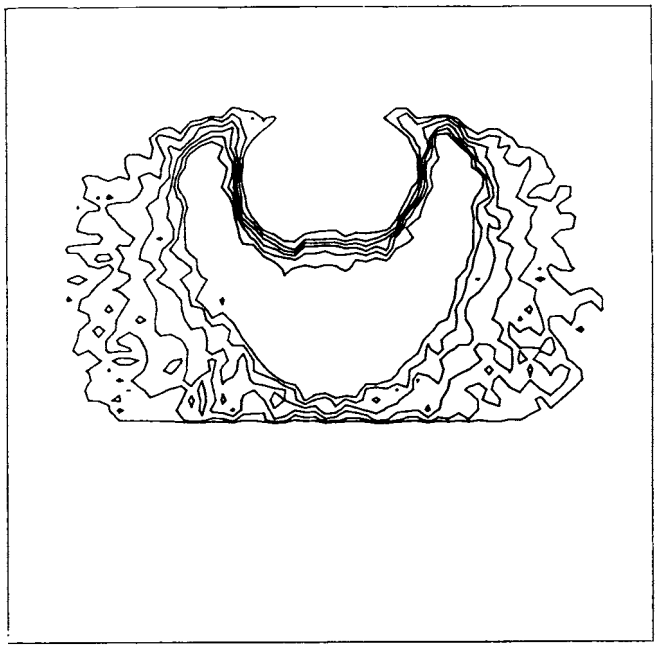

Figure 10. The resulting optimized two-dimensional dose map created by simulated annealing. The innermost dose contour is the 90% contour and the others (moving outward) are 80, 70, 60, 50, and 40%, respectively. The dose map is shown as a grey-scale image together with the beam sinogram in Webb [28].

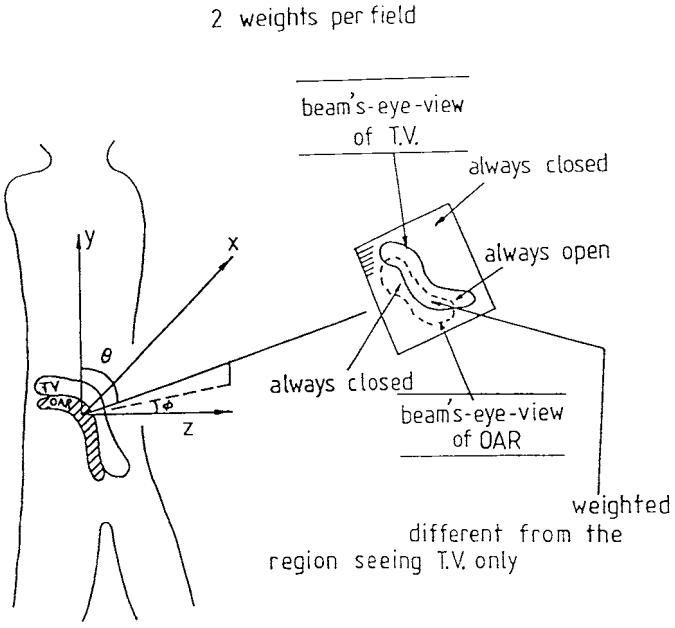

Figure 11. The way to optimize the separation between the DVH for PTV and OAR when multileaf-collimated beam's-eye-view ports are used. The multileaf collimator is shown to the right with the projected opening area corresponding to the views of the PTV and the OAR. These two curves overlap. The question arises how to handle the overlap region. A different beamweight is applied to the aperture viewing PTV only and the overlap aperture viewing PTV and OAR.

intensity-modulation across the MLC-shaped apertures for optimal three-dimensional conformal dose distributions [17]. Again, a number of difficult geometric model problems were studied, and this time the results were evaluated *a posteriori* by TCP and NTCP models. The first two applications were developed between March 1990 and July 1991.

The second application [with the original classical simulated annealing replaced by fast simulated annealing and the cost function of Equation (3)] has been implemented in a clinical context [24] (April 1992 onward) as part of the EC-funded AIM project A2003 called COVIRA, in collaboration with the German Cancer Research Centre (DKFZ) and the IBMUK Scientific Research Centre. The stand-alone system can now accept CT data from the image-handling package TOMAS, and the method has been implemented within the three-dimensional treatment planning package called VIRTUOS, which has grown out of VOXELPLAN.

The first application has been further studied to decide which method of delivering intensity-modulated beams may be most practical. Some preliminary results were presented at the 11th ICCR [21]. The tomotherapy technique seems preferable to creating IMBs from multiple static fields if only a few strata are used. However, a more thorough study [22] using a large number of strata for segmented delivery showed the two methods produced virtually indistinguishable results. Of much more relevance to outcome was the choice of tuning.

VIII. IMPLEMENTATION AT MSK, NEW YORK

Mohan [30] presented initial results of the New York work at the 10th ICCR. Mageras and Mohan [31] and Mohan et al. [23] investigated techniques for accelerating the convergence of the simulated annealing optimization technique for determining the beam weights for a large number of noncoplanar-shaped fields. Mageras and Mohan [31] investigated a model problem with 54 beams, arranged as three noncoplanar rings of 18 fields equispaced in 20° azimuth, one ring being transaxial and the other two at ±30° in latitude. The problem was to optimize a prostate treatment. Mohan et al. [23] chose fields not necessarily coplanar, so that no parallel-opposed fields occurred. These studies distinguished, for each orientation, two separate components of the field, namely, that "seeing" only PTV and that "seeing" PTV and OARs. The radiation beam weights for the former part-fields are traded off against those for the latter creating inhomogeneous dose distributions in the prostate. In this respect, the formalism was identical to that of Webb [17–20, 27].

Classical simulated annealing techniques generally choose to make a small change to one beam weight at each cycle of iteration, investigate the effect on some cost function, and then accept or reject the candidate change according to the criteria in Section III, which guarantee convergence to the global minimum cost. This involves some hill climbing to avoid trapping in local minima of the cost function, if these exist. Mageras and Mohan [31] implemented fast simulated annealing and compared it with classical simulated annealing.

Mageras and Mohan [31] and Mohan et al. [23] also proposed that at each cycle all beam weights are changed. Initially, the changes were large to coarsely explore the cost function. The cost function was based on biological response to radiation and considerations of NTCP and TCP, which

were derived from dose data using empirical models. The relative importance of TCP and NTCP was also accounted for in computing the cost or score function to be optimized. They proposed three distinct schemes for generating the candidate changes [classical simulated annealing with Gaussian and fixed-element generators (varying all beam weights simultaneously for the former per iteration and one beam weight only for the latter per iteration) and fast simulated annealing with a Cauchy generator (varying all beam weights simultaneously per iteration)], and each scheme requires specifying a function which updates the temperature, which controls the number of allowed hill climbs and the absolute size of the changes at each cycle.

Their results showed that with the two schemes in which all beam weights are simultaneously varied at each cycle, there is no need for hill climbing (i.e., zero temperature runs produce much the same result). This is because the wide search of the configuration space corresponds to tunnelling through from local minima as well as descent toward the global minimum.

Although for a model problem, the final cost function, TCP, and NTCP end up much the same with the new methods as with "one-change-per-cycle" simulated annealing, the beam weights can be quite different, reflecting the wide exploration of configuration space, and indeed, this allows them greatly to reduce (by eliminating beams with small weights) the number of fields needed (from 54 to 13 in the model problem) without radically altering the result. This would appear to be another example of the wide-bottomed cost function discussed earlier.

An additional advantage of fast simulated annealing with multiple beam weight changes per iteration is the increased speed of convergence by a factor of 10 or so.

Mohan et al. [23] found that "uneducated application of constraints" could thwart the optimisation altogether. Webb [27] similarly found that the choice of tuning in the cost function depended on what the goal was. Clearly, one cannot have the dose everywhere constrained *and* expect excellent PTV dose homogeneity. Mohan et al. [23] stated (although this is not formally proved) that optimization problems in radiotherapy involving TCP and NTCP probably have multiple minima and so simple descent methods cannot be relied on. There is scope for demonstrating the existence of local minima in specific circumstances and with specific cost functions.

IX. SOME COMMENTS ON COMPARATIVE ASPECTS OF ICR/RMH AND MSK IMPLEMENTATIONS

The work at the Memorial Sloan-Kettering Hospital and at the Royal Marsden Hospital is so closely parallel that some detailed points are extracted for comparison. Both approaches have the following features in common:

1. Both emphasize that there is a need for clear graphics to show the enormous wealth of information obtained by three-dimensional treatment planning systems.
2. Both calculate cost on a uniform dose grid.
3. Both point out that when using biological response data, it is important not to trust absolute values of TCP and NTCP, but that the use of relative values is acceptable.
4. Both ensure that there are no parallel-opposed beams. The beam locations are prespecified and a separate check must be done to see that the beam positions are practical without collisions.
5. Both used the biological data collated by Emami et al. and Burman et al.
6. Webb [17] used the NTCP model of Niemierko and Goitein and the effective volume at maximum dose method of reducing the dose-volume histogram (Kutcher–Burman method). Mohan et al. [23] used the Lyman equations and the effective dose-to-whole volume method of reducing the DVH. These are equivalent provided the NTCP is small.
7. Both methods incorporated the concept of "part-fields" seeing either PTV alone or PTV + OAR and created three-dimensional dose distributions which were highly conformal.

CONCLUSION

Simulated annealing is a powerful and flexible tool for treatment plan optimization. It has desirable features including controlling the positivity of beam weights and allowing a wide choice of cost function and flexibility to weight the importance of constraints in different regions in the patient. This same flexibility, however, demands considerable experimentation to determine optimum operating conditions. The first applications used classical simulated annealing, which is conceptually relatively simple but time consuming. Workers are now moving toward fast simulated annealing but still encountering the need to "tune" the algorithm.

ACKNOWLEDGMENTS

This review is an extended version of a review paper given in the International Course on Advances in Radiotherapy held at the Royal Marsden Hospital, 16–18 March 1994 just prior to the 11th ICCR in Manchester. The author is grateful to his colleagues in the Joint Department of Physics, Professor W. Swindell, Dr. A. Nahum, Dr. P. Mayles, Dr. P. Evans, and Dr. M. Oldham, for many discussions over the years on these subjects. He is also grateful to Professor R. Mohan for discussions at these conferences. He particularly wishes to acknowledge the active contributions to optimization in their Team made by Dr. M. Oldham, who since 1992 has been directly responsible for implementing the technique into VIRTUOS. The VIRTUOS implementation is funded under the EC AIM Project A2003 and has been carried out in collaboration with the German Cancer Research Centre (DKFZ) at Heidelberg and the IBMUK Scientific Research Centre in Hursley. The work of the Joint Department of Physics is supported by the Cancer Research Campaign.

REFERENCES

1. S. Webb, *The Physics of Three-Dimensional Radiation Therapy: Conformal Radiotherapy, Radiosurgery and Treatment Planning* (Institute of Physics Publishing, Bristol, 1993).
2. N. Metropolis, A. W. Rosenbluth, M. N. Rosenbluth, A. H. Teller, and E. Teller, "Equations of state calculations by fast computing machines," *J. Chem. Phys.* **21**, 1087–1092 (1953).
3. S. Kirkpatrick, C. D. Gelatt, and M. P. Vecci, "Optimisation by simulated annealing," *Science* **220**, 671–680 (1983).

4. S. Geman and D. Geman, "Stochastic relaxation, Gibbs distributions, and Bayesian restoration of images," *IEEE Trans. Patt. Anan. Mach. Int.* **PAMI6**, 721–741 (1984).
5. W. Jeffrey and R. Rosner, "Optimisation algorithms: Simulated annealing and neural network processing," *Astrophys. J.* **310**, 473–481 (1986).
6. W. H. Press, B. P. Flannery, S. A. Teukolsky, and W. T. Vetterling, *Numerical Recipes: The Art of Scientific Computing* (Cambridge University Press, Cambridge, 1986).
7. L. T. Willie. "Searching potential energy surfaces by simulated anealing," *Nature* **324**, 46–48 (1986).
8. N. Radcliffe and G. Wilson, "Natural solutions give their best," *New Scientist* **14th April**, 47–50 (1990).
9. W. H. Press and S. A. Teukolsky, "Simulated annealing optimisation over continuous spaces," *Comput. Phys.* **5**, 426–429 (1991).
10. H. Barrett, H. B. Barber, P. A. Ervin, K. J. Myers, R. G. Paxman, W. E. Smith, W. J. Wild, and J. M. Woolfenden, "New directions in coded-aperture imaging," in *Information Processing in Medical Imaging*. F. Deconinck, Ed., Martinus Nijhoff, Boston 1983, pp. 106–129.
11. R. G. Paxman, H. H. Barrett, W. E. Smith, and T. D. Milster, "Image reconstruction from coded data. 2: Code design," *J. Optical Soc. Amer.* **A2**, 501–509 (1985).
12. W. E. Smith, R. G. Paxman, and H. H. Barrett, "Image reconstruction from coded data. 1: reconstruction algorithms and experimental results," *J. Optical Soc. Amer.* **A2**, 491–500 (1985).
13. S. Webb, "SPECT reconstruction by simulated annealing," *Phys. Med. Biol.* **34**, 259–281 (1989).
14. S. Webb, "Optimisation of conformal radiotherapy dose distributions by simulated annealing," *Phys. Med. Biol.* **34**, 1349–1369 (1989).
15. S. Webb, "Inverse tomograph," *Nature* **344**, 284 (1990).
16. S. Webb, "A new dose optimising technique using simulated annealing," Proc. 9th Annual Meeting of ESTRO, Montecatini Sept. 1990, Leuven: ESTRO, p. 263.
17. S. Webb, "Optimisation by simulated annealing of three-dimensional conformal treatment planning for radiation fields defined by a multileaf collimator: 2. Inclusion of two-dimensional modulation of the X-ray intensity," *Phys. Med. Biol.* **37**, 1689–1704 (1992).
18. S. Webb, "Optimising dose with a multileaf collimator for conformal radiotherapy," Proc. of the 50th Annual Congress of the British Institute of Radiology, Birmingham, May 18–20 1992, London: BIR 1992, p. 15.
19. S. Webb, "Optimised three dimensional treatment planning for volumes with concave outlines, using a multileaf collimator," Proc. ART91 Munich, April 1991 (abstract book p. 66), in *Advanced Radiation Therapy: Tumour Response Monitoring and Treatment Planning*. A. Breit, Ed. Springer, Berlin 1992, pp. 495–502.
20. S. Webb, "Techniques for optimisation of dose with a multileaf collimator for conformal radiotherapy of target volumes with concave outlines," in *Three-Dimensional Treatment Planning*, P. Minet, Ed. and Publisher (Proceedings of the E.A.R. Conference in Geneva at W.H.O., October 1992), pp. 163–172.
21. S. Webb, "Tomotherapy and beamweight stratification," Proc. 11th I.C.C.R., Manchester, March 1994, in "*The use of computers in radiation therapy*" ed A. R. Hounsell et al p 58–59, Pub. Manchester ICCR.
22. S. Webb, "Optimising the planning of intensity-modulated radiotherapy," *Phys. Med. Biol.* **39**, 2229–2246.
23. R. Mohan, G. S. Mageras, B. Baldwin, L. J. Brewster, G. J. Kutcher, S. Leibel, C. M. Burman, C. C. Ling, and Z. Fuks, "Clinically relevant optimisation of 3D conformal treatments," *Med. Phys.* **19**, 933–944 (1992).
24. M. Oldham and S. Webb, "Optimisation by fast simulated annealing of three-dimensional conformal treatment plans of the prostate and theoretical limits of improvement in TCP and NTCP," *Br. J. Radiol.*, in press.
25. H. Szu, "Fast simulated annealing," AIP Conf. Proc. Neural Networks for Computing, Snowbird, UT, Apl 1986 151, 420–425, 1987.
26. H. Szu and R. Hartley, "Fast simulated annealing," *Phys. Lett.* **A122**, 157–162 (1987).
27. S. Webb, "Optimisation by simulated annealing of three-dimensional conformal treatment planning for radiation fields defined by a multileaf collimator," *Phys. Med. Biol.* **36**, 1201–1226 (1991).
28. S. Webb, "Optimisation of conformal radiotherapy dose distributions by simulated annealing 2: Inclusion of scatter in the 2D technique," *Phys. Med. Biol.* **36**, 1227–1237 (1991).
29. A. Silverman and J. Adler, "Animated simulated annealing," *Comput. Phys.* **6**, 277–281 (1992).
30. R. Mohan, "Clinically relevant optimisation of 3D conformal treatments," in *The Use of Computers in Radiation Therapy: Proceedings of the 10th International Conference on the Use of Computers in Radiation Therapy*. S. Hukku and P. S. Iyer Lucknow, Eds. ICCR Lucknow 1990, pp. 36–39.
31. G. S. Mageras and R. Mohan, "Application of fast simulated annealing to optimisation of conformal radiation treatments," *Med. Phys.* **20**, 639–647 (1992).

Exhibit D

IN THE UNITED STATES DISTRICT COURT

FOR THE DISTRICT OF DELAWARE

BEST MEDICAL INTERNATIONAL, INC.,	)	
	)	
Plaintiff,	)	
	)	
v.	)	C.A. No. 18-1599-MN
	)	
VARIAN MEDICAL SYSTEMS, INC. and VARIAN MEDICAL SYSTEMS INTERNATIONAL AG,	)	
	)	
Defendants.	)	

LETTER OF REQUEST FOR INTERNATIONAL JUDICIAL ASSISTANCE PURSUANT TO THE HAGUE CONVENTION OF 18 MARCH 1970 ON THE TAKING OF EVIDENCE ABROAD IN CIVIL OR COMMERCIAL MATTERS

The United States District Court for the District of Delaware presents its compliments to the appropriate judicial authority of the United Kingdom, and requests international judicial assistance to obtain evidence to be used in a civil proceeding before this Court in the above-captioned matter. A trial on this matter is scheduled at present for August 23, 2021, in Wilmington, Delaware. This request is made pursuant to Article 1 of the Hague Convention of 18 March 1970 on the Taking of Evidence Abroad in Civil or Commercial Matters (the "Hague Evidence Convention").

The Court requests the assistance described herein as necessary in the interests of justice. Specifically, this matter is a patent case, and the Court requests that appropriate judicial authority of the United Kingdom compel the production of documentary evidence and deposition testimony from the Institute of Cancer Research, London ("ICR"), 123 Old Brompton Road, Kensington, London Sw7 3RP, United Kingdom, regarding a medical treatment system developed at ICR that may be prior art to one or more of the asserted patents.

1. Sender

The Honorable Maryellen Noreika
United States District Court for the District of Delaware
J. Caleb Boggs Federal Building
844 N. King Street
Wilmington, DE 19801-3555
USA

2. Central Authority of the requested state

The Senior Master
For the attention of the Foreign Process Section
Room E16
Royal Courts of Justice
Strand
London WC2A 2 LL
United Kingdom

3. Person to whom the executed request is to be returned

Defendants' counsel:

Ryan K. Wong
KEKER, VAN NEST & PETERS LLP
633 Battery Street
San Francisco, CA 94111
USA

4. Specification of the date by which the requesting authority requires receipt of the response to the Letter of Request: **March 13, 2020**.

IN CONFORMITY WITH ARTICLE 3 OF THE HAGUE EVIDENCE CONVENTION, THE UNDERSIGNED APPLICANT HAS THE HONOR TO SUBMIT THE FOLLOWING REQUEST:

5. a. Requesting judicial authority (Article 3, *a*):

The Honorable Maryellen Noreika
United States District Court for the District of Delaware
J. Caleb Boggs Federal Building
844 N. King Street
Wilmington, DE 19801-3555
USA

b. To the competent authority of (Article 3, *a*):

The Senior Master
For the attention of the Foreign Process Section
Room E16
Royal Courts of Justice
Strand
London WC2A 2 LL
United Kingdom

c. Names of the case and any identifying number:

Best Medical International, Inc. v. Varian Medical Systems, Inc. and Varian Medical Systems International AG
Civil Action Number 18-1599-MN
United States District Court for the District of Delaware

6. Names and addresses of the parties and their representatives (Article 3, *b*)

Plaintiff:

Best Medical International, Inc.
7643 Fullerton Road
Springfield, Virginia 22153
USA

Plaintiff's U.S. legal representative:

Philip Hirschhorn
BUCHANAN INGERSOLL & ROONEY PC
640 5th Avenue, 9th Floor
New York, NY 10019-6102
USA

Defendants:

Varian Medical Systems, Inc.
3100 Hansen Way
Palo Alto, CA 94304
USA

Varian Medical Systems International AG
Hinterbergstrasse 14
6312 Steinhausen
Switzerland

Defendants' U.S. legal representative:

Ryan K. Wong
KEKER, VAN NEST & PETERS LLP
633 Battery Street
San Francisco, CA 94111
USA

Other parties: None

7. Nature of the proceedings, summary of complaint, and summary of defenses (Article 3, *c*):

Plaintiff Best Medical, Inc. ("BMI") accuses defendants Varian Medical Systems, Inc. and Varian Medical Systems International AG ("Varian") of infringing four asserted patents: U.S. Patent Nos. 7,266,175, 7,015,490, 6,038,283, and 6,393,096. BMI amended its complaint on September 9, 2019, and Varian has moved to dismiss certain allegations in the amended complaint regarding indirect and willful infringement.

8. Evidence to be obtained and purpose of the evidence sought (Article 3, *d*):

a. Evidence to be obtained

i. Documents sufficient to show the conception, design, and development of the following aspects of the computer optimization program developed under Computer Vision in Radiology (COVIRA), project A2003 of the AIM (Advanced Informatics in Medicine) program of the European Union, of which ICR was a participant (the "COVIRA Algorithm"), which was used in the IMRT treatment planning systems at ICR and is more fully disclosed in Mark Oldham, Anthony Neal, Steve Webb, *A Comparison of Conventional 'Forward Planning' With Inverse Planning for 3D Conformal Radiotherapy of the Prostate*, 35 Radiotherapy & Oncology 248 (1995), attached hereto as Attachment A-1, before May 27, 1998, and if such documents exist, before October 24, 1996:

cost function computation;

cost function minimization (including, *inter alia*, use of simulated annealing, logic for accepting or rejecting a beam-weight set on a given iteration, and logic for stopping the iteration);

use of partial volume data or dose volume constraints;

use of dose volume histograms;

importance factors; and

user interface(s) for receiving optimization input.

ii. Documents sufficient to identify each version of the COVIRA Algorithm in use before May 27, 1998, and if such documents exist, before October 24, 1996, the release date for each version, and differences between each version with respect to the aspects of the COVIRA Algorithm identified in Request No. i.

iii. Documents sufficient to show the design, operation, and functionality of the aspects of the COVIRA Algorithm identified in Request No. i for each version identified in response to Request No. ii.

iv. Documents sufficient to show that each version of the COVIRA Algorithm identified in response to Request No. ii was publicly available and/or in use anywhere in the world before May 27, 1998, and if such documents exist, before October 24, 1996, such as academic journal articles, industry publications, press releases, product specifications, manuals, user guides, brochures, and/or web pages describing or identifying that version of COVIRA and its availability.

v. Documents sufficient to identify any apparatus, system, or device using the COVIRA Algorithm before May 27, 1998, and if such documents exist, before October 24, 1996. This request may include the VIRTUOS System.

vi. Documents and communications sufficient to show the design, structure, function, operation, and availability of each apparatus, system, or device identified in response to Request No. v.

vii. Documents and communications sufficient to show the sale, offer for sale, or importation into the United States of each apparatus, system, or device identified in response to Request No. v before May 27, 1998, and if such documents exist, before October 24, 1996.

viii. Documents sufficient to show the conception, design, and development of the following aspects of the simulated annealing technique developed and implemented at ICR (the "Simulated Annealing Implementation"), as disclosed in S. Webb, *Optimization Radiation Therapy Inverse Treatment Planning Using the Simulated Annealing Technique*, 6 Int'l J. Imaging Sys. & Tech. 71 (1995), attached hereto as Attachment A-2, before May 27, 1998, and if such documents exist, before October 24, 1996:

cost function computation;

cost function minimization (including, *inter alia*, use of simulated annealing, logic for accepting or rejecting a beam-weight set on a given iteration, and logic for stopping the iteration);

use of partial volume data or dose volume constraints;

use of dose volume histograms;

importance factors; and

user interface(s) for receiving optimization input.

ix. Documents sufficient to identify each version of the Simulated Annealing Implementation in use before May 27, 1998, and if such documents exist, before October 24, 1996, the release date for each version, and differences between each version with respect to the aspects of the Simulated Annealing Implementation identified in Request No. viii.

x. Documents sufficient to show the design, operation, and functionality of the aspects of the Simulated Annealing Implementation identified in Request No. viii for each version identified in response to Request No. ix.

xi. Documents sufficient to show that each version of the Simulated Annealing Implementation identified in response to Request No. ix was publicly available and/or in use anywhere in the world before May 27, 1998, and if such documents exist, before October 24, 1996, such as academic journal articles, industry publications, press releases, product specifications, manuals, user guides, brochures, and/or web pages describing or identifying that version of the Simulated Annealing Implementation and its availability.

xii. Documents sufficient to identify any apparatus, system, or device using the Simulated Annealing Implementation before May 27, 1998, and if such documents exist, before October 24, 1996. This request may include the VIRTUOS System.

xiii. Documents and communications sufficient to show the design, function, operation, and availability of each apparatus, system, or device identified in response to Request No. xii.

xiv. Documents and communications sufficient to show the sale, offer for sale, or importation into the United States of each apparatus, system, or device identified in response to Request No. xii before May 27, 1998, and if such documents exist, before October 24, 1996.

b. Purpose of the evidence sought

The documents sought by these requests are directly relevant to the above-captioned litigation. These requests seek documents regarding specific features of a medical treatment system developed at ICR, which may be prior art to one or more of BMI's asserted patents under 35 U.S.C. § 102. If obtained, Varian would use these documents to develop its invalidity defenses for trial, and may rely on the documents to seek invalidation of one or more asserted patents.

9. Identity and address of any person to be examined (Article 3, *e*):

The Court requests that the Institute of Cancer Research, London ("ICR"), 123 Old Brompton Road, Kensington, London Sw7 3RP, United Kingdom, designate one or more witnesses who are knowledgeable about the subject matter identified in section 10 below.

10. Statement of the subject matter about which the persons are to be examined (Article 3, *f*):

i. The conception, design, development, operation, and functionality of the aspects of the COVIRA Algorithm and the Simulated Annealing Implementation set forth in Document Request Nos. i and viii before the date(s) specified in Document Request Nos. i and viii.

ii. Each version of the COVIRA Algorithm and the Simulated Annealing Implementation in use before the date(s) specified in Document Request Nos. i and viii, and the release date for each version.

iii. The date and circumstances of the first sale, offer for sale, and/or public use in the United States of the COVIRA Algorithm and the Simulated Annealing Implementation set forth in Document Request No. i and viii before the date(s) specified in Document Request Nos. i and viii.

iv. The identity, design, operation, and functionality of any apparatus, system, or device using the aspects of the COVIRA Algorithm and the Simulated Annealing Implementation set forth in Document Request Nos. i and viii before the date(s) specified in Document Request Nos. i and viii.

v. The date and circumstances of the first sale, offer for sale, and/or public use in the United States of any apparatus, system, or device covered by Deposition Topic No. iv.

vi. The authenticity of documents produced in response to this Letter of Request, the public availability and publication dates of documents produced in response to this Letter of Request, the creation and authorship of documents produced in response to this Letter of Request, and whether and how the documents produced in response to this Letter of Request were created and/or stored in the ordinary course of business.

11. Any requirement that the evidence be given on oath or affirmation and any special form to be used (Article 3, *h*):

Because the testifying witnesses are outside this Court's subpoena power and cannot be compelled to attend trial, the Court requests that the witnesses' testimony be taken under oath in such manner as provided by the laws of the United Kingdom for the formal taking of evidence.

12. Special methods or procedure to be followed (Articles 3, *i* and 9):

The Court requests that the testimony be taken by oral examination in such manner as provided by the laws of the United Kingdom for the formal taking of evidence. To the extent permitted by the laws of United Kingdom, the Court requests that the testimony be recorded by a videographer and transcribed by a stenographer.

13. Request for notification of the time and place for the execution of the Request and identity and address of any person to be notified (Article 7):

Please notify defendants' U.S. legal counsel at the following address:

Ryan K. Wong
KEKER, VAN NEST & PETERS LLP
633 Battery Street
San Francisco, CA 94111
USA

14. Specification of privilege or duty to refuse to give evidence under the law of the State of origin (Article 11, *b*):

Nothing in this Letter of Request is intended to interfere with any rights of MRC to assert privilege or refuse to give evidence under any applicable law of the United Kingdom or the United States of America.

15. Fees and costs

If the Senior Master incurs fees or costs in executing this Letter of Request that are reimbursable under the second paragraph of Article 14 or Article 26 of the Hague Evidence Convention, the Court requests that the Senior Master submit a bill of fees and costs to the Court and defendants' U.S. legal counsel:

Ryan K. Wong
KEKER, VAN NEST & PETERS LLP
633 Battery Street
San Francisco, CA 94111
USA

The Court guarantees that defendants' counsel will reimburse the Senior Master for all reimbursable fees and costs incurred in executing this Letter of Request.

This Court expresses its gratitude to the authorities of the United Kingdom for assisting with this Letter of Request, and will provide similar assistance to the judicial authorities of the United Kingdom when requested.

DATE OF REQUEST: _____

SIGNATURE AND SEAL OF THE REQUESTING AUTHORITY

_____
The Honorable Maryellen Noreika
United States District Judge

ATTACHMENT A-1

VOL. 35, NO. 3 JUNE 1995 ISSN 0167-8140
RAONDT (35) 177–274 (1995)

RADIOTHERAPY & ONCOLOGY

Journal of the European Society for Therapeutic Radiology and Oncology

ELSEVIER

Radiotherapy and Oncology, 1995, Volume 35, Number 3, June, pp. 177–274

CONTENTS

Cited in: Chemical Abstracts, Excerpta Medica (EMBASE), Current Contents (Clinical Medicine; Life Sciences), Index Medicus (MEDLINE), Current Awareness in Biological Sciences (CABS)

Original Papers

Epidermoid carcinomas of the floor of mouth treated by exclusive irradiation: statistical study of a series of 207 cases
M. Pernot, S. Hoffstetter, D. Peiffert, E. Luporsi, C. Marchal, P. Kozminski, D. Dartois, P. Bey (France) 177

Indications, techniques and results of postoperative brachytherapy in cancer of the oral cavity
M. Pernot, P. Aletti, J.M. Carolus, I. Marquis, S. Hoffstetter, F. Maaloul, D. Peiffert, M. Lapeyre, E. Luporsi, C. Marchal, A. Noël, P. Bey (France) 186

Low dose rate versus high dose rate intraluminal brachytherapy for malignant endobronchial tumors
T.C.M. Lo, L. Girshovich, G.A. Healey, J.F. Beamis, Jr., D.C. Webb-Johnson, A.G. Villanueva, A.W. Gray, Jr., T.R. Wu (USA) 193

Postoperative radiotherapy in carcinoma of the cervix: treatment results and prognostic factors
G. Atkovar, Ö. Uzel, M. Özşahin, S. Koca, İ. Şahinler, S. Okkan, R. Uzel (Turkey) 198

Radiation treatment of cervical lymph node metastases from an unknown primary: an analysis of outcome by treatment volume and other prognostic factors
L. Weir, T. Keane, B. Cummings, P. Goodman, B. O'Sullivan, D. Payne, P. Warde (Canada) 206

Intrarectal formalin application, an effective treatment for grade III haemorrhagic radiation proctitis
B.M. Biswal, P. Lal, G.K. Rath, N.K. Shukla, B.K. Mohanti, S. Deo (India) 212

Toxicity, biodistribution and radioprotective capacity of L-homocysteine thiolactone in CNS tissues and tumors in rodents: comparison with prior results with phosphorothioates
A.M. Spence, J.S. Rasey, L. Dwyer-Hansen, Z. Grunbaum, J. Livesey, L. Chin, N. Nelson, D. Stein, K.A. Krohn, F. Ali-Osman (USA) 216

A mathematical model of the volume effect which postulates cell migration from unirradiated tissues
H. Shirato, M. Mizuta, K. Miyasaka (Japan) 227

Clinical implementation of an objective computer-aided protocol for intervention in intra-treatment correction using electronic portal imaging
F. Van den Heuvel, W. De Neve, D. Verellen, M. Coghe, V. Coen, G. Storme (Belgium) 232

A diagnostic-quality electronic portal imaging system
R. Sephton, J. Hagekyriakou (Australia) 240

A comparison of conventional 'forward planning' with inverse planning for 3D conformal radiotherapy of the prostate
M. Oldham, A. Neal, S. Webb (UK) 248

ESTRO Meetings 263
ESTRO Courses 264
Calendar of Events 265

Volume contents 268
Author index 271
Subject index 273

0167-8140(199506)35:3;1-7

ELSEVIER

Radiotherapy and Oncology 35 (1995) 248–262

RADIOTHERAPY & ONCOLOGY

A comparison of conventional 'forward planning' with inverse planning for 3D conformal radiotherapy of the prostate

Mark Oldham*, Anthony Neal, Steve Webb

Joint Department of Physics, Institute of Cancer Research and the Royal Marsden Hospital, Downs Road, Sutton, Surrey, SM2 5PT, UK

Received 6 October 1994; revision received 20 March 1995; accepted 27 March 1995

Abstract

A radiotherapy treatment plan optimisation algorithm has been applied to 48 prostate plans and the results compared with those of an experienced human planner. Twelve patients were used in the study, and 3-, 4-, 6- and 8-field plans (with standard coplanar beam angles for each plan type) were optimised by both the human planner and the optimisation algorithm. The human planner 'optimised' the plan by conventional forward planning techniques. The optimisation algorithm was based on fast simulated annealing using a cost-function designed to achieve a homogenous dose in the 'planning-target-volume' and to minimise the integral dose to the organs at risk. 'Importance factors' assigned to different regions of the patient provide a method for controlling the algorithm, and it was found that the same values gave good results for almost all plans. A study of the convergence of the algorithm is presented and optimal convergence parameters are determined. The plans were compared on the basis of *both* dose statistics and 'normal-tissue-complication-probability' (NTCP) and 'tumour-control-probability' (TCP). The results of the comparison study show that the optimisation algorithm yielded results that were at least as good as the human planner for all plan types, and on the whole slightly better. A study of the beam-weights chosen by the optimisation algorithm and the planner revealed differences that increased with the number of beams in the plan. The planner was found to make small perturbations about a conceived optimal beam-weight set. The optimisation algorithm showed much greater variation, in response to individual patient geometry, frequently deselecting certain beams altogether from the plan. The algorithm is shown to be a useful tool for radiotherapy treatment planning. For simple (e.g., three-field) plans it was found to consistently achieve slightly higher TCP and lower NTCP values. For more complicated (e.g., eight-field) plans the optimisation also achieved slightly better results with generally less numbers of beams, unfavourable beams being deselected from the plan. Probably the greatest benefit is the reduced time taken by the optimisation to compute optimised beam-weights. This time was always ≤ 5 min; a factor of up to 20-times faster than the human planner.

Keywords: Conformal therapy; Treatment planning; Optimisation; Biological modelling; Simulated annealing

1. Introduction

The aim of conformal radiotherapy is to achieve tumour control with as low normal tissue morbidity as possible. In terms of radiation-dose, and making the assumption of uniform clonogenic cell density within the PTV, this goal translates to achieving a high uniform dose throughout the planning target volume (PTV) and as low a dose as possible elsewhere, specifically in organs at risk (OAR). With the advent of computer controlled multileaf collimators attached to computer controlled linacs, conformal radiotherapy is entering a new era with the possibility of significant improvement in treatment delivery. It is now becoming feasible to deliver plans with large numbers of beams, each shaped to the beam's eye view of the PTV, in reasonable times under computer control [8].

The technical ability to implement more complicated plans presents a new challenge to the treatment planner who traditionally has used 'forward planning' (manual trial-and-error based on informed experience) to calculate the best field arrangements and beam-weights. Whilst forward planning is acceptable for plans with only a few fields, the process becomes impossibly

* Corresponding author.

0167-8140/95/$09.50
SSDI 0167-8140(95)01556-V

tedious for plans with larger numbers of fields [23]. Much effort has been devoted recently to the challenge of designing algorithms to compute optimised beam-weights for such complicated plans [2,4,6,7,9,10, 13–22,24,27–30].

To date, the majority of these new algorithms and planning techniques have illustrated their potential with the application to just one or two sample cases. Our own developments have been no exception [20,21,27–30]. This paper presents a detailed study comparing the performance of an inverse optimisation algorithm with conventional planning techniques over a wide range of patient cases. The aim of the study was to investigate the effectiveness, reliability, and time saving potential of an optimisation algorithm which has been under development at the Royal Marsden Hospital over the past 4 years. The algorithm is inverse in the sense that a dose prescription is specified a priori, and an algorithm used to work backwards to find the dose distribution (and corresponding beam-weights) that match as closely as possible the prescription. Details of the algorithm (COVIRAOPT) have already been published [20] and it remains the same except for some minor modifications which are discussed in the text. COVIRAOPT has been developed under the European COVIRA programme (see Acknowledgements).

The optimisation algorithm we have developed currently only has the facility to optimise beam-weights and wedge angles. Ideally it would also optimise the orientation and energy of the beams, and even the number of beams in the plan. These last facilities are the subject of current research but are not simple problems to solve. In this paper we have used the algorithm solely to optimise the beam-weights of plans that have been pre-defined by a human planner. The planner used standard beam arrangements on which to base his plans but was free to individually customise the wedge angle and the beam orientation for each patient as required. This procedure is the same as that used in the clinic. The inclusion of wedge angle optimisation will be the subject of later work. This paper is primarily concerned with evaluating the likely benefits associated with optimising the beam-weights of predefined, standard plans.

2. Method

2.1. The optimisation algorithm

To optimise the beam-weights of an arbitrary treatment plan, a numerical method is employed to find the set of beam-weights that corresponds to the minimum of a cost function. The cost function is a measure of fit between a dose distribution and some ideal, user-specified, dose distribution. In this paper the numerical method used is fast simulated annealing (FSA) with zero temperature [25,13] and the cost function is based on attaining a uniformly homogenous dose in the planning target volume (PTV) and minimising the integral doses to the organs at risk (OAR). Full details of both the numerical method and the cost function are given in [20], and here only a brief overview is included highlighting some modifications that have been made.

2.1.1. Fast simulated annealing with zero temperature

The numerical method used to find the cost-function minimum was fast simulated annealing. In this iterative method, at each iteration all beam-weights are independently perturbed by adding a 'grain' of beam-weight which is selected randomly from a Cauchy distribution. (The grains are randomly positive or negative and hence individual beam-weights can independently increase or decrease, the only restriction being that the beam-weight must remain zero or positive.) A cost function is evaluated for the current beam-weight set and compared to the running cost-function value (i.e., the lowest cost-function value found from previous iterations). If the new cost function is lower than the running value, then the running value is set equal to the new value and the new beam-weight set is stored. If the new cost-function value is greater than the running value then no change is made to the running value and the algorithm moves to the next iteration.

In this manner the algorithm finds beam-weight sets that successively converge to that set which corresponds to the minimum of the cost function. There are two differences between the method outlined above and that of our previous paper [20]. The first is that all beam-weights are now perturbed at each iteration (or cost-function evaluation) instead of just one beam-weight per iteration. This change was made in accordance with the approach of [13] and allows for more efficient convergence. The second change is that no beam-weight sets that make the cost function greater are ever accepted. This is equivalent to setting the temperature to zero in FSA, thereby disallowing all up-hill changes. For the linear-quadratic cost function used in this paper (Section 2.1.2), there is only a single minimum, and therefore the acceptance of up-hill changes to escape from local minima is not required. This approach applied to a biological cost function has previously been investigated [13] and it was found that even if local minima are present there is no need to accept up-hill changes with FSA because of an alternative 'tunnelling' mechanism. Tunnelling arises because of the broad wings of the Cauchy distribution which allow occasional large grains to be selected.

In this scenario (FSA with zero temperature) the efficiency of the optimisation depends only on the Cauchy probability distribution from which the grains of beam-weight are selected. This distribution gradually collapses as the iterations increase so as to more finely probe the cost-function structure near the minimum. The collapse

of the distribution is controlled by the parameter $W(n)$, the full-width at half-maximum of the distribution, which varies according to Eq. 1 [20].

$$W(n) = \frac{W(0)}{(1 + n/R)} \quad (1)$$

In Eq. 1, $W(0)$ is the full-width at half-maximum at the start of the optimisation, n is the iteration number and R is a constant that controls the speed with which the distribution collapses. Appropriate values of R to produce efficient convergence are determined in Section 2.3.1.

2.1.2. Cost-function structure

The minimum of the cost function defines the theoretical ideal dose distribution (and beam-weight set) which the optimisation algorithm attempts to achieve. It is therefore critical that the cost function should reflect what is clinically desired in each different region of the patient. In accord with our previous paper [20], the cost function was segmented into component terms from each of the regions PTV, OAR and BODY (i.e., all tissue that is not in the PTV or in an OAR). The following mathematical formulae were used, reflecting the desired clinical dose to each region.

$$C_{\mathrm{PTV}} = \Sigma_{i \text{ in PTV}} (D_i - 100)^2 \quad (2)$$

$$C_{\mathrm{OAR}} = \Sigma_{i \text{ in OAR}} (D_i) \quad (3)$$

$$C_{\mathrm{BODY}} = \Sigma_{i \text{ in BODY}} (D_i) \quad (4)$$

where D_i is the dose to the ith cubic voxel of each segmented region. The figure 100 appearing in Eq. 2 represents the desired 100% uniform dose to the PTV. The quadratic cost function is used in Eq. 2, as opposed to the modulus for example, because it is inherently better at controlling the dose in extreme regions (either very hot or cold).

A useful feature of the linear OAR and BODY cost function terms is that the voxel summation need only be done once, for each beam, at the start of the optimisation. All future changes in the C_{OAR} and C_{BODY} terms due to the addition of a grain of beam-weight can simply be calculated by multiplying the 'global' contribution of that beam, for unit weight, by the grain size. This shortcut leads to a reduction of about a factor 30 in the computation time necessary to evaluate the cost function. For plans with ≥ 4 beams, almost all the computer time taken to optimise the plan comes from evaluating the cost function over many iterations and therefore this is a significant time saving.

The component terms (2)–(4) were merged linearly to form the total cost function (Eq. 5). Each term was weighted by an 'importance factor' to define its relative importance at the start of the optimisation. In Eq. (5), n is the iteration number, the subscript ST denotes the starting value of the term (i.e., at $n = 1$), and m is the number of OARs. (Note, the value of the $\mathrm{WEIGHT_{OAR}}$ factor can be arbitrarily set for each OAR.)

$$C_{\mathrm{TOTAL}}(n) = \mathrm{WEIGHT_{PTV}} \times C_{\mathrm{PTV}}(n)/C_{\mathrm{PTVST}}(1) + \sum_{j=1}^{m} (\mathrm{WEIGHT_{OAR}}_j \times C_{\mathrm{OAR}_j}(n)/C_{\mathrm{OARST}_j}(1)) + \mathrm{WEIGHT_{BODY}} \times C_{\mathrm{BODY}}(n)/C_{\mathrm{BODYST}}(1) \quad (5)$$

Minimising the cost function C_{TOTAL} thus corresponds to minimising the integral dose in the OAR and BODY regions, while attempting to achieve a uniform dose of 100% in the PTV. Although of simple design, without the sophistication to model complicated volume effects, the cost function is designed to be effective at differentially reducing the dose received by segmented regions. The algorithm and cost function should therefore be effective for tumours at locations other than the prostate via judicious choice of importance factors.

2.2. The patient data set

The 12 patients in the study were all diagnosed with early prostate cancer (either stage T1 or T2), and underwent a pelvic CT scan as part of their routine treatment planning. The CT data sets consisted of 5-mm contiguous axial images, acquired when the patient had a full bladder. The only difference with standard CT imaging protocol was that the number of CT slices per patient was extended so that the complete bladder was contained in the 3D data set. This was done for the purposes of calculating meaningful dose-volume histograms (DVH) and normal tissue-complication probabilities (NTCP) for the bladder. For each patient, the PTV was segmented in 3D by first outlining the gross tumour volume (macroscopic disease spread), then adding a margin of 5 mm to create the clinical target volume (including microscopic tumour spread), and finally adding a further 5 mm to create the PTV (this extra margin accounting for random and systematic treatment delivery and set-up errors). The rectum, bladder, and left and right femoral heads were also segmented in 3D. In most patients there was a small region which was classified as both PTV and rectum. In the optimisation algorithm, this overlap region was considered as being PTV only. The consequences of this overlap region have been explored in [20].

2.2.1. Conventional 'forward' treatment planning

For each patient, four plans were created by a human planner (A.J. Neal) using the fully 3D VIRTUOS (VIRTUal radiOtherapy Simulator) treatment planning system [1]. The plans consisted of a 3-, 4-, 6- and an 8-field plan (Fig. 1a–d). Beam configurations were adhered to whenever possible but gantry angles and

ANTERIOR

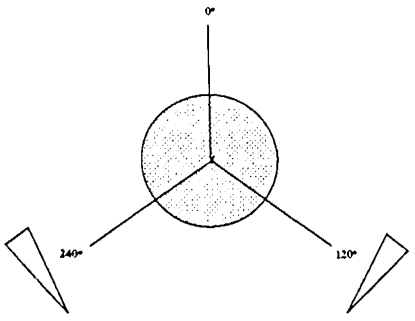

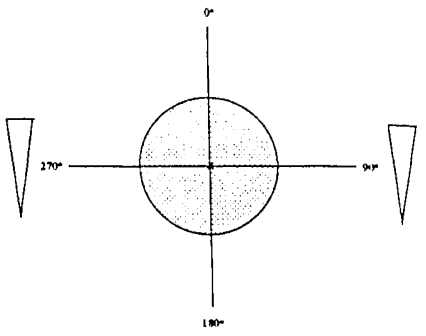

POSTERIOR

Fig 1a

Fig 1b

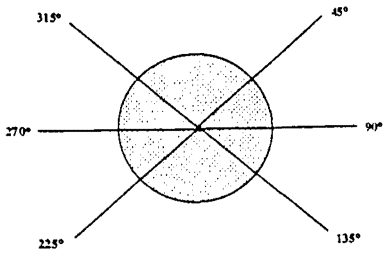

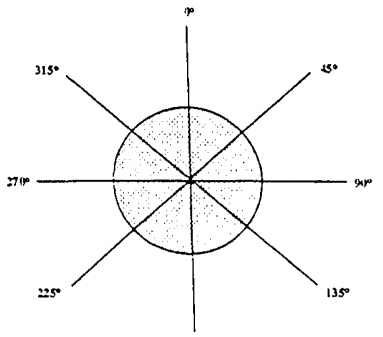

Fig 1c

Fig 1d

Fig. 1. (a) the 3-field arrangement of an anterior field and two posterior wedged oblique fields; (b) the 4-field arrangement of opposed anterior/posterior and right lateral/left lateral wedged fields; (c) the 6-field arrangement of opposed left anterior oblique/right posterior oblique fields, opposed right anterior oblique/left posterior oblique fields and opposed right lateral/left lateral fields; and (d) the 8-field arrangement as 6-field arrangement but with the addition of opposed anterior and posterior fields.

wedge compensators were adjusted individually to optimise the plan for that particular patient's anatomy. In all cases where the plan was adjusted, it was the adjusted plan that was also optimised by the algorithm. All fields were coplanar and shaped to the beam's eye view of the PTV. A margin of 6 mm around the PTV was added to allow for beam penumbra. This study was retrospective in that all the patients had been previously treated with 3-field wedged plans. The delivery plans were not necessarily exactly the same as the 3-field plans reproduced here because they were created using a different planning system, by a different planner.

Beam weights were iteratively adjusted, in the conventional forward planning manner, from an initial 'best guess' to give a satisfactory dose distribution. The acceptability of the plan was determined from isodoses overlaid upon the CT data in transverse, sagittal and coronal views. Priority was given to treating the PTV to a homogeneous dose, using the isocentre as a reference point. A PTV dose homogeneity of ±5% was aimed for. Once attained, consideration was given to reducing irradiation of the adjacent OARs. In practice, the bladder and rectum were considered to be the OARs which determined the acceptance or rejection of a particular plan. The femoral heads were considered in the comparison of plans but was not a major factor in the human optimisation of individual plans.

The dose calculation algorithm was of the Bentley-

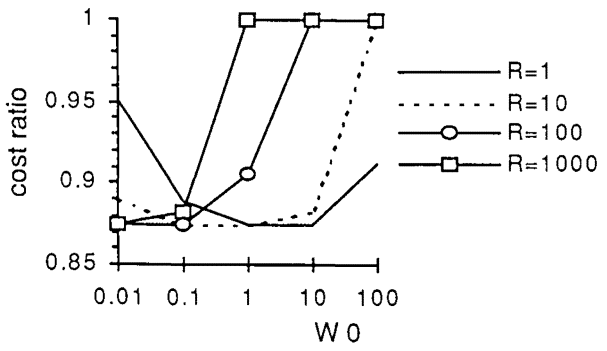

Fig. 2. Plot of the dependence of the cost ratio (the ratio of the final cost-function value to the starting cost-function value) on the annealing parameters $W(0)$ (the starting full-width–half-maximum of the Cauchy distribution), and R which is a constant that controls the speed of collapse of the distribution (Eq. 1).

Milan ray-tracing type which took into account tissue inhomogeneity for the primary beam, and equivalent field-size scatter effects. The effects of tissue inhomogeneity on the scatter was not modelled. The beam data used was that of 15-MV photons from a Siemens Mevatron 77 linear accelerator.

2.3. Optimised treatment planning

Before the optimisation algorithm was applied to the patient data set, suitable optimisation parameters needed to be found. These parameters fall into two categories; annealing parameters, and importance factors. The annealing parameters, $W(0)$ and R in Eq. 1, control the convergence of the optimisation and, if badly set, the algorithm may converge to a value that is not the minimum of the cost function in the allowed space, or converge ineffectively. The importance factors, $\text{WEIGHT}_{\text{PTV}}$, $\text{WEIGHT}_{\text{OAR}_i}$, and $\text{WEIGHT}_{\text{BODY}}$ (Eq. 5) determine the minimum of the cost function and thus the final beam-weights.

2.3.1. Finding suitable annealing parameters

A series of optimisation runs on the 3-field plan of an arbitrary patient were performed where the parameters $W(0)$ and R were varied over several orders of magnitude. These runs represented a coarse sampling to estimate $W(0)$, R combinations that produced fast convergence. Each run was allowed to progress for a 1000

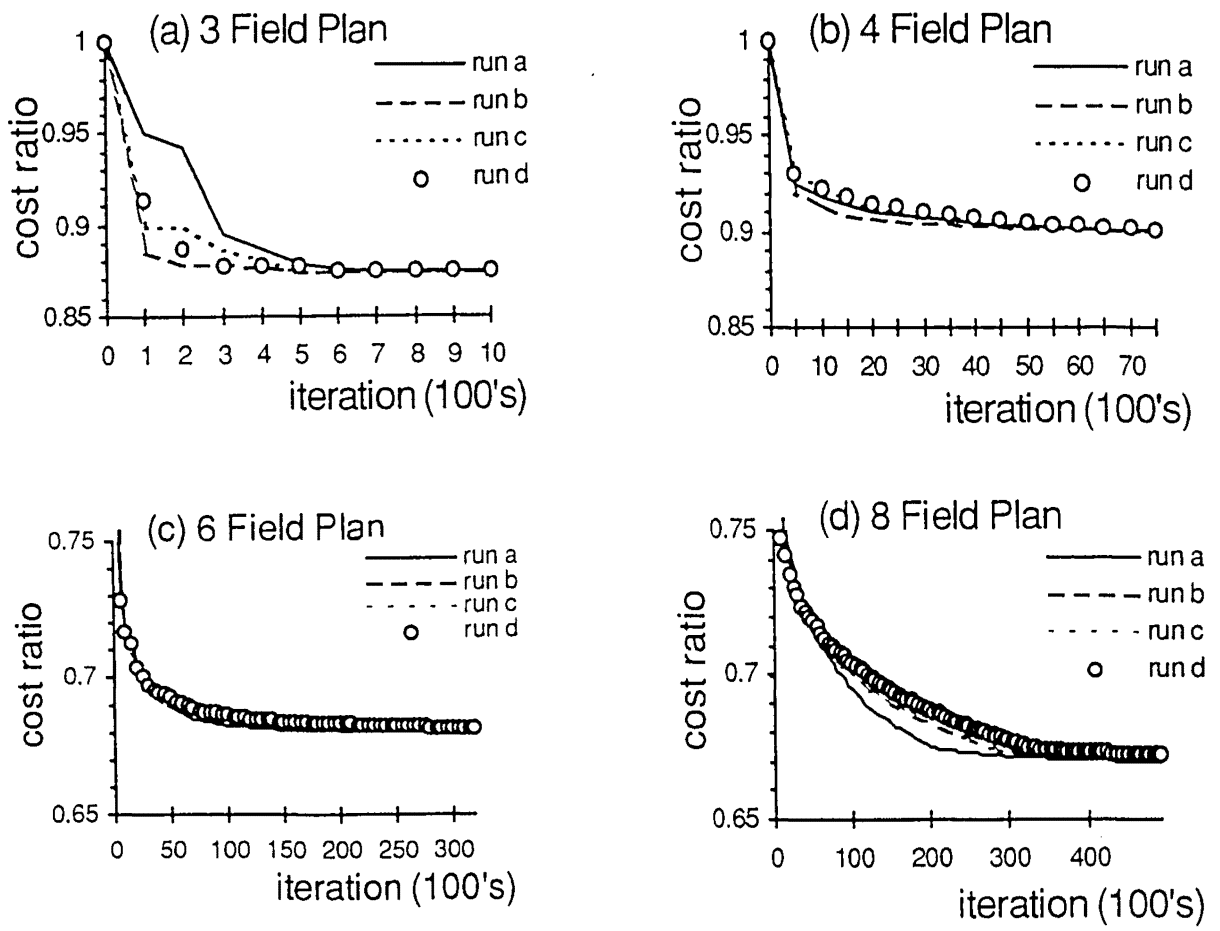

Fig. 3. Plots of the cost ratio (the ratio of the final cost-function value to the starting cost-function value), vs. iteration number, for four $W(0)$, R combinations. Runs a, b, c and d correspond to $W(0)$,R combinations of 0.01,1000; 0.05,100; 0.5,10; 5.0,1.

iterations and the efficiency of convergence was then quantified by evaluating the 'cost ratio', i.e., the ratio of the final cost function to the starting cost function. The plot of the value of the cost ratio after a 1000 iterations for different $W(0)$, R combinations is shown in Fig. 2. The cost function minimum in allowed space corresponds to the smallest value of the cost ratio which, for the 3-field plan of this patient is about 0.875. For some runs (i.e., $W(0)$, R combinations) it is clear that the algorithm has not found the minimum, indicating false convergence.

Four ($W(0)$, R) combinations were selected from Fig. 2 that all produced convergence to the minimum within the 1000 iterations. These four combinations (which were $W(0) = 0.01$, $R = 1000$ (run a); $W(0) = 0.05$, $R = 100$ (run b); $W(0) = 0.5$, $R = 10$ (run c); and $W(0) = 5.0$, $R = 1$ (run d)) were then studied further by plotting the cost ratio against iteration number for all four plan types (Fig. 3a–d). The aim was to find a parameter set that guaranteed fast convergence for all plan types. Fig. 3a–c shows that for the 3-, 4- and 6-field plans, despite initial differences in the rate of convergence, all four runs arrived at the minimum in roughly the same number of iterations. This indicates that for these few-beam plans, rapid collapse of the Cauchy distribution from an initially large $W(0)$ is equivalent to slow collapse from an initially small $W(0)$. In Fig. 3d a trend is seen that we have observed in all plans with more than eight fields, that of the fastest convergence being achieved by the runs with the slower collapse schedules (and correspondingly smaller $W(0)$ value). Fig. 3a–d indicates that all runs truly converged (given enough time) and therefore the algorithm is robust concerning the exact settings of the annealing parameters in this range.

Although the results shown here are for a single patient (this patient actually needed more iterations to converge than any others studied), a similar series of runs was also performed on the physically largest and smallest prostate patients, respectively. These runs confirmed the trends found in Fig. 3a–d, although there were slight inter-patient variations ($\leq 10\%$) in the number of iterations needed to reach the minimum. On the basis of Fig. 3a–d, the parameter values of run a ($W(0) = 0.01$, $R = 1000$) were selected as producing true convergence for all patients, for all plan types, in close to the minimum number of iterations possible. The final beam-weights produced by the optimisation algorithm thus correspond to the minimum of the cost function in allowed space and are independent of small variations in the parameter settings.

2.3.2. Finding suitable importance factors

In this paper we are interested in evaluating the performance of a practical and usable optimisation algorithm. The practicality of the algorithm would be severely reduced if it was necessary to individually adjust the importance factors (Eq. 5) for each patient and each plan type. The difficulty here is that in reality each patient may have a slightly different importance factor set that is 'optimal', depending on inter-patient variables like patient size, organ positioning, target size, etc. Furthermore the optimal set might be expected to vary between plan types with very different geometries (the 3- and 8-field plans for example). This section details work undertaken to identify a 'practical' importance factor set; practical in the sense of consistently giving good dose distributions over the 48 plans. (In the rest of the paper this importance factor set is referred to as the 'practical' set, and was used for all patients.)

An exhaustive study comparing the resulting dose distributions arising from all possible sets of importance factors, each set evaluated over 48 plans, is clearly not feasible. Instead, informed importance factor set 'guesses' were made and these then evaluated on the physically largest and smallest patients, hopefully ensuring the set would yield good results over as wide a range of patient geometry as possible. In practice it was found surprisingly easy to find a practical set that gave good dose distributions for both patients, for all four plan types. This set was arrived at after three 'guesses' shown in Table 1. (The first guess was loosely based on the perceived clinical importance of structures. Although the contour region obviously does not have zero importance, it was set to zero in order to give the algorithm a high degree of freedom. In subsequent tests we did not find it necessary to increase this value. The second and third guesses were refinements of the first guess, attempting to get a better dose distribution. All subsequent refinements after the third guess showed no benefit.)

Table 1
Three 'guesses' were necessary to identify a practical importance factor set that gave good results for all patients and all plan types in the patient data set

Guess	PTV	Rectum	Bladder	Femorals	Contour
1	2	20	5	1	0
2	10	10	5	1	0
3 (practical set)	18	20	5	1	0

The numbers refer to the importance factors guessed for that region of the patient.

Table 2
NTCP and TCP values for three importance factor set guesses for an arbitrary patient

Guess	B-NTCP	R-NTCP	LFH-NTCP	TCP	RFH-NTCP
1 (64 Gy)	<0.1	3.6	<0.1	86.1	<0.1
2 (64 Gy)	<0.1	3.4	<0.1	86.0	<0.1
3 (64 Gy)	<0.1	3.4	<0.1	86.0	<0.1
1	<0.1	5.0	<0.1	87.2	<0.1
2	<0.1	5.0	<0.1	87.4	<0.1
3	<0.1	5.0	<0.1	87.4	<0.1

The column heading notation (B-, R-, LFH- and RFH-) corresponds to the bladder, rectum, and left and right femoral heads, respectively. The first three rows correspond to when a dose of 64 Gy is prescribed to the isocentre. In the last three rows, the prescribed dose was scaled until a rectal NTCP of 5% was obtained.

The dose distribution corresponding to each guess was analysed primarily on the basis of TCP and NTCP values and also careful study of the DVH. (The calculation of TCP and NTCP is discussed in Section 2.4.). The greater reliance on NTCP and TCP numbers simply reflects the great time saving incurred over studying DVHs for a large patient data set. The NTCP and TCP values for the three guesses as applied to the largest patient are given in Table 2. Although the values are the same for guesses 2 and 3, and in all patients studied these two guesses gave very similar results, the latter was judged to be marginally superior on investigation of the DVH. The NTCP and TCP values of guess 1 are similar to those of guesses 2 and 3 because, even with a relatively low importance factor, the quadratic nature of the cost function in the PTV ensures a quite uniform dose. Further investigations into modifications of the practical importance factor set showed no improvement in the NTCP or TCP values for any of the plan types of the two patients selected for this evaluation. It was thus assumed that this set could be applied to all the patients in the data set.

2.4. Normal tissue-complication probability (NTCP) and tumour-control probability (TCP) computation

NTCP values were calculated using the Lyman model [12] combined with the DVH reduction scheme of Kutcher and Burman [11] and the biological parameters given in Burman et al. [5] (full details can be found in Oldham and Webb [20]). TCP was computed using the model of Webb and Nahum [31] (Eq. 6), with the values $\alpha = 0.547$, $\sigma_\alpha = 0.19$, clonogenic cell density = 10^7 per cm^3, and the number of patients averaged over to account for inter-patient variation in radio-sensitivity was 40 000 (guaranteeing a precision of $\leq 0.1\%$). It is stressed that these biological models are at an early stage of development. In the absence of good quality data, the parameters used in the model have been derived from a mixture of very sparse data and clinician's estimates [5]. The errors in absolute values of NTCP may be quite large. However, the models embody the general principles that are believed to approximate the response of organs to radiation. In this respect we have relied upon the models to rank dose distributions according to clinical benefit. The uncertainties in model parameters, we believe, will not affect the central conclusions of this paper which are based on comparative 'average rankings'.

$$\mathrm{TCP_{TOT}} = \frac{1}{K} \sum_{n=1}^{k} \left(\Pi_{i \text{ in PTV}} \, e^{-N_i e^{-\alpha_n D_i}} \right) \tag{6}$$

In Eq. 6, i is an index looping over voxels in the PTV, D_i and N_i are the dose and number of clonogenic cells of the ith voxel, respectively, and K is a number of the order 10^4 which represents averaging over a patient population. A discussion of the fitting of Eq. 6 to clinical data, and its use in predicting TCP is given in [20].

3. Results

Each of the four plan types for all patients were optimised according to the algorithm outlined above with the importance factors set to the practical set of Table 1 and with the appropriate annealing parameters R and $W(0)$ (Section 2.3.1). The optimised dose distributions were then compared with those obtained by the human planner on the basis of dose statistics in the PTV, dose-volume histograms for the OARs, and NTCP and TCP calculations. To determine any consistent, significant difference between the results obtained from the optimisation algorithm and those of the human planner, the mean of the individual patient differences, the 95% confidence interval of this mean, and a two-tailed paired Student's t-test were computed. The 95% confidence interval describes the magnitude of any effect and the t-test quantifies the statistical significance of the mean difference. For each plan the mean dose in the PTV (D), and standard deviation (σ_D) of the dose in the PTV about this mean was computed. σ_D represents the uniformity of dose in the PTV. The average standard deviation ($\bar{\sigma}_D$) over the 12 patients was computed as

Table 3
Comparison of the dose homogeneity in the PTV achieved by the human planner and the optimisation algorithm

	Average S.D.		Mean Diff	95% C.I. for	*P* value of
	$\overline{\sigma_D}$	$\sigma_{\overline{\sigma D}}$	$\overline{\delta}$	Mean diff.	Mean diff.
3-F Human	0.012 (0.001)				
3-F Optimised	0.011 (0.002)		−0.002	−0.002 to −0.001	0.004
4-F Human	0.015 (0.005)				
4-F Optimised	0.011 (0.003)		−0.004	−0.006 to −0.001	0.022
6-F Human	0.014 (0.007)				
6-F Optimised	0.010 (0.004)		−0.004	−0.006 to −0.002	0.002
8-F Human	0.012 (0.003)				
8-F Optimised	0.008 (0.003)		−0.004	−0.005 to −0.003	>0.001

The first column 'Average S.D.' is the average of the standard deviations in the PTV over the 12-patient sample. The 'Mean diff.' column is the average of the individual patient differences of the S.D. in the PTV achieved by the optimisation and the human planner. The *P* value was computed from a two-tailed paired Student's *t*-test. C.I. is the confidence interval.

well as the standard deviation of this average ($\sigma_{\overline{\sigma}D}$), the latter representing the variability over the sample. Next, the mean difference ($\overline{\delta}$) in the PTV dose homogeneity achieved by the optimisation and the human planner was computed (i.e., $\overline{\delta} = \overline{\sigma_{D,\text{opt}} - \sigma_{D,\text{human}}}$). The more negative this quantity is, the better the optimisation is in terms of uniformity of dose in the PTV.

The quantities $\overline{\sigma_D}$, $\sigma_{\overline{\sigma D}}$ and $\overline{\delta}$ for each plan type are shown in Table 3, and the individual δ values for each patient and each plan type are given in Fig. 4. (In order to make the standard deviations of the dose in the PTV for different plans directly comparable, dose distributions were scaled so that the mean in the PTV was the same for all plans: an arbitrary value of unity was selected. In Table 3 it is shown that $0.008 \leq \overline{\sigma_D} \leq 0.015$ for the different plan types (i.e., the average standard deviation of dose in the PTV ranges between 0.8 and 1.5%.) DVH comparisons were made by noting down the percentage volume of the OAR in each of the four dose bins <20, 20–50, 50–80 and >80%, and

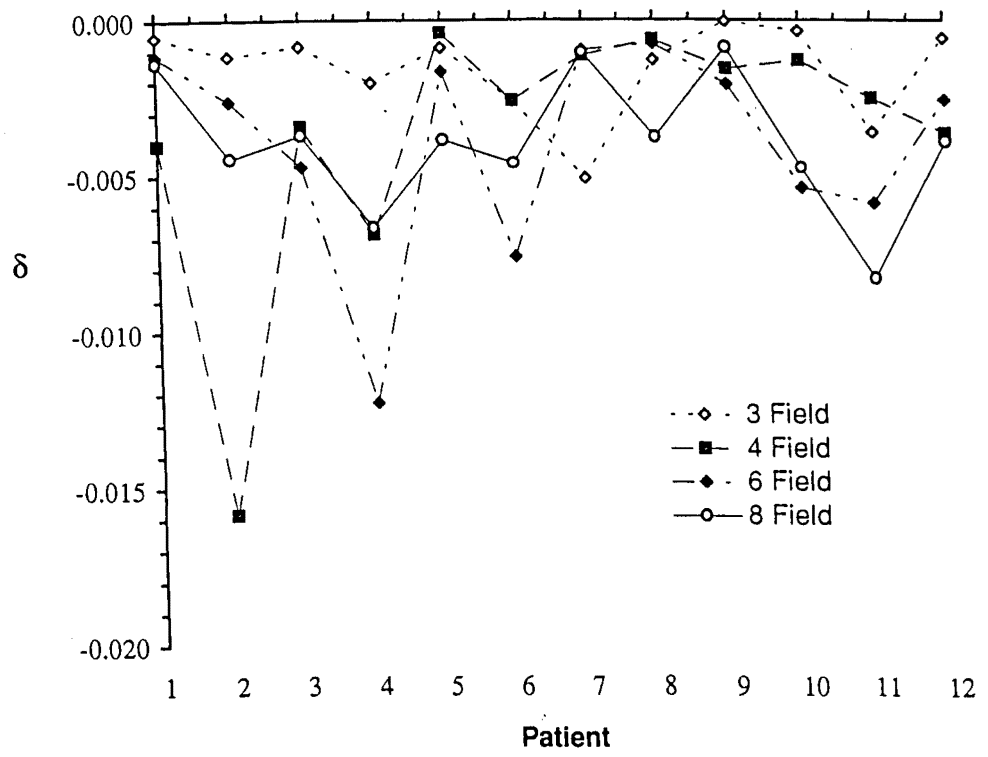

Fig. 4. Graph showing the δ values (i.e., the difference in the standard deviation of the dose in the PTV achieved by the optimisation algorithm and the human planner) for all 12 patients, and for each plan type.

averaging over the 12 patients (Fig. 5a–p). For all plans the DVHs were normalised to the dose at the isocentre. In Fig. 5a–p, the one standard deviation limit of the 12 patient sample is indicated by the upper and lower curves. In Tables 4 and 5, average TCP and NTCP values are shown after the dose to the isocentre was scaled to give a rectal NTCP of 5%. The average beam-weights selected by the human planner are compared to those computed by the optimisation algorithm in Fig. 6, and the average planning times (i.e., the time taken to determine optimal beam-weights once the beam orientations and field shape have been defined and implemented) are compared in Table 6. The optimisation times are real-times, recorded on an IBM RS6000 530H mainframe under conditions of light usage by other users.

4. Discussion

Both Fig. 4 and the '$\overline{\sigma_D}$' column of Table 3 show that the optimisation algorithm has achieved a more homogenous PTV dose for all plan types. The standard deviation of the average ('$\sigma_{\overline{\sigma D}}$' column in Table 3) are similar for the 3-, 4- and 8-field plan types, indicating a similar level of inter-patient consistency. For the 6-field plans there is greater inter-patient consistency in the optimised plans. A more revealing analysis comes from studying the mean of the individual differences (optimised — human) given in the '$\overline{\delta}$' column. A statistically significant effect was observed for all plan types, particularly for 3-, 6- and 8-field plans. The magnitude of the improvement, as indicated by the 95% confidence interval, is greatest for the 8-field plans and least for the 3-field plans (as expected, because the optimisation algorithm has more degrees of freedom in the 8-field plan). However, there is no obvious trend towards greater improvement with larger numbers of beams. In studying the individual results of the human planner it was observed that occasionally a plan was accepted that, although acceptable, was noticeably sub-optimal with regards to PTV dose homogeneity. The optimisation algorithm provides an effective method of reducing these anomalies. The increased dose inhomogeneity in the planner's plans was found to be largely due to patient-specific tumour shapes (odd bulges, etc.) rather than to any systematic under or overdosing.

The dose distributions in the OARs are summarised in Fig. 5a–p. By and large, the distribution of dose between the four bins (<20, 20–50, 50–80 and >80%), for the bladder and rectum, are similar for the human planner and the optimisation, for all plan types. The optimisation does, however, produce about 1–2% more rectal volume in the >80% bin for the 3-, 4- and 8-field plans, and 1–2% less for the 6-field plans. For the left and right femoral heads there is a significant difference in distribution of dose for the 4-, 6- and 8-field plans. In the 4-field plans, the optimisation produces a higher volume in the 20–50% bin, and a lower volume in the 50–80% bin. This trend is reversed for the 6-field plans, and in the 8-field plans the optimisation produces less volume in both bins. The precise cause of these trends is difficult to ascertain but an important feature is certainly that in trying to achieve a homogenous PTV dose the optimisation consistently favours beam orientations differently from the human planner.

The salient point from the PTV homogeneity data of Table 3 and the OAR DVH data of Fig. 5, is that compared with the human planner the optimisation algorithm achieves a more homogenous PTV dose by slight re-distribution of dose in the bladder and rectum, and significant re-distribution in the femoral heads. Of particular importance to NTCP is the amount of OAR volume in the >80% dose bin. From Fig. 5 we expect that the optimisation has slightly worsened the rectal dose for the 3-, 4- and 8-field plans, and slightly improved it for the 6-field plans. The femoral head dose also appears worse for the 3-, 4- and 6-field plans, but better for the 8-field plans. The TCP and NTCP values in Table 4 can be used to assess the relative merit of a more homogenous PTV dose against the worsening of the rectal and femoral heads dose. By scaling the dose so that the rectal NTCP is 5% for all plans, the best plans can be judged as those having the highest TCP, providing that the NTCP of other organs are acceptable.

From Table 4, the optimisation has achieved a slightly higher average TCP for all plan types than the human planner. The internal consistency (indicated by the S.D. column) is similar for the 3-, 4- and 8-field plans, and better for the 6-field plans. Surprisingly, the optimisation does not appear to attain relatively better results for the more complicated 6- and 8-field plans. In fact the opposite is observed where the largest benefit is obtained for the 3-field plans. In the 4-field plans, the optimisation achieved a significantly worse NTCP in both femoral heads (first row). Analysis of the NTCP values for both right and left femoral heads revealed that they were less than 5% for all except three patients who had extremely high values (up to 20%). It was obvious that the practical parameter set was inappropriate for these few patients and so they were recalculated with the 'importance factor' for the femoral head increased from 1 to 3. An increase of more than this resulted in the anterior-posterior beams being too strongly favoured. The corrected average NTCP and TCP values are shown as the lower italicised row in the Table. (All other relevant Tables and figures incorporate the results of these three corrected runs.) A marked decrease in NTCP values for the femoral heads was thus achieved for the 3- and 4-field plans.

A more revealing analysis is again obtained by studying the individual patient TCP and NTCP differences (Table 5). (The 'Bladder' data has been omitted from

this table because the mean differences as indicated in Table 4 were always too small to be significant.) One may see from the 'TCP' column that the optimisation algorithm achieved a statistically significant improvement of about 0.5% for the 3- and 4-field plans. It must be stressed here that statistical significance is not the same as clinical significance. Although a 0.5% improvement in TCP is not of great importance clinically, the implication is that the optimisation performs at least as well as the human planner. The real benefit of the optimisation algorithm comes in the planning time saved (see below). There is also a suggestion of a benefit for the 6- and 8-field plans although the effect is not proved significant at the 95% level. The femoral head NTCP values in Table 5 suggest the optimisation achieves a small (<1.0%) improvement in all cases except for the right femoral head in the 6-field plan.

Tables 3–5 and Fig. 5a–p indicate that the optimisation algorithm produced dose distributions that were as good as the human planner and often slightly better. For

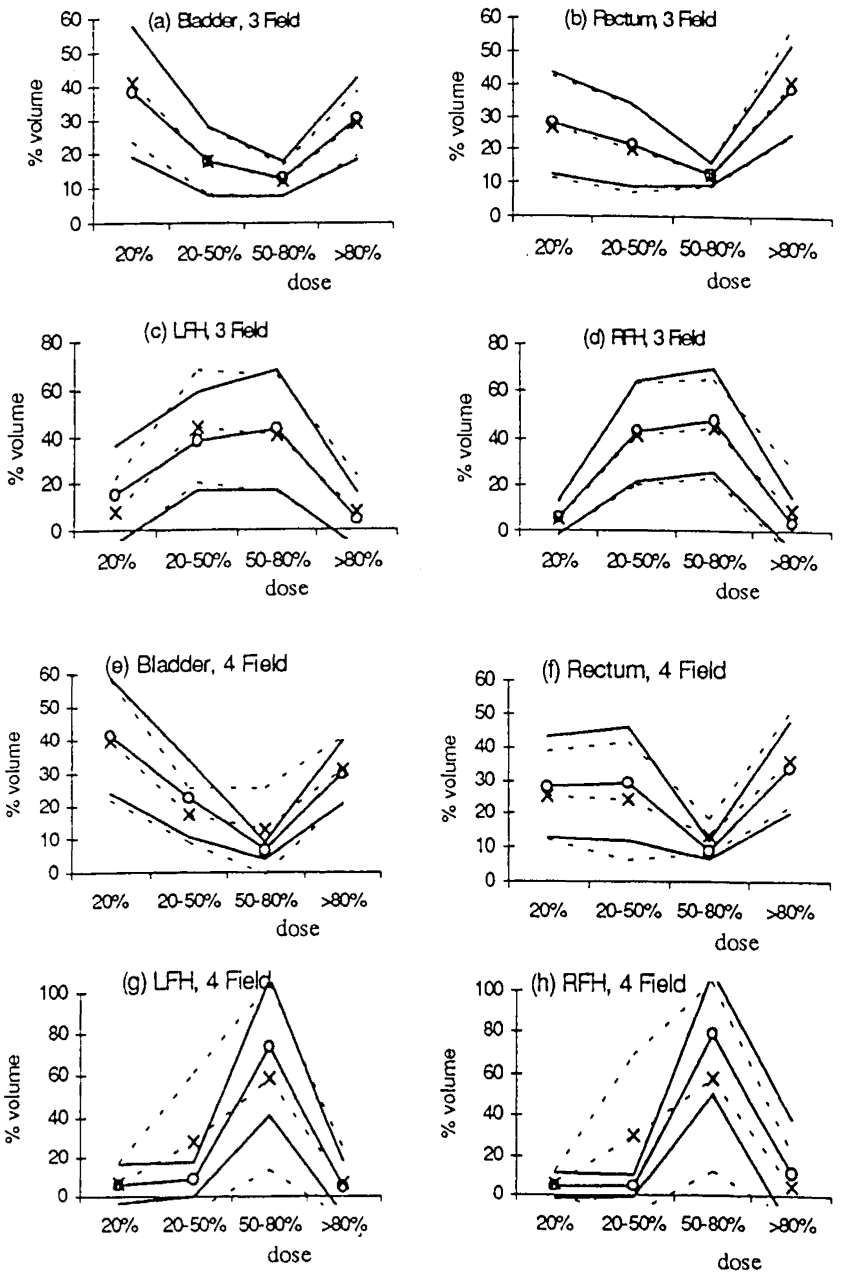

Fig. 5 (a)–(h). Each plot surnmarises average extracted dose-volume histogram statistics over the 12 patients. The central solid line with circle marker is the average achieved by the human planner; the upper and lower solid lines are one standard deviation bounds. Similarly, the central dashed line with cross marker is the average achieved by the optimisation algorithm, with the one standard deviation bound shown as the upper and lower dashed lines.

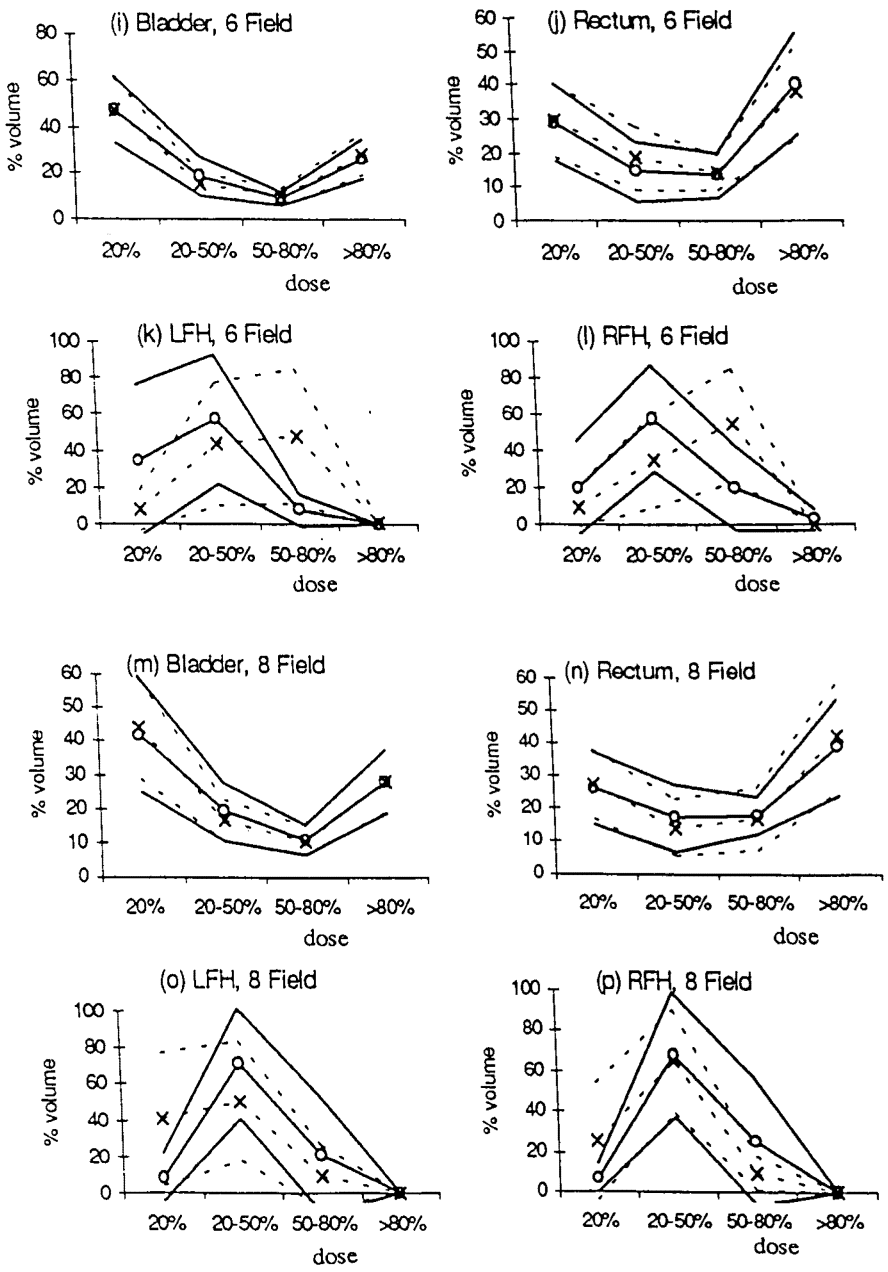

Fig. 5 (i)–(p).

the four plan types studied, the optimisation achieved a more homogenous PTV dose whilst keeping the NTCPs acceptable (i.e., <5%). From the statistical data alone (Table 3 and Fig. 5) one might have expected a more significant benefit to have translated into the TCP and NTCP values. We believe that this is not observed because of the 'overlap factor' which has been shown to limit the therapeutic advantage for radiotherapy of the prostate [20]. The overlap factor is the phenomenon where part of the rectum is inside (or overlaps with) the PTV. Achieving a homogenous PTV dose thus raises the overlap part of the rectum to a high dose and this high dose region is almost entirely responsible for the NTCP.

A comparison study of the beam-weights selected by the human planner and the optimisation algorithm is presented in Fig. 6. It is clear that as the number of beams in the plan increases, there is increasing divergence between the human and the optimisation algorithm. For the 4-, 6- and 8-field plans, the low standard deviations on the beam-weights selected by the human

Table 4
Comparison of the average TCP and NTCP values achieved by the human planner (using conventional forward planning) and the optimisation algorithm over 12 prostate patients, and the corresponding standard deviations

	TCP		NTCP					
	Mean (%)	S.D.	Bladder		Left femoral head		Right femoral head	
			Mean (%)	S.D.	Mean (%)	S.D.	Mean (%)	S.D.
3-F Human	87.9	1.5	<0.1	0.0	1.1	3.4	1.5	4.1
3-F Optimised	88.5	1.4	<0.1	0.0	0.6	1.5	0.7	1.8
4-F Human	88.1	1.6	<0.1	0.0	2.9	2.8	2.7	2.6
4-F Optimised	88.7	1.7	<0.1	0.0	5.0	7.1	5.0	7.2
	88.7	*1.7*	*<0.1*	*0.0*	*1.7*	*1.8*	*1.8*	*1.8*
6-F Human	87.8	1.7	<0.1	0.0	0.0	0.1	0.1	0.1
6-F Optimised	88.1	1.5	<0.1	0.0	0.0	0.0	0.2	0.6
8-F Human	87.9	1.6	<0.1	0.0	0.0	0.0	0.0	0.0
8-F Optimised	88.1	1.5	<0.1	0.0	0.0	0.0	0.0	0.0

Values are shown for 3-, 4-, 6- and 8-field (F) plans. The dose for each plan was normalized so that the rectal NTCP was 5%. The results in the italicised row are for the patient sample after three patients were re-optimised with the femoral head importance factor increased to 3 (see main text Section 4).

planner suggest that small perturbations were made about a perceived 'optimal' beam-weight set. For the 4-field plans the optimisation algorithm found a moderately similar ($\leq 10\%$) optimal set, but had significantly greater variation about these values. For the 6- and 8-field plans the optimal sets of the human and the optimisation show almost no correlation at all. In fact, for the 6-field plan, the beam-weight pattern is almost opposite. The fact that acceptable plans can be produced by such differences in beam-weight patterns indicates that there exists a remarkable degree of flexibility in the planning process. Our results support the idea that many different beam-weight sets can give a similar dose distribution, and particularly, similar TCP and NTCP values.

It is of interest to note that for the 6- and 8-field plans the optimisation algorithm sometimes set certain beam-weights to zero. Three out of the twelve 6-field plans had at least one beam-weight set to zero and were thus actually 5-field plans (in one case, two beam-weights were set to zero). For the 8-field plans the effect was more pronounced with only one actual 8-field plan, six 7-field plans, three 6-field plans and a 5-field plan. This, together with the inter-patient beam-weight variability discussed above, is evidence that the optimum number of beams and their beam-weights for complicated standard plan arrangements are significantly dependent on the patients geometry. It also suggests that significant gains might be had in optimising beam orientations. The implications for clinical practice are a significant reduc-

Table 5
An analysis of the difference in TCP and NTCP values achieved by the optimisation and the human planner over the 12 patient sample

	TCP		NTCP			
	Mean diff. (%) (95% C.I.)	*P* value	Left femoral head		Right femoral head	
			Mean diff. (%) (95% C.I.)	*P* value	Mean diff. (%) (95% C.I.)	*P* value
3-Field	0.56 (0.43 to 0.69)	<0.01	−0.53 (−1.69 to 0.64)	0.39	−0.89 (−2.14 to 0.55)	0.27
4-Field	0.57 (0.34 to 0.79)	<0.01	−1.12 (−2.11 to −0.13)	0.05	−0.84 (−1.77 to 0.08)	0.10
6-Field	0.29 (−0.01 to 0.60)	0.09	−0.13 (−0.08 to 0.02)	0.22	0.13 (−0.20 to 0.45)	0.46
8-Field	0.13 (−0.08 to 0.34)	0.24	0.0	—	0.0	

The 'Mean diff.' columns are the average of the differences between the results obtained by the optimisation algorithm and by the human planner. The *P* value was computed from a two-tailed paired Student's *t*-test, and the dose was scaled for all plans so that the rectal NTCP was 5%. C.I. is the confidence interval.

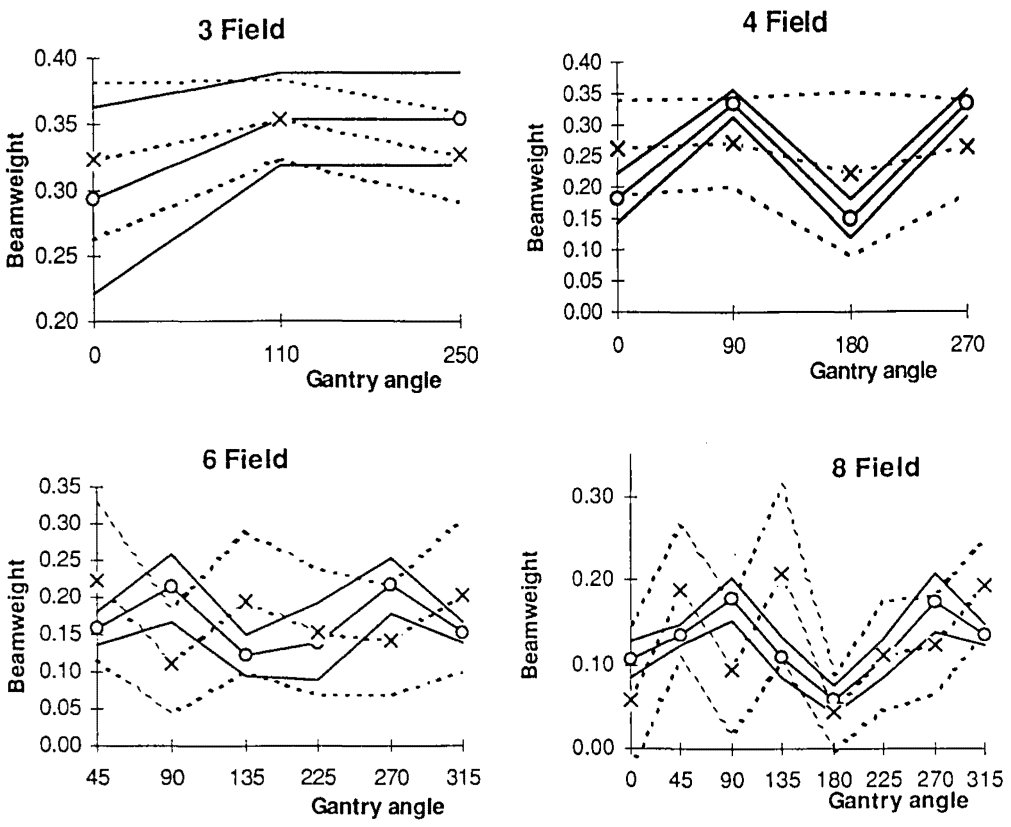

Fig. 6. Average beam-weight statistics over the 12 patient sample. As with Fig. 5, the central solid line with circle marker is the average achieved by the human planner; the upper and lower solid lines are one standard deviation bounds. The central dashed line with cross marker is the average achieved by the optimisation algorithm, with the one standard deviation bound shown as the upper and lower dashed lines.

tion in the delivery time and a general simplification of the delivery process. The deselection of beams seems to be dependent on the shape of the tumour. An irregular tumour with, for example, a large protuberance, is more likely to have a beam deselected from the plan than a spherically shaped tumour. This is due to the inherently strong (Section 2.1.2) quadratic nature of the cost function in the PTV which is sensitive to beams that cause inhomogeneity.

Table 6
Average values over five patients of the time taken (min) to determine optimal beam-weights by a human planner and the optimisation algorithm

	Planner		Optimisation (a)		Optimisation (b)	
	Mean	S.D.	Mean	S.D.	Mean	S.D.
3-Field	21.6	4.4	1.4	0.1	0.5	0.0
4-Field	28.4	8.0	1.6	0.2	1.0	0.1
6-Field	20.2	3.9	2.7	0.3	2.0	0.2
8-Field	22.0	2.4	5.0	0.5	4.1	0.4

The optimisation column (a) includes the time taken by the dose calculation algorithm, and is therefore the total time taken to plan a patient for the first time. The optimisation column (b) is the time for subsequent optimisations of the patient for which the dose calculation does not need to be called again.

The results of the timing study (Table 6) show the most significant advantage of the optimisation algorithm. The times shown are average values over the last five patients in the study, when the planner was fully familiar with the planning system and was therefore working with high efficiency. For all plan types the optimisation was much faster at computing optimised beam-weights (by a factor of 4 for the 8-field plans to 20 for the 3-field plans). Furthermore, whilst the optimisation is computing the beam-weights, the human planner is free to perform other tasks (e.g., further inspection of patient anatomy displayed on the screen). For the three patients where it was necessary to increase the importance factor for the femoral heads, the total time taken to optimise the beam-weights is estimated by adding the mean 'optimisation (a)' time and the mean 'optimisation (b)' time in Table 6. Significant time savings are still observed.

5. Conclusions

The dose distributions produced by the optimisation algorithm were compared with those of the human plan-

ner by studying both dose statistics and biological NTCP and TCP values. The more descriptive dose statistics study broadly supported the more quantitative biological modelling study. The studies have shown two advantages of the optimisation algorithm. Firstly the optimisation consistently achieved a more homogenous PTV dose (Table 3) while maintaining the dose to the OAR at acceptable levels (Figs. 5a–p). This translated into a small but statistically significant increase in TCP (about 0.5%) for the 3- and 4-field plans and there was also the suggestion of a benefit for the 6- and 8-field plans (Table 5). The predicted improvement in treatment outcome associated with the optimisation algorithm, applied to the plan types studied, is thus quite small (0.5%). The second and probably more significant advantage is in the time saving incurred by the optimisation algorithm (a factor of between 20 and 4 for 3- and 8-field plans, respectively).

The clinical implications of the benefits that the optimisation algorithm could bring to routine treatment planning are significant. A reduction in planning time would increase the efficiency of the planning process allowing more patients to be planned and a reduction in costs. The consistency of the algorithm has been demonstrated to be high, which could result in more reliable plan production. From the clinician's viewpoint the algorithm can be used to quickly generate optimised beam-weights for a range of plan types, and for different organ weightings (via the importance factors). The relative merits of these rival plans can then be assessed and the best plan selected for treatment. Finally, the quality of the optimised plans were found to be slightly better on average than the planners plans indicating a potential therapeutic benefit.

Acknowledgements

This work is part of COVIRA (Computer Vision in Radiology), project A2003 of the AIM (Advanced Informatics in Medicine) programme of the European Union.

Participants in the COVIRA consortium are:

Philips Medical Systems. Best (NL) (prime contractor) and Madrid (E); Philips Corporate Research, Hamburg (D); Siemens AG, Eriangen (D) and Munich (D); IBM UK Scientific Centre, Winchester (UK); Gregorio Maranon General Hospital, Madrid (E); University of Tübingen, Neuroradiology and Theoretical Astrophysics (D); German Cancer Research Centre, Heidelberg (D); University of Leuven, Neurosurgery, Radiology and Electrical Engineering (B); University of Utrecht, Neurosurgery and Computer Vision (NL); Royal Marsden Hospital and Institute of Cancer Research, Sutton (UK); National Hospital for Neurology and Neurosurgery, London (UK) Foundation of Research and Technology, Crete (GR); University of Sheffield (UK); University of Genoa (I); University of Aachen (D); University of Hamburg (D); Federal Institute of Technology, Zurich (CH).

We would especially like to thank Ms A. Hoess, Dr R. Bendl, Mr C. Schulze, Dr J. Pross and Prof Schlegel, at DKFZ, for their support, stimulating discussion and providing VIRTUOS; also to Dr P. Evans, Dr P. Mayles, Mrs V. Hansen, Professor W. Swindell, and Dr A.Nahum for discussions at RMH/ICR; Dr P. Elliot, Dr K. Goodson, Dr R. Riste-Smith, Dr G. Sivewright at IBMUKSC. Dr R. Bentley and Mr S. Bashford have provided invaluable help with computing and networking support.

References

[1] Bendl, R., Pross, J., Hoess, A., Keller, M.A., Preiser, K. and Schlegel, W. "VIRTUOS — A Program for Virtual Radiotherapy Simulation and Verification". In: Proc. of the 11th Int. Conf. on the Use of Computers in Radiation Therapy, p. 226. Editors: A.R. Hounsell, J.M. Wilkinson and P.C. Williams. Manchester, 1994.

[2] Boyer, A.L., Desobry, G.E. and Wells, N.H. Potential and limitations of invariant kernel conformal therapy. Med. Phys. 18: (4) 703–712, 1991.

[3] Bortfeld, T.R., Kahler, D.L., Waldron, T.J. and Boyer, A.L. X-ray field compensation with a multi-leaf collimators. Int. J. Radiat. Oncol. Biol. Phys. 28: 3, 1993.

[4] Brahme, A. Treatment optimisation using physical and radiobiological objective functions. In: Radiation Therapy Physics. Editor: A. Smith. Springer, Berlin, 1992.

[5] Burman, C., Kutcher G.J., Emami, D. and Goitein, M., Fitting of normal tissue tolerance data to an analytic function. Int. J. Radiat. Oncol. Biol. Phys. 21: 123–135, 1991.

[6] Censor, Y., Altschuler, M.D. and Powlis, W.D. On the use of Cimmino's simultaneous projections method for computing a solution of the inverse problem in radiation therapy treatment planning. Invest. Prob. 4: 607–623, 1988.

[7] Censor, Y., Powlis, W.D. and Altschuler, M.D. On the fully discretised model for the inverse problem of radiation therapy treatment planning. Proc 13th Annual Northeast Bioengineering Conference. Editor: K.R. Foster. IEEE 87-CH2436-4 Library of Congress catalog card number 87-80502: 211–214, 1987.

[8] Galvin, J.M., Smith, R.M. and Chen, X.-G. Modulation of photon beam intensity with a multileaf collimator. Proc. 1st Biennial ESTRO Meeting on Physics in Clinical Radiotherapy. Budapest, 14–17 October, 1991.

[9] Holmes, T. A model for the physical optimisation of external beam radiotherapy. PhD thesis, University of Winsconsin, Madison, 1993.

[10] Holmes, T. and Mackie, T.R. Simulation studies to characterise the search space of a radiotherapy optimisation algorithm. Proc AAPM Conference, August, 1992.

[11] Kutcher, G.J. and Burman, C. Calculation of complication probability factors for non-uniform normal tissue irradiation: the effective volume method. Int. J. Radiat. Oncol. Biol. Phys. 16: 1623–1630, 1989.

[12] Lyman, J.T. Complication probability as assessed from dose volume histograms. Radiat. Res. 104: S-13–S-19, 1985.

[13] Mageras, G.S. and Mohan, R. Application of fast simulated annealing to optimisation of conformal radiation treatments. Med. Phys. 20: 639–647, 1992.

[14] Mohan, R., Mageras, G.S., Baldwin, B., Brewster, L.J., Kutcher, G.J., Leibel, S, Burman, C.M., Ling, C.C. and Fuks, Z. Clinically relevant optimisation of 3D conformal treatments. Med. Phys. 19 (4): 933–944, 1992.

[15] Mohan, R., Mageras, G. and Podmaniczky, K.C. A model for computer-controlled delivery of 3D conformal treatments. Med. Phys. 18: 612, 1991.

[16] Morrill, S.M., Lane, R.G., Jacobson, G. and Rosen, I. Treatment planning optimization using constrained simulated annealing. Phys. Med. Biol. 36: 1341–1361, 1991.

[17] Niemierko, A. Random search algorithm (RONSC) for optimisation of radiation therapy with both physical and biological endpoints and constraints. Int. J. Radiat. Oncol. Biol. Phys. 23: 89–98, 1992.

[18] Niemierko, A., Urie, M. and Goitein, M. Optimisation of 3D radiation therapy with both physical and biological endpoints and constraints. Int. J. Radiat. Oncol. Biol. Phys. 23: 99–108, 1992.

[19] Oldham, M. and Webb, S. Clinical implementation of Inverse Treatment Planning. Br. J. Radiol. 66: 162.

[20] Oldham, M. and Webb, S. The optimisation and inherent limitations of 3D conformal radiotherapy treatment plans of the prostate. Br. J. Radiat. 1994a (in press).

[21] Oldham, M. and Webb, S. Inverse planning and the optimisation of radiotherapy plans by simulated annealing incorporating dual weighting p. 60. Proc. of the 11th Int Conf. on the Use of Computers in Radiation Therapy. Editors: A.R. Hounsell, J.M. Wilkinson and P.C. Williams. Manchester, 1994b.

[22] Rosen, I.I., Lane, R.G., Morrill, S.M. and Belli, J.A. Treatment plan optimisation using linear programming. Med. Phys. 18: 141–152, 1991.

[23] Smith, R.M., Galvin, J.M. and Chen, X.G. The use of a multileaf collimator to optimise dose distributions. Med. Phys. 18: 613, 1991.

[24] Starkschall, G. and Eifel, P.J. An interactive beam-weight optimisation tool for three-dimensional radiotherapy treatment planning. Med. Phys. 19: 155–163, 1992.

[25] Szu, H. and Hartley, R. Fast simulated annealing. Phys. Lett. A122: 157–162, 1987.

[26] Vance, R., Sandham, W.A. and Durrani, T.S. Optimisation of beam profiles in conformal radiotherapy using genetic algorithms. Phys. Med. Biol., 39a, Abstracts of the World Congress on Medical Physics and Biomedical Engineering. Editors: L.N. Rodrigues and J. Nadal. Rio de Janeiro, 1994.

[27] Webb, S. Optimisation by simulated annealing of three-dimensional conformal treatment planning for radiation fields defined by a multileaf collimator. Phys. Med. Biol. 36: 1201–1226, 1991.

[28] Webb, S. Optimisation by simulated annealing of three-dimensional conformal treatment planning for radiation fields defined by a multileaf collimator: 2. Inclusion of two-dimensional modulation of the X-ray intensity. Phys. Med. Biol. 37: 1689–1704, 1992a.

[29] Webb, S. Techniques for optimisation of dose with a multileaf collimator for conformal radiotherapy of target volumes with concave outlines. In: Three-Dimensional Treatment Planning. Editor: P. Minet. (Proceedings of the E.A.R Conference in Geneva at W.H.O., October, 1992) 163–172, 1992b.

[30] Webb, S. Optimised three dimensional treatment planning for volumes with concave outlines, using a multileaf collimator. Proc. ART91 Munich, April 1991 (Abstract book p. 66). In: Advanced Radiation Therapy: Tumour Response and Treatment Planning, pp. 495–502. Editor: A. Breit. Springer, Berlin, 1992c.

[31] Webb, S. and Nahum, A.E. A model for calculating tumour control probability including the effects of inhomogenous distributions of dose and clonogenic cell density. Phys. Med. Biol. 38: 653–666, 1993.

ATTACHMENT A-2

Optimizing Radiation Therapy Inverse Treatment Planning Using the Simulated Annealing Technique

Steve Webb

Joint Department of Physics, Institute of Cancer Research and Royal Marsden Hospital, Downs Road, Sutton, Surrey SM2 5PT, London, United Kingdom

ABSTRACT

The role of simulated annealing in therapy planning is discussed from a historical, theoretical and practical viewpoint. The properties of the method are discussed in detail together with available options and specific implementations. © 1995 John Wiley & Sons, Inc.

I. WHAT IS TREATMENT PLAN OPTIMIZATION?

The aim of radiotherapy of local disease is to achieve a high dose to the planning target volume (PTV), simultaneously keeping the dose to organs at risk (OAR) as low as possible. When a small number of rectangular fields with or without wedges and blocking is intended for use, the treatment planning technique is to try a number of different beam weightings, compute the dose distribution, evaluate the plan, and then repeat the task until the plan meets prescribed criteria satisfactorily. This is known as forward treatment planning. It is the traditional method and is still in widespread use. It might be called "human optimization," but in fact the resulting plan has no more status than "acceptable."

As we move toward an era of increased automation and precision in three-dimensional radiotherapy, a number of desirable treatment options will increasingly be called upon, including:

1. the use of a larger number (than simply two or three) of fields;
2. the use of noncoplanar fields;
3. the use of fields shaped to the beam's-eye-view (BEV) of the PTV by a multileaf collimator (MLC);
4. the introduction of intensity-modulated beams (IMBs) (Figure 1) via:
   a. multiple exposures with different static MLC settings;
   b. dynamic sweeping of MLC leaves;
   c. apparatus for tomotherapy;
   d. electronically steered, time-modulated pencil beams.

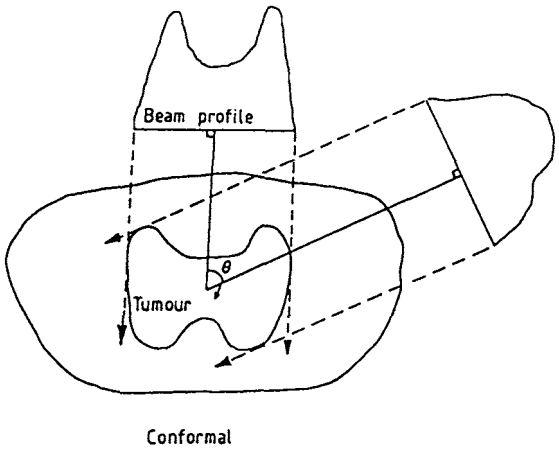

Figure 1. The concept of intensity-modulated beams. Two (of a large set of) such beams with one-dimensional intensity modulation are shown irradiating a two-dimensional slice. The beams combine to create a high-dose treatment volume spanning the PTV, which has a concave outline in which might lie OARs. Such uniform high-dose treatment volumes cannot be achieved using beams without intensity modulation. Planning such treatments relies on tools, such as simulated annealing, for solving the inverse problem.

As these quite technologies become increasingly more common, it becomes impossible to create treatment plans by forward treatment planning, because there are just too many possibilities to explore and not enough human time to do this task; there is little chance of arriving at the optimum treatment plan by trial and error; and if an acceptable plan could be found, there is no guarantee it would be the best, nor any criteria to specify its precision in relation to an optimum plan.

For this reason, the treatment planning process has to be radically changed to solve the problem, "Given a prescription of desired outcomes, compute the best beam arrangement." Stated this way, the problem is solved by inverse treatment planning. The task has to be solved by a computer with human guidance rather than by human experience alone.

II. CLASSES OF INVERSE TREATMENT PLANNING TECHNIQUES

Inverse treatment planning was first discussed by Brahme in the early 1980s. Since then, several groups of workers have developed inverse treatment planning tools. They fall into two broad classes:

1. Analytic techniques. These involve deconvolving a dose-kernel from a desired dose distribution to obtain the distribution of photon fluence and forward projecting this fluence with attenuation factors to create profiles of beam intensity. Because of the formal similarity

International Journal of Imaging Systems and Technology, Vol. 6, 71–79 (1995)

CCC 0899-9457/95/010071-09

with X-ray slice imaging, these methods have sometimes been called inverse computed tomography. The first tools were used for two-dimensional planning, later extended to three dimensions.

2. Iterative techniques. Both linear-programming algorithms (Simplex) and the Cimmino algorithm have been exploited, together with simulated annealing.

Some optimization tools combine a mixture of analytic and iterative-refinement stages. In particular, negative beam weights, created by analytic inversions, have to be removed in some way.

Optimization is a vast field, not further reviewed here. The reference list in this review is restricted to papers on simulated annealing, since other articles in this Special Issue and the references in Webb [1] point to this vast field.

III. SIMULATED ANNEALING: GENERAL CONCEPTS AND PROPERTIES

Simulated annealing is an iterative optimization technique. It is a method of finding the global minimum of some function when the state-space of this function may possess multiple local minima. Because of this property it may have advantages compared to other iterative methods which may become trapped in a local minimum. Simulated annealing has been used in a variety of different fields with many applications [e.g., 2–9]. It was first introduced into the field of medical physics (coded aperture reconstruction of images of radioactive distributions) by Professor Harry Barrett and colleagues in Tucson, Arizona, who applied the method to minimizing a quadratic cost function [10–12]. The present author continued this application into SPECT [13] and then into radiotherapy treatment planning (see Section VII) [14–22]. Recently, Mageras and Mohan [31] have further extended the method and application with other cost functions and techniques to accelerate convergence (see Section VIII).

To give the discussion substance in the radiotherapy context, let us imagine that a number of beam orientations have been selected and the problem is to determine the optimum set of beam weights for beams with intensity modulation [i.e., it is required to compute the beam weight sinogram (Figure 2)]. The analogy with medical imaging is shown in Figure 3.

A large number of combinations of beam weights are explored in some iterative manner (see Section IV). Define a quadratic cost function V_n at the nth iteration (i.e., nth choice of such beam weights) to be:

$$V_n = \left[\left(\frac{1}{M} \right) \sum_{\underline{r}} I(\underline{r}) (D_p(\underline{r}) - D_n(\underline{r}))^2 \right]^{0.5} \qquad (1)$$

where $D_p(\underline{r})$ means the prescribed dose value at some point $\underline{r}$ in the patient and $D_n(\underline{r})$ denotes the actual dose at the same point at the nth iteration, and the mean is taken over a large number M of specified dose points. $I(\underline{r})$ is a term which allows the user to weight the importance of contributions to the cost from different parts of the body. For example, it may be more important to have the dose conform in the PTV than in the OAR, or conversely, protection of the OAR may be the desired goal at the expense of some dose inhomogeneity in the PTV. The choice of the parameters $I(\underline{r})$ greatly influences

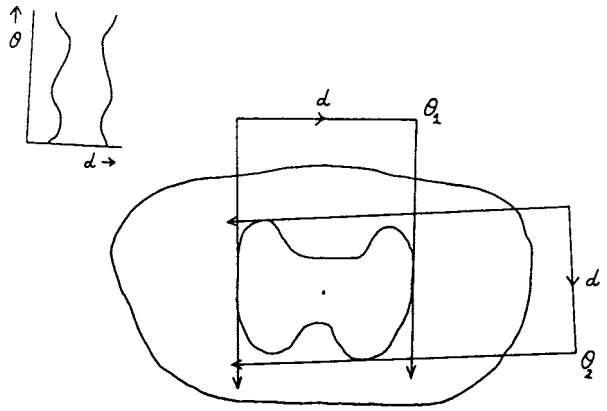

Figure 2. The concept of the beam weight sinogram. The butterfly-shaped region is the PTV, and a number of beams with intensity modulation are arranged to span the PTV. The angle θ labels each beam and the parameter d labels each element of each beam. If the beamweights are stacked as shown in the upper left, then the resulting image is a beamweight sinogram by analogy with medical imaging (see Figure 3).

the outcome of the optimization. The aim of the optimization is to compute the lowest value of V_n, since this corresponds to the calculated dose distribution best matching the prescription in a least-squares sense (Figures 4 and 5).

This suffices for the purpose of discussion, although this is only one of many possible functions to minimize and the quadratic cost function does not actually have any local minima when optimising beam weights. Bortfeld has shown that the same dose quadratic cost function does have local minima when optimizing beam directions. We return later (see Section IV) to discuss other cost functions, including those

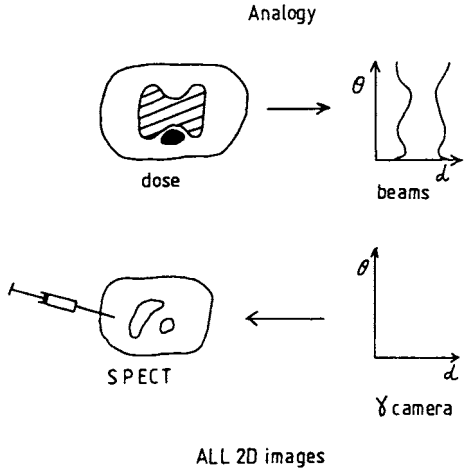

Figure 3. The analogy of inverse treatment planning when the one-dimensional beams are intensity modulated, and emission tomography imaging. In the former, the dose prescription is known on a two-dimensional matrix (top left), and it is required to compute the beam weight sinogram (top right). In the latter, a γ camera makes a measurement of the projection sinogram (bottom right) of the distribution of activity; this is reconstructed (bottom left) from these data. Simulated annealing has been used to solve *both* problems, the latter problem providing the stimulus and motivation for introducing simulated annealing into radiotherapy treatment planning.

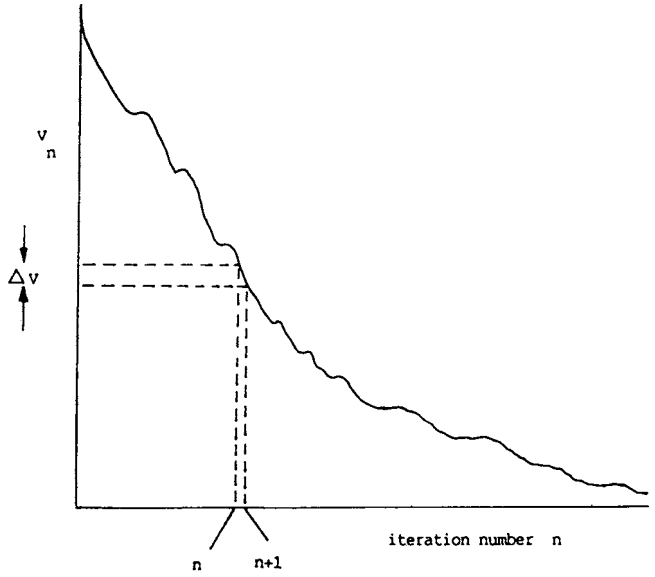

Figure 4. In one dimension, a general cost function V_n which may have local minima as shown as well as a global minimum.

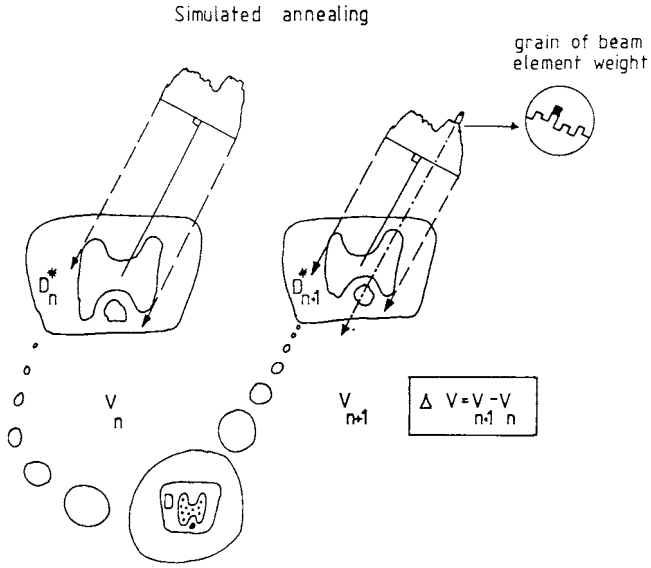

Figure 6. The way the addition of a grain changes the cost function. On the left at the nth iteration the current estimate of the dose distribution is D_n^* and the cost function is V_n, computed by comparing the running estimate of the dose distribution with the prescription D (shown as bubbles). Then (right) one particular element of beam weight has a grain added (black), the new dose distribution becomes D_{n+1}^*, and the new cost function is V_{n+1}. The change of the cost function ΔV_n controls what happens next.

embodying biological end points, which almost certainly do have local minima.

For some general cost function it is not possible to know ahead of time the form of the multidimensional surface in state space of the function for all possible beam arrangements. As different beam arrangements are tested, the cost function will change (Figure 6). The problem is to compute a very large number of elemental beam weights which combine to give a dose distribution evaluated on all the pixels contributing to the cost function.

Sometimes the cost function will be larger than at the previous iteration, and sometimes smaller. At first sight it would seem obvious to accept only each new beam weight set that *lowers* the cost function, and those that achieve this reduction are indeed substituted for the previous best estimate. However, in simulated annealing a mechanism for accepting changes which lead to an *increase* in the cost function is also built in. This mechanism allows the system to climb out of local minima in the cost function, should there be any, and eventually reach the global minimum. If the cost function changes by ΔV_n in progressing from the nth to the $(n+1)$th iteration and if ΔV_n is positive, then this change is accepted with a small probability

$$\exp(-\Delta V_n/kT) \tag{2}$$

where k is the Boltzmann constant and T is the temperature (Figure 7).

In practice, kT is simply a quantity ascribed the same dimensions as ΔV_n. Initially in the iterative process, the temperature is large allowing many "wrong-way" changes of the cost function (and thus a wide exploration of state space). In so-called classical simulated annealing provided the temperature in equation 2 is reduced slower than, or as $(1/\ln(n))$ this guarantees progression toward the global minimum as iterations proceed [6].

The method gets its name from the process by which metals are annealed. If the temperature falls too fast, then amorphous states can arise, whereas annealed metals form from slow cooling. Consider also the analogy with a skier descending a slope (Figure 8). Imagine the slope is the graph of the cost function. The skier starts at the top (large value of the cost function) and wishes to reach the hotel at the bottom (global minimum of cost function).

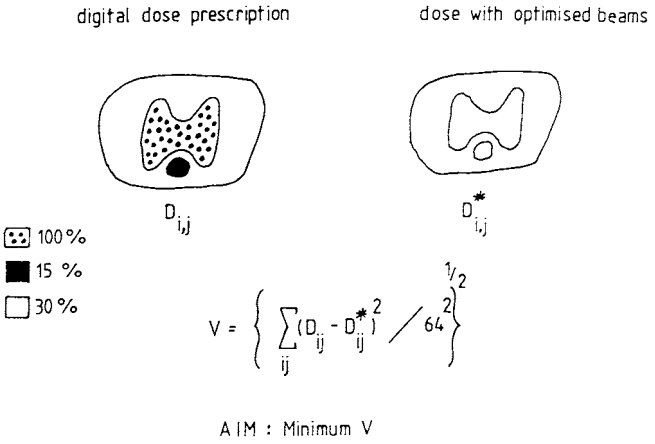

Figure 5. The left part shows a possible dose prescription (D is $D_p(r)$ in the text). The aim is to have a high dose in the PTV (dots) and a low dose in the OAR (black). The right part shows the "running estimate" of the dose on a two-dimensional grid specified by i, j (D^* is $D_n(r)$ in the text) and this example illustrates the computation of a dose quadratic cost function on a 64^2 grid. For simplicity the importance of all regions is considered to be the same (unity). In practice (see Section VII) tuning the importance changes the outcome. The aim of simulated annealing is to minimize the cost function V.

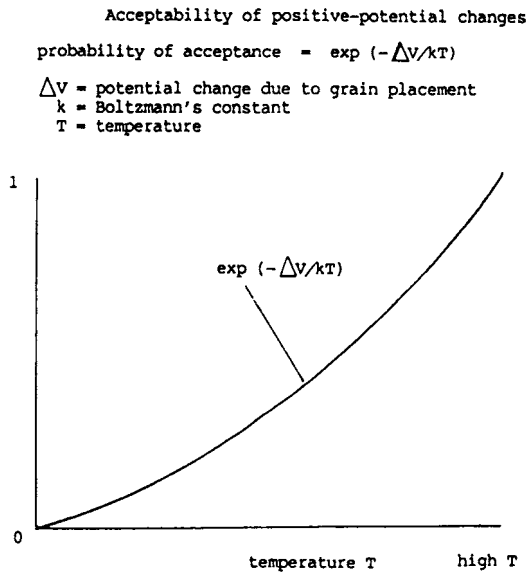

Figure 7. The graph controlling the acceptability or otherwise of wrong-way (uphill) changes in the cost function. When ΔV_n is positive, Equation (2) gives the probability with which such changes should be accepted. At high temperatures the probability will be high, and vice-versa.

In general, the skier must aim to go downhill, of course. But if our skier is overprincipled and refuses ever to suffer a potential energy rise (i.e., go uphill), then that skier will be trapped behind any snow bump blocking his path (see Figure 8) and will not reach the bottom. Just as a skier requires some momentum to rise over the snow bump, so the optimization requires the described mathematical step for overcoming local minima. However, in multidimensional problems, simultaneous minima in many directions are rare.

IV. THE POWER OF SIMULATED ANNEALING: COST FUNCTIONS

The great power of simulated annealing lies in its flexibility. The cost function can be as simple or as complicated as one likes. The quadratic cost function in dose [Eq. (1)] is a popular choice because it has an intuitive meaning. The outcome can be tuned via the importance parameters $I(\underline{r})$. As the name "cost function" suggests, what is achieved depends on what the user is prepared to pay for. A pure quadratic cost function in dose for beam weight optimisation has no local minima, and the matrix linking three-dimensional dose to a set of beam weights could, in principle, be analytically inverted. However, such inversions would be lengthy and ill conditioned. The enormous matrices would be hard to compute and would require huge computer storage. The analytic inversion may well be impossible, would almost certainly lead to the inclusion of negative beam weights; simulated annealing still provides a convenient way to solve the problem and build in the constraint of positivity and flexible tuning. In the case of beam weight optimization with the dose quadratic cost function, simulated annealing at zero temperature reduces to constrained iterative least-squares optimization. If beam orientation is optimized with the quadratic cost function in

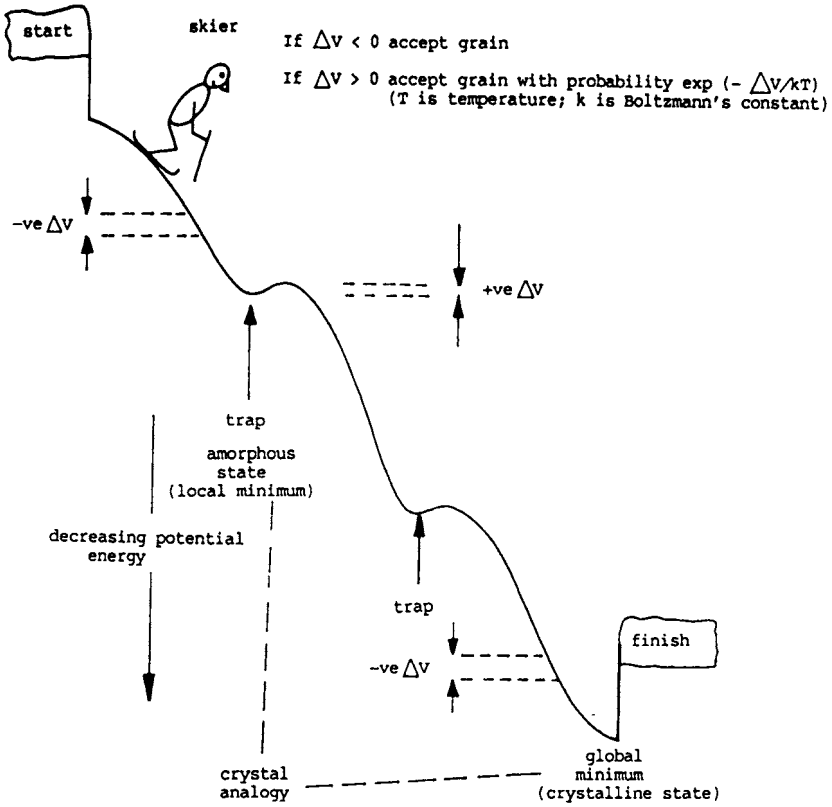

Figure 8. The analogy of minimizing a cost function by simulated annealing and the technique of a skier descending a slope (see text for discussion).

dose, nonzero–temperature simulated annealing must be implemented.

An alternative cost function still based on dose is to use a quadratic term in the PTV and a linear term in the OAR, representing integral dose to the OAR and the rest of the body B. Oldham and Webb [24] used

$$V_n = a_1 \frac{C_{\mathrm{PTV}}}{C_{\mathrm{PTV}_{st}}} + a_2 \frac{C_{\mathrm{OAR}}}{C_{\mathrm{OAR}_{st}}} + a_3 \frac{C_B}{C_{B_{st}}} \tag{3}$$

where C_{PTV} has the same form as in Equation (1) and

$$C_{\mathrm{OAR}} = \sum_{\underline{r}} D_n(\underline{r}) \quad \text{with } \underline{r} \text{ in OAR} \tag{4}$$

and

$$C_B = \sum_{\underline{r}} D_n(\underline{r}) \quad \text{with } \underline{r} \text{ in } B \tag{5}$$

and the subscript $_{st}$ indicates the starting value when all beam weights are uniform. a_1, a_2, and a_3 are constants which control the optimization allowing different initial importance to be ascribed to each region of interest in the fit.

Since dose is only a surrogate for biological outcome, some workers have argued that instead of trying to match a dose prescription, it is better to optimize biological outcome. The argument applies equally to analytic and iterative techniques. Using models supported by observational data, tumor control probability (TCP) and normal tissue complication probability (NTCP) can both be computed knowing the three-dimensional dose distribution in the PTV and OAR. Formally, the TCP at the nth iteration is

$$\mathrm{TCP}_n = f_1[D_n(\underline{r})] \quad \text{with } \underline{r} \text{ in PTV} \tag{6}$$

where f_1 represents the function linking inhomogeneous dose and TCP. Similarly, the NTCP at the nth iteration is

$$\mathrm{NTCP}_n = f_2[D_n(\underline{r})] \quad \text{with } \underline{r} \text{ in OAR} \tag{7}$$

where f_2 represents the function linking inhomogeneous dose and NTCP.

It is then possible to specify different cost functions for optimization involving biological outcome—e.g., maximize TCP subject to some maximum-allowed NTCP; minimize NTCP subject to some minimum-allowed TCP; and maximize the probability of uncomplicated tumor control TCP × (1 − NTCP).

Not all of these objectives are endorsed. For example, the third option might correspond to too-high NTCP. Clinicians usually regard an upper NTCP as a constraint and the first option is often the preferred clinical rationale in determining a treatment.

It would even be possible to construct cost functions involving both dose and biological outcome. Cost functions based on TCP and NTCP almost certainly have local minima. Note, however, that a physical parameter cannot both be a constraint and a goal for optimization simultaneously.

The argument in favor of optimizing biological outcome is that this is, of course, the aim of radiotherapy, dose being a traditional surrogate. The argument against it is that the biological models are relatively new and not universally accepted. To an extent there exists a difference in philosophy between some workers in the United Kingdom who have preferred to optimize dose and compute TCP and NTCP *a posteriori* and some in the United States who have taken a bolder approach and bypass dose (see Section VIII). There is plenty of scope for debate on the issue, which has received some attention already [17].

V. CLASSICAL AND FAST SIMULATED ANNEALING

Imagine that the system of beam weights are changed at each iteration by the addition of a "grain" g of beam weight to one particular beam element (see Figure 6). In classical simulated annealing the system is perturbed only slightly at each iteration, sometimes with a Gaussian generating function for g

$$\exp(-g^2/T_n) \tag{8}$$

where T_n is the temperature at iteration n. The author's early work had a generating function, which was simplified to a delta-function choice of either a positive or negative grain g, initially constant and then reduced in size toward the closing stages of iteration. The cooling proceeds as, or slower than,

$$\frac{T_0}{\ln(1+n)}. \tag{9}$$

In fast simulated annealing [25, 26], the grains are generated by a Cauchy distribution

$$\frac{T_n}{(T_n^2 + g^2)}. \tag{10}$$

The cooling proceeds as

$$\frac{T_0}{(1+n)}. \tag{11}$$

The faster cooling (and hence quicker computational times) is allowed because the form of the Cauchy distribution generates occasional large grains which allow the system to tunnel out of a local minimum. Depending on the cost function there may be no need for classical hill climbing (see Section VIII).

VI. PRACTICALITIES OF IMPLEMENTING SIMULATED ANNEALING FOR INVERSE TREATMENT PLANNING

First, it should be made clear that simulated annealing substitutes for only one part of the planning process, the calculation of beam weights by otherwise traditional forward planning. Thus, it requires to be fed exactly the same data as the forward planning problem, including:

1. specification of the PTV and OAR contours, derived from high-quality three-dimensional imaging data (e.g., X-ray CT, MRI, SPECT, and PET);
2. specification of the dose to each dose-space voxel per unit beam weight;
3. relevant biological models and data if a biological cost function is used; and
4. prescription/constraints on the treatment plan and/or on the beam weights themselves.

Similarly, the results of the calculation (three-dimensional dose maps) must be evaluated by the same tools as would be used to evaluate the outcome of forward treatment planning [i.e., DVHs, display of isodoses, three-dimensional shaded-surface display of dose, dose ribbons, display of dose super-

posed on anatomical sections, *a posteriori* TCP, and NTCP calculations (if simulated annealing was dose-based), etc.].

Hence, simulated annealing should properly form part of an integrated three-dimensional treatment planning system. When first introduced into the armamentarium of planning tools [14], this was not possible. A stand-alone implementation demanded that all these tasks be worked up independently for the application. How this was done is not central to understanding simulated annealing, but is described at length in a suite of papers [14–20, 27, 28].

The following features must be included:

1. Both positive and negative grains must be sampled so that there is a mechanism to "undo" structures which may be created early in the optimization but which may need to be removed once a wide search of state space has been made.
2. In classical simulated annealing the grain size should be reduced at the later stages of iteration to fine-tune the solution. In fast simulated annealing the Cauchy distribution should become increasingly more narrow.
3. Beam weights must be constrained positive. Any candidate change which passes the acceptance criterion for annealing is nevertheless rejected if it would lead to a beam weight going negative. This is an important step. Analytic inversion techniques on the other hand generally generate negative beam weights and then artificially, these have to be set to zero *a posteriori*, somewhat massaging the status of the result. Constrained iterative solution never gets into this difficulty.
4. Attention must be paid to the computational aspects of the calculation of the cost function, because this is at the heart of each iteration. This part must be computer-optimized. For example, there are tricks whereby the change in a quadratic cost function can be computed without evaluating the full function for each of two successive iterations [13, 14]. Also, when large three-dimensional arrays are being manipulated, care must be exercised in handling the order of sequencing through the dimensions of the array.
5. Other constraints can be applied to beam weights (e.g., requirement for smoothness in intensity-modulated beam profiles). The application of constraints leads to its being impossible to reach a zero of the cost function (which would require disallowed negative beam weights). The optimization will achieve some finite global minimum, which in turn will depend on the constraints.

Although simulated annealing appeals because of its wide flexibility, this very same ability to be tailored in many ways has a drawback. In the author's experience it is necessary to experiment somewhat in choice of grain sizes, number of iterations, and the importance weighting in the cost function, which in turn depends on the desired clinical outcome. If the cost function is expected to have local minima and uphill moves are to be included, then attention must be paid to the cooling scheme and the initial temperature (which determines both the initial and the total number of "wrong-way" changes accepted). The early papers by Barrett et al. [10] did not address these points, and in discussion with Professor Barrett he was of the opinion that the choices depended to some extent on the nature of the cost function in parameter space. Yet, this function is not well known *a priori*, hence the need to experiment [29].

Barrett (private communication, 1994) commented that problems such as the one used here for illustration may have cost functions with a very broad region with shallow curvature in the vicinity of the global minimum, and that consequently, different schemes for optimization can arrive at different parts of this "floor," with the global minimum being hard to reach. Put another way, there can be a large number of possible beam arrangements which correspond to much the same final dose distribution, the inversion from three-dimensional dose to beam weights being ill conditioned. Simulated annealing and least-squares iterative optimization provide a tool to control the optimization via the tuning features.

VII. IMPLEMENTATIONS AT ICR/RMH, LONDON

The work at ICR/RMH has proceeded in several stages:

The first application was to compute the one-dimensional intensity-modulated beam profiles which would create a two-dimensional dose distribution for a PTV with a concave outline in which might lie OARs. A series of model problems and clinical cases from the literature was solved, first with a simple beam model [14] and then with a model including scattered radiation [28]. This work occupied the period July 1988 to March 1990, and at that time there was a lot of interest in the potential uses of intensity-modulated radiation even though it was almost impossible to deliver radiation with this feature at the time (Figures 9 and 10).

The second application was to compute the beam weights for fields defined by an MLC [27]. The main advance was to recognize that each field could be divided into two, with one part seeing only PTV and the other seeing both PTV and OAR. The application was for those problems where it was not possible to create beams whose primary radiation only intersected PTV. For example, when irradiating the prostate, the rectum is in the field of view and indeed often overlaps the PTV. Simulated annealing was used to find the optimum set of pairs of beam weights. A number of "difficult" geometric model problems were studied where the PTV wrapped around the OAR (Figure 11).

The third application was to compute the two-dimensional

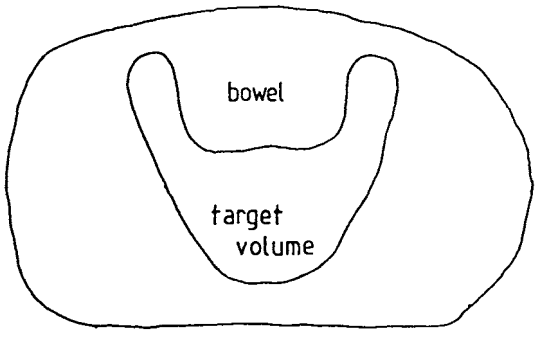

Figure 9. A two-dimensional planning problem where the aim is to obtain a high-dose treatment volume within the irregular PTV shown, while simultaneously sparing the dose to the bowel (OAR). This is a clinical planning problem first presented by Chin.

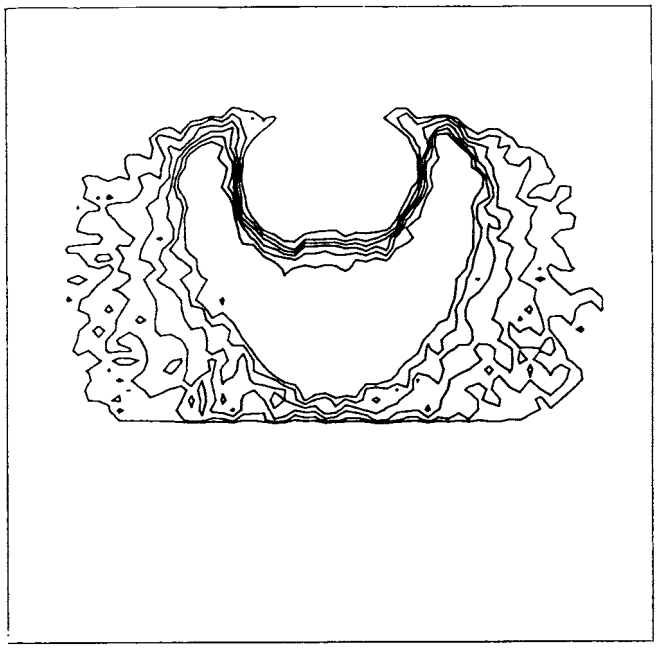

Figure 10. The resulting optimized two-dimensional dose map created by simulated annealing. The innermost dose contour is the 90% contour and the others (moving outward) are 80, 70, 60, 50, and 40%, respectively. The dose map is shown as a grey-scale image together with the beam sinogram in Webb [28].

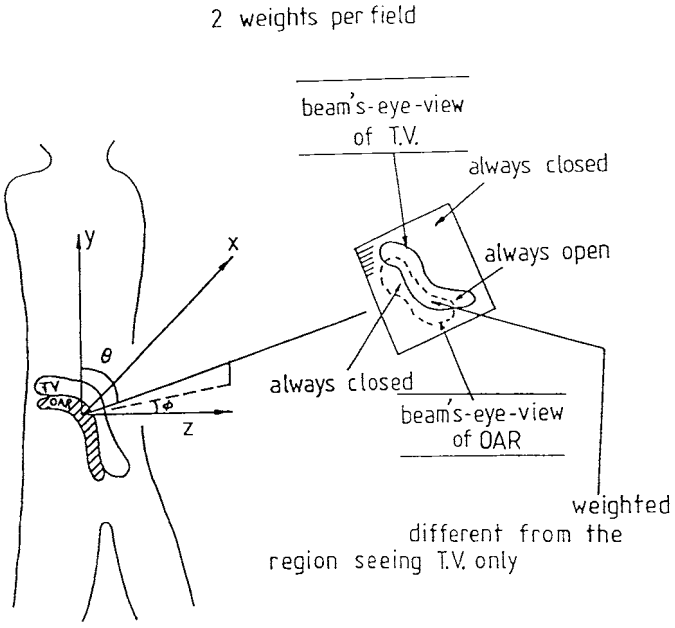

Figure 11. The way to optimize the separation between the DVH for PTV and OAR when multileaf-collimated beam's-eye-view ports are used. The multileaf collimator is shown to the right with the projected opening area corresponding to the views of the PTV and the OAR. These two curves overlap. The question arises how to handle the overlap region. A different beamweight is applied to the aperture viewing PTV only and the overlap aperture viewing PTV and OAR.

intensity-modulation across the MLC-shaped apertures for optimal three-dimensional conformal dose distributions [17]. Again, a number of difficult geometric model problems were studied, and this time the results were evaluated *a posteriori* by TCP and NTCP models. The first two applications were developed between March 1990 and July 1991.

The second application [with the original classical simulated annealing replaced by fast simulated annealing and the cost function of Equation (3)] has been implemented in a clinical context [24] (April 1992 onward) as part of the EC-funded AIM project A2003 called COVIRA, in collaboration with the German Cancer Research Centre (DKFZ) and the IBMUK Scientific Research Centre. The stand-alone system can now accept CT data from the image-handling package TOMAS, and the method has been implemented within the three-dimensional treatment planning package called VIRTUOS, which has grown out of VOXELPLAN.

The first application has been further studied to decide which method of delivering intensity-modulated beams may be most practical. Some preliminary results were presented at the 11th ICCR [21]. The tomotherapy technique seems preferable to creating IMBs from multiple static fields if only a few strata are used. However, a more thorough study [22] using a large number of strata for segmented delivery showed the two methods produced virtually indistinguishable results. Of much more relevance to outcome was the choice of tuning.

VIII. IMPLEMENTATION AT MSK, NEW YORK

Mohan [30] presented initial results of the New York work at the 10th ICCR. Mageras and Mohan [31] and Mohan et al. [23] investigated techniques for accelerating the convergence of the simulated annealing optimization technique for determining the beam weights for a large number of noncoplanar-shaped fields. Mageras and Mohan [31] investigated a model problem with 54 beams, arranged as three noncoplanar rings of 18 fields equispaced in 20° azimuth, one ring being transaxial and the other two at ±30° in latitude. The problem was to optimize a prostate treatment. Mohan et al. [23] chose fields not necessarily coplanar, so that no parallel-opposed fields occurred. These studies distinguished, for each orientation, two separate components of the field, namely, that "seeing" only PTV and that "seeing" PTV and OARs. The radiation beam weights for the former part-fields are traded off against those for the latter creating inhomogeneous dose distributions in the prostate. In this respect, the formalism was identical to that of Webb [17–20, 27].

Classical simulated annealing techniques generally choose to make a small change to one beam weight at each cycle of iteration, investigate the effect on some cost function, and then accept or reject the candidate change according to the criteria in Section III, which guarantee convergence to the global minimum cost. This involves some hill climbing to avoid trapping in local minima of the cost function, if these exist. Mageras and Mohan [31] implemented fast simulated annealing and compared it with classical simulated annealing.

Mageras and Mohan [31] and Mohan et al. [23] also proposed that at each cycle all beam weights are changed. Initially, the changes were large to coarsely explore the cost function. The cost function was based on biological response to radiation and considerations of NTCP and TCP, which

were derived from dose data using empirical models. The relative importance of TCP and NTCP was also accounted for in computing the cost or score function to be optimized. They proposed three distinct schemes for generating the candidate changes [classical simulated annealing with Gaussian and fixed-element generators (varying all beam weights simultaneously for the former per iteration and one beam weight only for the latter per iteration) and fast simulated annealing with a Cauchy generator (varying all beam weights simultaneously per iteration)], and each scheme requires specifying a function which updates the temperature, which controls the number of allowed hill climbs and the absolute size of the changes at each cycle.

Their results showed that with the two schemes in which all beam weights are simultaneously varied at each cycle, there is no need for hill climbing (i.e., zero temperature runs produce much the same result). This is because the wide search of the configuration space corresponds to tunnelling through from local minima as well as descent toward the global minimum.

Although for a model problem, the final cost function, TCP, and NTCP end up much the same with the new methods as with "one-change-per-cycle" simulated annealing, the beam weights can be quite different, reflecting the wide exploration of configuration space, and indeed, this allows them greatly to reduce (by eliminating beams with small weights) the number of fields needed (from 54 to 13 in the model problem) without radically altering the result. This would appear to be another example of the wide-bottomed cost function discussed earlier.

An additional advantage of fast simulated annealing with multiple beam weight changes per iteration is the increased speed of convergence by a factor of 10 or so.

Mohan et al. [23] found that "uneducated application of constraints" could thwart the optimisation altogether. Webb [27] similarly found that the choice of tuning in the cost function depended on what the goal was. Clearly, one cannot have the dose everywhere constrained *and* expect excellent PTV dose homogeneity. Mohan et al. [23] stated (although this is not formally proved) that optimization problems in radiotherapy involving TCP and NTCP probably have multiple minima and so simple descent methods cannot be relied on. There is scope for demonstrating the existence of local minima in specific circumstances and with specific cost functions.

IX. SOME COMMENTS ON COMPARATIVE ASPECTS OF ICR/RMH AND MSK IMPLEMENTATIONS

The work at the Memorial Sloan-Kettering Hospital and at the Royal Marsden Hospital is so closely parallel that some detailed points are extracted for comparison. Both approaches have the following features in common:

1. Both emphasize that there is a need for clear graphics to show the enormous wealth of information obtained by three-dimensional treatment planning systems.
2. Both calculate cost on a uniform dose grid.
3. Both point out that when using biological response data, it is important not to trust absolute values of TCP and NTCP, but that the use of relative values is acceptable.
4. Both ensure that there are no parallel-opposed beams. The beam locations are prespecified and a separate check must be done to see that the beam positions are practical without collisions.
5. Both used the biological data collated by Emami et al. and Burman et al.
6. Webb [17] used the NTCP model of Niemierko and Goitein and the effective volume at maximum dose method of reducing the dose-volume histogram (Kutcher–Burman method). Mohan et al. [23] used the Lyman equations and the effective dose-to-whole volume method of reducing the DVH. These are equivalent provided the NTCP is small.
7. Both methods incorporated the concept of "part-fields" seeing either PTV alone or PTV + OAR and created three-dimensional dose distributions which were highly conformal.

CONCLUSION

Simulated annealing is a powerful and flexible tool for treatment plan optimization. It has desirable features including controlling the positivity of beam weights and allowing a wide choice of cost function and flexibility to weight the importance of constraints in different regions in the patient. This same flexibility, however, demands considerable experimentation to determine optimum operating conditions. The first applications used classical simulated annealing, which is conceptually relatively simple but time consuming. Workers are now moving toward fast simulated annealing but still encountering the need to "tune" the algorithm.

ACKNOWLEDGMENTS

This review is an extended version of a review paper given in the International Course on Advances in Radiotherapy held at the Royal Marsden Hospital, 16–18 March 1994 just prior to the 11th ICCR in Manchester. The author is grateful to his colleagues in the Joint Department of Physics, Professor W. Swindell, Dr. A. Nahum, Dr. P. Mayles, Dr. P. Evans, and Dr. M. Oldham, for many discussions over the years on these subjects. He is also grateful to Professor R. Mohan for discussions at these conferences. He particularly wishes to acknowledge the active contributions to optimization in their Team made by Dr. M. Oldham, who since 1992 has been directly responsible for implementing the technique into VIRTUOS. The VIRTUOS implementation is funded under the EC AIM Project A2003 and has been carried out in collaboration with the German Cancer Research Centre (DKFZ) at Heidelberg and the IBMUK Scientific Research Centre in Hursley. The work of the Joint Department of Physics is supported by the Cancer Research Campaign.

REFERENCES

1. S. Webb, *The Physics of Three-Dimensional Radiation Therapy: Conformal Radiotherapy, Radiosurgery and Treatment Planning* (Institute of Physics Publishing, Bristol, 1993).
2. N. Metropolis, A. W. Rosenbluth, M. N. Rosenbluth, A. H. Teller, and E. Teller, "Equations of state calculations by fast computing machines," *J. Chem. Phys.* **21**, 1087–1092 (1953).
3. S. Kirkpatrick, C. D. Gelatt, and M. P. Vecci, "Optimisation by simulated annealing," *Science* **220**, 671–680 (1983).

4. S. Geman and D. Geman, "Stochastic relaxation, Gibbs distributions, and Bayesian restoration of images," *IEEE Trans. Patt. Anan. Mach. Int.* **PAMI6**, 721–741 (1984).
5. W. Jeffrey and R. Rosner, "Optimisation algorithms: Simulated annealing and neural network processing," *Astrophys. J.* **310**, 473–481 (1986).
6. W. H. Press, B. P. Flannery, S. A. Teukolsky, and W. T. Vetterling, *Numerical Recipes: The Art of Scientific Computing* (Cambridge University Press, Cambridge, 1986).
7. L. T. Willie. "Searching potential energy surfaces by simulated anealing," *Nature* **324**, 46–48 (1986).
8. N. Radcliffe and G. Wilson, "Natural solutions give their best," *New Scientist* **14th April**, 47–50 (1990).
9. W. H. Press and S. A. Teukolsky, "Simulated annealing optimisation over continuous spaces," *Comput. Phys.* **5**, 426–429 (1991).
10. H. Barrett, H. B. Barber, P. A. Ervin, K. J. Myers, R. G. Paxman, W. E. Smith, W. J. Wild, and J. M. Woolfenden, "New directions in coded-aperture imaging," in *Information Processing in Medical Imaging*. F. Deconinck, Ed., Martinus Nijhoff, Boston 1983, pp. 106–129.
11. R. G. Paxman, H. H. Barrett, W. E. Smith, and T. D. Milster, "Image reconstruction from coded data. 2: Code design," *J. Optical Soc. Amer.* **A2**, 501–509 (1985).
12. W. E. Smith, R. G. Paxman, and H. H. Barrett, "Image reconstruction from coded data. 1: reconstruction algorithms and experimental results," *J. Optical Soc. Amer.* **A2**, 491–500 (1985).
13. S. Webb, "SPECT reconstruction by simulated annealing," *Phys. Med. Biol.* **34**, 259–281 (1989).
14. S. Webb, "Optimisation of conformal radiotherapy dose distributions by simulated annealing," *Phys. Med. Biol.* **34**, 1349–1369 (1989).
15. S. Webb, "Inverse tomograph," *Nature* **344**, 284 (1990).
16. S. Webb, "A new dose optimising technique using simulated annealing," Proc. 9th Annual Meeting of ESTRO, Montecatini Sept. 1990, Leuven: ESTRO, p. 263.
17. S. Webb, "Optimisation by simulated annealing of three-dimensional conformal treatment planning for radiation fields defined by a multileaf collimator: 2. Inclusion of two-dimensional modulation of the X-ray intensity," *Phys. Med. Biol.* **37**, 1689–1704 (1992).
18. S. Webb, "Optimising dose with a multileaf collimator for conformal radiotherapy," Proc. of the 50th Annual Congress of the British Institute of Radiology, Birmingham, May 18–20 1992, London: BIR 1992, p. 15.
19. S. Webb, "Optimised three dimensional treatment planning for volumes with concave outlines, using a multileaf collimator," Proc. ART91 Munich, April 1991 (abstract book p. 66), in *Advanced Radiation Therapy: Tumour Response Monitoring and Treatment Planning*. A. Breit, Ed. Springer, Berlin 1992, pp. 495–502.
20. S. Webb, "Techniques for optimisation of dose with a multileaf collimator for conformal radiotherapy of target volumes with concave outlines," in *Three-Dimensional Treatment Planning*, P. Minet, Ed. and Publisher (Proceedings of the E.A.R. Conference in Geneva at W.H.O., October 1992), pp. 163–172.
21. S. Webb, "Tomotherapy and beamweight stratification," Proc. 11th I.C.C.R., Manchester, March 1994, in "*The use of computers in radiation therapy*" ed A. R. Hounsell et al p 58–59, Pub. Manchester ICCR.
22. S. Webb, "Optimising the planning of intensity-modulated radiotherapy," *Phys. Med. Biol.* **39**, 2229–2246.
23. R. Mohan, G. S. Mageras, B. Baldwin, L. J. Brewster, G. J. Kutcher, S. Leibel, C. M. Burman, C. C. Ling, and Z. Fuks, "Clinically relevant optimisation of 3D conformal treatments," *Med. Phys.* **19**, 933–944 (1992).
24. M. Oldham and S. Webb, "Optimisation by fast simulated annealing of three-dimensional conformal treatment plans of the prostate and theoretical limits of improvement in TCP and NTCP," *Br. J. Radiol.*, in press.
25. H. Szu, "Fast simulated annealing," AIP Conf. Proc. Neural Networks for Computing, Snowbird, UT, Apl 1986 151, 420–425, 1987.
26. H. Szu and R. Hartley, "Fast simulated annealing," *Phys. Lett.* **A122**, 157–162 (1987).
27. S. Webb, "Optimisation by simulated annealing of three-dimensional conformal treatment planning for radiation fields defined by a multileaf collimator," *Phys. Med. Biol.* **36**, 1201–1226 (1991).
28. S. Webb, "Optimisation of conformal radiotherapy dose distributions by simulated annealing 2: Inclusion of scatter in the 2D technique," *Phys. Med. Biol.* **36**, 1227–1237 (1991).
29. A. Silverman and J. Adler, "Animated simulated annealing," *Comput. Phys.* **6**, 277–281 (1992).
30. R. Mohan, "Clinically relevant optimisation of 3D conformal treatments," in *The Use of Computers in Radiation Therapy: Proceedings of the 10th International Conference on the Use of Computers in Radiation Therapy*. S. Hukku and P. S. Iyer Lucknow, Eds. ICCR Lucknow 1990, pp. 36–39.
31. G. S. Mageras and R. Mohan, "Application of fast simulated annealing to optimisation of conformal radiation treatments," *Med. Phys.* **20**, 639–647 (1992).

Exhibit E

IN THE UNITED STATES DISTRICT COURT

FOR THE DISTRICT OF DELAWARE

BEST MEDICAL INTERNATIONAL, INC.,	)	
	)	
Plaintiff,	)	
	)	
v.	)	C.A. No. 18-1599-MN
	)	
VARIAN MEDICAL SYSTEMS, INC. and VARIAN MEDICAL SYSTEMS INTERNATIONAL AG,	)	
	)	
Defendants.	)	

LETTER OF REQUEST FOR INTERNATIONAL JUDICIAL ASSISTANCE PURSUANT TO THE HAGUE CONVENTION OF 18 MARCH 1970 ON THE TAKING OF EVIDENCE ABROAD IN CIVIL OR COMMERCIAL MATTERS

The United States District Court for the District of Delaware presents its compliments to the appropriate judicial authority of Germany, and requests international judicial assistance to obtain evidence to be used in a civil proceeding before this Court in the above-captioned matter. A trial on this matter is scheduled at present for August 23, 2021, in Wilmington, Delaware. This request is made pursuant to Article 1 of the Hague Convention of 18 March 1970 on the Taking of Evidence Abroad in Civil or Commercial Matters (the "Hague Evidence Convention").

The Court requests the assistance described herein as necessary in the interests of justice. Specifically, this matter is a patent case, and the Court requests that appropriate judicial authority of Germany compel the production of documentary evidence and deposition testimony from MRC Systems GmbH – Medizintechnische Systeme ("MRC"), Hans-Bunte-Straße 8, 69123 Heidelberg, Germany, regarding a medical treatment system developed at MRC that may be prior art to one or more of the asserted patents.

1. Sender

The Honorable Maryellen Noreika
United States District Court for the District of Delaware
J. Caleb Boggs Federal Building
844 N. King Street
Wilmington, DE 19801-3555
USA

2. Central Authority of the requested state

Präsident des Amtsgerichts Freiburg
Holzmarkt 2
D-79098 Freiburg
Germany

3. Person to whom the executed request is to be returned

Defendants' counsel:

Ryan K. Wong
KEKER, VAN NEST & PETERS LLP
633 Battery Street
San Francisco, CA 94111
USA

4. Specification of the date by which the requesting authority requires receipt of the response to the Letter of Request: **March 13, 2020**.

IN CONFORMITY WITH ARTICLE 3 OF THE HAGUE EVIDENCE CONVENTION, THE UNDERSIGNED APPLICANT HAS THE HONOR TO SUBMIT THE FOLLOWING REQUEST:

5. a. Requesting judicial authority (Article 3, *a*):

The Honorable Maryellen Noreika
United States District Court for the District of Delaware
J. Caleb Boggs Federal Building
844 N. King Street
Wilmington, DE 19801-3555
USA

b. To the competent authority of (Article 3, *a*):

Präsident des Amtsgerichts Freiburg
Holzmarkt 2
D-79098 Freiburg
Germany

c. Names of the case and any identifying number:

Best Medical International, Inc. v. Varian Medical Systems, Inc. and Varian Medical Systems International AG
Civil Action Number 18-1599-MN
United States District Court for the District of Delaware

6. Names and addresses of the parties and their representatives (Article 3, *b*)

Plaintiff:

Best Medical International, Inc.
7643 Fullerton Road
Springfield, Virginia 22153
USA

Plaintiff's U.S. legal representative:

Philip Hirschhorn
BUCHANAN INGERSOLL & ROONEY PC
640 5th Avenue, 9th Floor
New York, NY 10019-6102
USA

Defendants:

Varian Medical Systems, Inc.
3100 Hansen Way
Palo Alto, CA 94304
USA

Varian Medical Systems International AG
Hinterbergstrasse 14
6312 Steinhausen
Switzerland

Defendants' U.S. legal representative:

Ryan K. Wong
KEKER, VAN NEST & PETERS LLP
633 Battery Street
San Francisco, CA 94111
USA

Other parties: None

7. Nature of the proceedings, summary of complaint, and summary of defenses (Article 3, *c*):

Plaintiff Best Medical, Inc. ("BMI") accuses defendants Varian Medical Systems, Inc. and Varian Medical Systems International AG ("Varian") of infringing four asserted patents: U.S. Patent Nos. 7,266,175, 7,015,490, 6,038,283, and 6,393,096. BMI amended its complaint on September 9, 2019, and Varian has moved to dismiss certain allegations in the amended complaint regarding indirect and willful infringement.

8. Evidence to be obtained and purpose of the evidence sought (Article 3, *d*):

a. Evidence to be obtained

i. Documents sufficient to show the conception, design, and development of the following aspects of the inverse the inverse treatment planning system developed at and/or commercialized by MRC ("KONRAD"), as referenced in Bortfeld and Oelfke, *IMRT with Mini Multi-Leaf Collimators and Compensators*, Course Compendium of the 1st IMRT Winter School (Heidelberg, 9-11) pp 53-63 (December 1999), and as described in the document available at https://www.accessdata.fda.gov/cdrh_docs/pdf2/K022307.pdf, at MRC before the stated date:

(a) Before August 11, 2003:

cost function computation for determining, selecting, or optimizing a collimator angle of a multi-leaf collimator;

cost function minimization relating to the determination, selection, or optimization of a collimator angle (including, *inter alia*, use of simulated annealing, logic for accepting or rejecting a beam-weight set on a given iteration, and logic for stopping the iteration);

consideration of target conformity and/or treatment plan delivery efficiency as cost terms in a cost function to determine, select, or optimize a collimator angle; and

user interface(s) for receiving optimization input relating to the determination of a collimator angle.

(b) Before July 11, 2003:

cost function computation;

cost function minimization (including, *inter alia*, use of simulated annealing, logic for accepting or rejecting a beam-weight set on a given iteration, and logic for stopping the iteration);

use of treatment plan delivery efficiency;

treatment delivery time;

total beam segments and/or total monitor units as part of treatment plan optimization;

use of dosimetric fitness as part of treatment plan optimization; and

user interface(s) for receiving optimization inputs and/or controlling tradeoffs between treatment plan delivery efficiency and dosimetric fitness.

ii. Documents sufficient to identify each version of KONRAD in use before August 11, 2003, the release date for each version, and differences between each version with respect to the aspects of KONRAD identified in Request No. i.

iii. Documents sufficient to show the design, operation, and functionality of the aspects of KONRAD identified in Request No. i for each version identified in response to Request No. ii.

iv. Documents sufficient to show that each version of KONRAD identified in response to Request No. ii was publicly available and/or in use anywhere in the world before August 11, 2003, such as academic journal articles, industry publications, press releases, product specifications, manuals, user guides, brochures, and/or web pages describing or identifying that version of KONRAD and its availability.

v. Documents sufficient to identify any apparatus, system, or device using KONRAD before August 11, 2003, and if such documents exist, before July 11, 2003. This request includes intensity-modulated radiation therapy

systems that comprise linear accelerators, treatment planning programs, and multi-leaf collimators.

vi. Documents and communications sufficient to show the design, structure, function, operation, and availability of each apparatus, system, or device identified in response to Request No. v.

vii. Documents and communications sufficient to show the sale, offer for sale, or importation into the United States of each apparatus, system, or device identified in response to Request No. v before August 11, 2003, and if such documents exist, before July 11, 2003.

b. Purpose of the evidence sought

The documents sought by these requests are directly relevant to the above-captioned litigation. These requests seek documents regarding specific features of a medical treatment system developed at MRC, which may be prior art to one or more of BMI's asserted patents under 35 U.S.C. § 102. If obtained, Varian would use these documents to develop its invalidity defenses for trial, and may rely on the documents to seek invalidation of one or more asserted patents.

9. Identity and address of any person to be examined (Article 3, *e*):

The Court requests that MRC Systems GmbH – Medizintechnische Systeme, Hans-Bunte-Straße 8, 69123 Heidelberg, Germany, designate one or more witnesses who are knowledgeable about the subject matter identified in section 10 below.

10. Statement of the subject matter about which the persons are to be examined (Article 3, *f*):

i. The conception, design, development, operation, and functionality of the aspects of KONRAD at MRC set forth in Document Request No. i before the date(s) specified in Document Request No. i.

ii. Each version of KONRAD in use before the date(s) specified in Document Request No. I, and the release date for each version.

iii. The date and circumstances of the first sale, offer for sale, and/or public use in the United States of KONRAD before the date(s) specified in Document Request No. i.

iv. The identity, design, operation, and functionality of any apparatus, system, or device using the aspects of KONRAD set forth in Document Request No. i before the date(s) specified in Document Request No. i.

v. The date and circumstances of the first sale, offer for sale, and/or public use in the United States of any apparatus, system, or device covered by Deposition Topic No. iv.

vi. The authenticity of documents produced in response to this Letter of Request, the public availability and publication dates of documents produced in response to this Letter of Request, the creation and authorship of documents produced in response to this Letter of Request, and whether and how the documents produced in response to this Letter of Request were created and/or stored in the ordinary course of business.

11. Any requirement that the evidence be given on oath or affirmation and any special form to be used (Article 3, *h*):

Because the testifying witnesses are outside this Court's subpoena power and cannot be compelled to attend trial, the Court requests that the witnesses' testimony be taken under oath in such manner as provided by the laws of Germany for the formal taking of evidence.

12. Special methods or procedure to be followed (Articles 3, *i* and 9):

The Court requests that the testimony be taken by oral examination in such manner as provided by the laws of Germany for the formal taking of evidence. To the extent permitted by the laws of Germany, the Court requests that the testimony be recorded by a videographer and transcribed by a stenographer.

13. Request for notification of the time and place for the execution of the Request and identity and address of any person to be notified (Article 7):

Please notify defendants' U.S. legal counsel at the following address:

Ryan K. Wong
KEKER, VAN NEST & PETERS LLP
633 Battery Street
San Francisco, CA 94111
USA

14. Specification of privilege or duty to refuse to give evidence under the law of the State of origin (Article 11, *b*):

Nothing in this Letter of Request is intended to interfere with any rights of MRC to assert privilege or refuse to give evidence under any applicable law of Germany or the United States of America.

15. Fees and costs

If the Präsident des Amtsgerichts Freiburg incurs fees or costs in executing this Letter of Request that are reimbursable under the second paragraph of Article 14 or Article 26 of the Hague Evidence Convention, the Court requests that the Präsident des Amtsgerichts Freiburg submit a bill of fees and costs to the Court and defendants' U.S. legal counsel:

Ryan K. Wong
KEKER, VAN NEST & PETERS LLP
633 Battery Street
San Francisco, CA 94111
USA

The Court guarantees that defendants' counsel will reimburse the Präsident des Amtsgerichts Freiburg for all reimbursable fees and costs incurred in executing this Letter of Request.

This Court expresses its gratitude to the authorities of Germany for assisting with this Letter of Request, and will provide similar assistance to the judicial authorities of Germany when requested.

DATE OF REQUEST: _____

SIGNATURE AND SEAL OF THE REQUESTING AUTHORITY

_____
The Honorable Maryellen Noreika
United States District Judge

Exhibit F

IN THE UNITED STATES DISTRICT COURT

FOR THE DISTRICT OF DELAWARE

BEST MEDICAL INTERNATIONAL, INC.,	)	
	)	
Plaintiff,	)	
	)	
v.	)	C.A. No. 18-1599-MN
	)	
VARIAN MEDICAL SYSTEMS, INC. and VARIAN MEDICAL SYSTEMS INTERNATIONAL AG,	)	
	)	
Defendants.	)	

LETTER OF REQUEST FOR INTERNATIONAL JUDICIAL ASSISTANCE PURSUANT TO THE HAGUE CONVENTION OF 18 MARCH 1970 ON THE TAKING OF EVIDENCE ABROAD IN CIVIL OR COMMERCIAL MATTERS

The United States District Court for the District of Delaware presents its compliments to the appropriate judicial authority of the Netherlands, and requests international judicial assistance to obtain evidence to be used in a civil proceeding before this Court in the above-captioned matter. A trial on this matter is scheduled at present for August 23, 2021, in Wilmington, Delaware. This request is made pursuant to Article 1 of the Hague Convention of 18 March 1970 on the Taking of Evidence Abroad in Civil or Commercial Matters (the "Hague Evidence Convention").

The Court requests the assistance described herein as necessary in the interests of justice. Specifically, this matter is a patent case, and the Court requests that appropriate judicial authority of the Netherlands compel the production of documentary evidence and deposition testimony from the Netherlands Cancer Institute ("NKI"), Plesmanlaan 121, 1066 CX Amsterdam, Netherlands, regarding a medical treatment system developed at NKI that may be prior art to one or more of the asserted patents.

1. Sender

The Honorable Maryellen Noreika
United States District Court for the District of Delaware
J. Caleb Boggs Federal Building
844 N. King Street
Wilmington, DE 19801-3555
USA

2. Central Authority of the requested state

The District Court in The Hague (Rechtbank Den Haag)
Team Administratie Civiel—Algemene Zaken
Postbus 20302
2500 EH THE HAGUE
Netherlands

3. Person to whom the executed request is to be returned

Defendants' counsel:

Ryan K. Wong
KEKER, VAN NEST & PETERS LLP
633 Battery Street
San Francisco, CA 94111
USA

4. Specification of the date by which the requesting authority requires receipt of the response to the Letter of Request: **March 13, 2020**.

IN CONFORMITY WITH ARTICLE 3 OF THE HAGUE EVIDENCE CONVENTION, THE UNDERSIGNED APPLICANT HAS THE HONOR TO SUBMIT THE FOLLOWING REQUEST:

5. a. Requesting judicial authority (Article 3, *a*):

The Honorable Maryellen Noreika
United States District Court for the District of Delaware
J. Caleb Boggs Federal Building
844 N. King Street
Wilmington, DE 19801-3555
USA

b. To the competent authority of (Article 3, *a*):

The District Court in The Hague (Rechtbank Den Haag)
Team Administratie Civiel—Algemene Zaken
Postbus 20302
2500 EH THE HAGUE
Netherlands

c. Names of the case and any identifying number:

Best Medical International, Inc. v. Varian Medical Systems, Inc. and Varian Medical Systems International AG
Civil Action Number 18-1599-MN
United States District Court for the District of Delaware

6. Names and addresses of the parties and their representatives (Article 3, *b*)

Plaintiff:

Best Medical International, Inc.
7643 Fullerton Road
Springfield, Virginia 22153
USA

Plaintiff's U.S. legal representative:

Philip Hirschhorn
BUCHANAN INGERSOLL & ROONEY PC
640 5th Avenue, 9th Floor
New York, NY 10019-6102
USA

Defendants:

Varian Medical Systems, Inc.
3100 Hansen Way
Palo Alto, CA 94304
USA

Varian Medical Systems International AG
Hinterbergstrasse 14
6312 Steinhausen
Switzerland

Defendants' U.S. legal representative:

Ryan K. Wong
KEKER, VAN NEST & PETERS LLP
633 Battery Street
San Francisco, CA 94111
USA

Other parties: None

7. Nature of the proceedings, summary of complaint, and summary of defenses (Article 3, *c*):

Plaintiff Best Medical, Inc. ("BMI") accuses defendants Varian Medical Systems, Inc. and Varian Medical Systems International AG ("Varian") of infringing four asserted patents: U.S. Patent Nos. 7,266,175, 7,015,490, 6,038,283, and 6,393,096. BMI amended its complaint on September 9, 2019, and Varian has moved to dismiss certain allegations in the amended complaint regarding indirect and willful infringement.

8. Evidence to be obtained and purpose of the evidence sought (Article 3, *d*):

a. Evidence to be obtained

i. Documents sufficient to show the conception, design, and development of the following aspects of the treatment planning system used at NKI to calculate 3-D dose distributions in conformal radiotherapy (the "U-M Plan"), as referenced in A. Bel, et al., *Target Margins for Random Geometrical Treatment Uncertainties in Conformal Radiotherapy*, 23 Med. Phys. 1537 (Sept. 1996), attached hereto as Attachment A-1, before May 27, 1998, and if such documents exist, before October 24, 1996:

cost function computation;

cost function minimization (including, *inter alia*, use of simulated annealing, logic for accepting or rejecting a beam-weight set on a given iteration, and logic for stopping the iteration);

use of partial volume data or dose volume constraints;

use of dose volume histograms;

importance factors; and

user interface(s) for receiving optimization input.

ii. Documents sufficient to identify each version of the U-M Plan in use before May 27, 1998, and if such documents exist, before October 24, 1996, the release date for each version, and differences between each version with respect to the aspects of the U-M Plan identified in Request No. i.

iii. Documents sufficient to show the design, operation, and functionality of the aspects of the U-M Plan identified in Request No. i for each version identified in response to Request No. ii.

iv. Documents sufficient to show that each version of the U-M Plan identified in response to Request No. ii was publicly available and/or in use anywhere in the world before May 27, 1998, and if such documents exist, before October 24, 1996, such as academic journal articles, industry publications, press releases, product specifications, manuals, user guides, brochures, and/or web pages describing or identifying that version of the U-M Plan and its availability.

v. Documents sufficient to identify any apparatus, system, or device using the U-M Plan before May 27, 1998, and if such documents exist, before October 24, 1996. This request includes multi-leaf collimators and linear accelerators.

vi. Documents and communications sufficient to show the design, structure, function, operation, and availability of each apparatus, system, or device identified in response to Request No. v.

vii. Documents and communications sufficient to show the sale, offer for sale, or importation into the United States of each apparatus, system, or device identified in response to Request No. v before May 27, 1998, and if such documents exist, before October 24, 1996.

b. Purpose of the evidence sought

The documents sought by these requests are directly relevant to the above-captioned litigation. These requests seek documents regarding specific features of a medical treatment system developed at NKI, which may be prior art to one or more of BMI's asserted patents under 35 U.S.C. § 102. If obtained, Varian would use these documents to develop its invalidity

defenses for trial, and may rely on the documents to seek invalidation of one or more asserted patents.

9. Identity and address of any person to be examined (Article 3, *e*):

The Court requests that the Netherlands Cancer Institute, Plesmanlaan 121, 1066 CX Amsterdam, Netherlands, designate one or more witnesses who are knowledgeable about the subject matter identified in section 10 below.

10. Statement of the subject matter about which the persons are to be examined (Article 3, *f*):

i. The conception, design, development, operation, and functionality of the aspects of the U-M Plan at NKI set forth in Document Request No. i before the date(s) specified in Document Request No. i.

ii. Each version of the U-M Plan in use before the date(s) specified in Document Request No. i, and the release date for each version.

iii. The date and circumstances of the first sale, offer for sale, and/or public use in the United States of the U-M Plan before the date(s) specified in Document Request No. i.

iv. The identity, design, operation, and functionality of any apparatus, system, or device using the aspects of the U-M Plan set forth in Document Request No. i before the date(s) specified in Document Request No. i.

v. The date and circumstances of the first sale, offer for sale, and/or public use in the United States of any apparatus, system, or device covered by Deposition Topic No. iv.

vi. The authenticity of documents produced in response to this Letter of Request, the public availability and publication dates of documents produced in response to this Letter of Request, the creation and authorship of documents produced in response to this Letter of Request, and whether and how the documents produced in response to this Letter of Request were created and/or stored in the ordinary course of business.

11. Any requirement that the evidence be given on oath or affirmation and any special form to be used (Article 3, *h*):

Because the testifying witnesses are outside this Court's subpoena power and cannot be compelled to attend trial, the Court requests that the witnesses' testimony be taken under oath in such manner as provided by the laws of the Netherlands for the formal taking of evidence.

12. Special methods or procedure to be followed (Articles 3, *i* and 9):

The Court requests that the testimony be taken by oral examination in such manner as provided by the laws of the Netherlands for the formal taking of evidence. To the extent permitted by the laws of the Netherlands, the Court requests that the testimony be recorded by a videographer and transcribed by a stenographer.

13. Request for notification of the time and place for the execution of the Request and identity and address of any person to be notified (Article 7):

Please notify defendants' U.S. legal counsel at the following address:

Ryan K. Wong
KEKER, VAN NEST & PETERS LLP
633 Battery Street
San Francisco, CA 94111
USA

14. Specification of privilege or duty to refuse to give evidence under the law of the State of origin (Article 11, *b*):

Nothing in this Letter of Request is intended to interfere with any rights of NKI to assert privilege or refuse to give evidence under any applicable law of the Netherlands or the United States of America.

15. Fees and costs

If the Rechtbank Den Haag incurs fees or costs in executing this Letter of Request that are reimbursable under the second paragraph of Article 14 or Article 26 of the Hague Evidence

Convention, the Court requests that the Rechtbank Den Haag submit a bill of fees and costs to the Court and defendants' U.S. legal counsel:

Ryan K. Wong
KEKER, VAN NEST & PETERS LLP
633 Battery Street
San Francisco, CA 94111
USA

The Court guarantees that defendants' counsel will reimburse the Rechtbank Den Haag for all reimbursable fees and costs incurred in executing this Letter of Request.

This Court expresses its gratitude to the authorities of the Netherlands for assisting with this Letter of Request, and will provide similar assistance to the judicial authorities of the Netherlands when requested.

DATE OF REQUEST: _____

SIGNATURE AND SEAL OF THE REQUESTING AUTHORITY

_____
The Honorable Maryellen Noreika
United States District Judge

ATTACHMENT A-1

C-RAD

SEE THE DIFFERENCE

Superior Surface Image Guided Radiation Therapy Solutions

Contact us to schedule your personalized product demonstration at info@c-rad.com

CATALYST HD™ SRT CYRPA LASER

Learn more at C-RAD.COM

Target margins for random geometrical treatment uncertainties in conformal radiotherapy

A. Bel,[a] M. van Herk, and J. V. Lebesque
Netherlands Cancer Institute, Antoni van Leeuwenhoek Huis, Plesmanlaan 121, 1066 CX Amsterdam, The Netherlands

(Received 18 September 1995; accepted for publication 19 February 1996)

In this study we investigate a method for positioning the margin required around the clinical target volume (CTV) to account for the random geometrical treatment uncertainties during conformal radiotherapy. These uncertainties are introduced by patient setup errors and CTV motion within the patient. Three-dimensional dose distributions are calculated for two four-field box techniques and a three-field technique, using rectangular fields. In addition, dose calculations are performed for four prostate cases, treated with a three-field conformal technique. The effects of random rotational and translational deviations on the delivered dose are described as a convolution of the ''static'' dose with the distribution of the deviations. For the rectangular field techniques, these convolutions are performed with a range of standard deviations (SDs) of the distribution of random translations (0–7 mm in the three directions) and rotations (0°–5° around the main axes). Two centers of rotation are considered: the isocenter and a position that is 3.5 cm shifted with respect to the isocenter. For the prostate cases, the random deviations are estimated by combining the results from organ motion and setup accuracy studies. The required margin is defined as the change in the position of the static 95% isodose surface by the convolution and it is approximated by a morphological erosion operator, applied to the static 95% isodose surface. When the center of rotation coincides with the isocenter the change in the position of the static 95% isodose surface can accurately be described by an erosion operator. For the rectangular field techniques, the margin is equal to about 0.7 SD of the distribution of translations, independent of the distribution of rotations. When the center of rotation does not coincide with the isocenter and rotations are considerable, the margin is strongly place dependent, and the accuracy of the approximation by an erosion operator is much lower. In conclusion, margins for random uncertainties can be approximated by a dilation operator (inverse of an erosion operator) when the center of rotational deviations coincides with the isocenter. The size of the margin is about 0.7 SD of the distribution of translations. When rotational deviations are present and the center of rotation does not coincide with the isocenter, the margin can become strongly place dependent and the convolution computation should be incorporated in the planning system.

Key words: 3-D treatment planning, geometrical treatment uncertainties, target margins, morphological image processing

I. INTRODUCTION

During radiotherapy, setup accuracy is important, since geometrical misses can result in a failure to eradicate the tumor. In clinical practice, however, uncertainties in the position of the tumor are inevitable. The recent ICRU Report 50[1] gave guidelines regarding the definition of the tumor and ''safety'' margins to ensure an adequate dose. The gross tumor volume (GTV) containing the macroscopic visible tumor is defined first. Subsequently the clinical target volume (CTV) that includes microscopic tumor extension around the GTV, is defined. To account for uncertainties in its position, the CTV is extended with a margin to the planning target volume (PTV). The treatment planning should be designed in such way that the high dose region (e.g., the 95% isodose surface) matches the PTV as closely as possible.

The size of the margin around the CTV is very important. Making this margin larger than necessary can lead to excessive irradiation of surrounding healthy tissues, while a small margin can result in underdosage of the CTV. The ICRU Report 50, however, did not discuss what the size of the margin should be for specific treatment techniques. The size of the margin is closely related to the magnitude and statistical character of positional uncertainties of the CTV. Therefore, quantitative knowledge of these uncertainties for specific treatment techniques is essential.

Variations in the position of the CTV during the course of a multifractionated treatment arise from setup uncertainties and organ motion. Portal imaging studies showed that setup deviations can be described statistically by a systematic and a random component.[2–5] Both types of deviations can be corrected by on-line repositioning the patient during each treatment session.[6–9] However, application of these procedures involve an additional treatment time of nearly 60%.[6] Therefore, for routine clinical practice, an off-line procedure is often preferred.[2,3] With such a procedure, decisions on repositioning of the patient are taken after the treatment ses-

sion. Consequently, only systematic deviations can be corrected in this way and random deviations remain present.

The other source of geometrical uncertainties is organ motion. The motion of the prostate during treatment has been studied by several authors.[10–15] Van Herk *et al.*[10] have shown that the combined motion of the prostate and seminal vesicles can be described by a translation and a rotation. The largest rotations were found around the left–right axis. In their analysis, the rotations were calculated around the center of gravity of the combined contours of the prostate and seminal vesicles, while it was assumed that the deformations of the prostate and seminal vesicles were negligible.

Several methods have been described to estimate the effect of geometrical uncertainties on the actual delivered dose. A method to deal with systematic deviations was proposed by Kutcher *et al.*[16] They computed a range of dose-volume histograms (DVHs) for the CTV and organs at risk by sampling the distribution of systematic deviations. By comparing the DVHs, it was determined if the treatment plan (including a margin) was satisfactory.

To study the effect of random deviations, the actual delivered dose distribution can be approximated by a convolution of the "static" dose distribution, obtained from the treatment plan, with the distribution of random deviations. Leong[17] was the first investigator to show the consequences of such a convolution in two dimensions. In general, the convolution leads to a blurring of the dose distribution, which can be visualized by shrinking the high-dose area.

Rudat *et al.*[18] determined the distribution of translational setup deviations of thoracic and pelvic treatments. Using this distribution, a convolution of the static three-dimensional dose distribution was performed. As a result of the convolution, the tumor control probability reduced considerably, indicating that the safety margin around the GTV was not large enough. Stroom *et al.*[19] studied the effect of the convolution in three dimensions on dose distributions for prostate treatment. They included rotational deviations in the convolution, leading to a (further) blurring of the dose distribution. However, none of these authors[17–19] used the convolution method for determining the required margin for ensuring a sufficient dose to the CTV.

Using different approaches, some other authors suggested a size for the margin[20,21] around the CTV. Urie *et al.*[21] defined a margin in such a way that at the 85% level of confidence, the CTV was within that margin. However, they took neither the actual dose distribution into account nor distinguished random from systematic deviations. Lind *et al.*[20] used a one-dimensional biological model to find margins for random deviations. They optimized the probability of uncomplicated tumor control and found a margin that depended on the proximity of organs at risk (0.5 SD–0.8 SD of the distribution of translations).

In the present paper, we elucidate the effect of a convolution of three-dimensional dose distributions with rotations and translations. The aim of this study is to determine which margins should be used clinically for several treatment techniques and various distributions of random deviations.

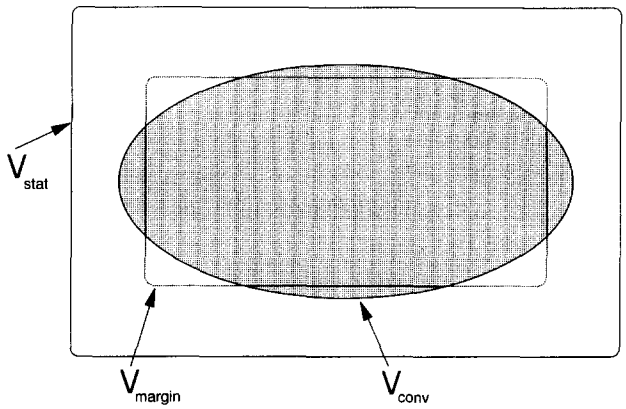

FIG. 1. Schematic two-dimensional representation of the definition of the "inverse" margins. By performing a convolution of the dose distribution, the volume enclosed by the static 95% isodose surface (V_{stat}) (solid line) shrinks to V_{conv} (shaded area). This latter volume was approximated by an erosion operator, working on V_{stat}, resulting in V_{margin} (dotted line). The mismatch between V_{conv} and its approximation (V_{margin}) is minimized with a cost function.

II. METHODS AND MATERIALS

A. Definition of margins

In this study, the 95% isodose level is chosen for coverage of clinical target volume (CTV).[1] This is accomplished by extending the CTV with a margin for the random and systematic geometrical deviations to the planning target volume (PTV).[1] Subsequently, the treatment planning should be performed in such way that the 95% isodose surface surrounds the PTV as closely as possible. For the purpose of this study, we do not consider systematic deviations.

It is assumed that random deviations are generally so small that a shift of the CTV can be considered as a shift of the dose distribution in the opposite direction,[17] neglecting the effects of inhomogeneities, irregularities of the outer contours, and a different source–skin distance. For a multifractionated treatment, the actual delivered dose can be described by a convolution of the static dose distribution with the distribution of random deviations.[17]

One procedure for establishing treatment margins starts by defining the CTV, extending it with a margin to obtain the PTV, positioning and shaping the treatment fields, and calculating the dose distribution. At this point the convolution can be performed. The margin and the treatment plan have to be modified until the convolved dose distribution is satisfactory, i.e. the 95% isodose surface of the convolved dose distribution matches the CTV.

To find the size of the margins in this study, an approach was used in which the static dose distribution was the starting point. The convolution of the static dose distribution results in a "shrinkage" of the static 95% isodose surface (Fig. 1). Therefore, the current investigation examines the possibility of using an "inverse" margin to approximate this shrinkage.

B. Convolution of the dose distribution

Several assumptions regarding the random deviations were made. The random deviations were assumed to be normally distributed, and the distributions of setup deviations and organ motions were combined to normal distributions for translations and rotations. All variables were assumed to be uncorrelated. A positional deviation of the dose distribution was described by performing rotations first and subsequently translations, but this order is in practice irrelevant for the result of the convolution.

The effect of the random deviations on the actual delivered dose distribution was described by a convolution of the static three-dimensional (3-D) dose distribution $D_0(\mathbf{r})$ with the distribution of the translations $N_t(\mathbf{r})$, and rotations $N_r(\alpha,\beta,\gamma)$:

$$D(\mathbf{r})=\int_{-\infty}^{\infty}d\mathbf{r}'\int_{-\pi}^{\pi}d\alpha\int_{-\pi}^{\pi}d\beta\int_{-\pi}^{\pi}d\gamma \times D_0[R^{-1}(\alpha,\beta,\gamma)\mathbf{r}-\mathbf{r}']N_r(\alpha,\beta,\gamma)N_t(\mathbf{r}'). \quad (1)$$

$R^{-1}(\alpha,\beta,\gamma)\mathbf{r}$ denotes the rotation of the vector $\mathbf{r}$ by the inverse 3×3 rotation matrix $R^{-1}(\alpha,\beta,\gamma)$.

The distribution of the translations is given by a 3-D normal distribution:

$$N_t(\mathbf{r})=\frac{e^{-(x^2/2\sigma_x^2+y^2/2\sigma_y^2+z^2/2\sigma_z^2)}}{\sigma_x\sigma_y\sigma_z(2\pi)^{3/2}}, \quad (2)$$

with σ_x, σ_y, and σ_z the standard deviation (SD) of the distribution along the X, Y, and Z axis, respectively. The distribution of rotations is given by the analog equation, with the SD equal to σ_α, σ_β, and σ_γ for rotations around the X, Y, and Z axis, respectively.

When the convolution with translations and rotations is performed consecutively, the calculation time can be shortened considerably. Therefore, a substitution of variables was introduced in the integration in Eq. (1): $\boldsymbol{\rho}=\mathbf{r}-\mathrm{R}(\alpha,\beta,\gamma)\mathbf{r}'$. Equation (1) can now be rewritten as

$$D(\mathbf{r})=\int_{-\infty}^{\infty}d\boldsymbol{\rho}\int_{-\pi}^{\pi}d\alpha\int_{-\pi}^{\pi}d\beta\int_{-\pi}^{\pi}d\gamma\, D_0[R^{-1}(\alpha,\beta,\gamma)\boldsymbol{\rho}] \times N_r(\alpha,\beta,\gamma)N_t[R^{-1}(\alpha,\beta,\gamma)(\mathbf{r}-\boldsymbol{\rho})]. \quad (3)$$

When the normal distribution of the translational deviations is spherical symmetric (i.e., the SDs are equal in all directions), the convolution with rotations and translations in Eq. (3) can be separated since $N_t[R^{-1}(\alpha,\beta,\gamma)(\mathbf{r}-\boldsymbol{\rho})]=N_t(\mathbf{r}-\boldsymbol{\rho})$. For the actual numerical calculation, Eq. (3) was rewritten in discrete form, with the convolution for translations and rotations separated:

$$D[x,y,z]=N_t[x,y,z] \otimes\left[\sum_{\alpha=-3\sigma_\alpha}^{\alpha=3\sigma_\alpha}\sum_{\beta=-3\sigma_\beta}^{\beta=3\sigma_\beta}\sum_{\gamma=-3\sigma_\gamma}^{\gamma=3\sigma_\gamma}N_r[\alpha,\beta,\gamma] \times D_0[x_r,y_r,z_r]\right]. \quad (4)$$

Here, x_r,y_r,z_r denote the coordinates x,y,z rotated by the matrix $R^{-1}(\alpha,\beta,\gamma)$. The spatial convolution is denoted by $\otimes$. For some cases in this study, the convolution was performed with SDs of the distribution of translations that were different in the three directions. In these cases, the convolution, as given by Eq. (4), could not be used and a discrete version of Eq. (1) was used instead.

The convolution was implemented by rotating the static dose distribution over the discrete angles α,β,γ separately, using trilinear interpolation. The dose distribution was first rotated over a discrete angle α, next over β, and finally, over the whole range of angles γ. After each rotation over γ, the voxel values of the rotated dose distribution were multiplied with the corresponding weight $N_r[\alpha,\beta,\gamma]$ and summed. Finally, a convolution for translations of the total sum was performed, consecutively in the three main directions (using a kernel), resulting in the convolved dose distribution $D[x,y,z]$.

The spacing between the discrete angles α,β,γ was taken equal to 0.5 times the SD of the corresponding distribution. The distributions of the rotations and translations were truncated at three times the SD and were renormalized to 1.

The convolution was implemented using integer arithmetic. With a typical number of grid points (100 in each direction), the computation time of the convolution with only translations took 3–15 s on a Pentium PC (90 MHz), depending on the SD of the distribution of translations. The convolution with translations and rotations was more time consuming [about 30 min, using Eq. (4) and about 8 h, using Eq. (1)].

C. Approximation of margins

The required margin was defined as the change in the position of the 95% isodose surface by the convolution. This change was approximated by a morphologic filter. An erosion operation[22] results in a shrinkage of a geometrical structure and the applicability of this operator to describe the required margin was tested. The margin as described by the erosion operator shall be referred to as the approximated margin.

A cost function was defined as the volume of the nonoverlapping voxels of the volume enclosed by the convolved 95% isodose surface (V_{conv}) and it approximation (V_{margin}) (the terminology is described in Table I and illustrated in Fig. 1). This cost function was minimized to find the optimal size of the erosion operator. The size of the erosion operator increased with one voxel in each of the three main directions.

To obtain the optimal size of the erosion operator with adequate accuracy, the static and convolved dose distribution

TABLE I. Definitions of volumes.

Volume	Definition
V_{stat}	Volume enclosed by the static 95% isodose surface
V_{conv}	Volume enclosed by the convolved 95% isodose surface
V_{margin}	Volume defined by the erosion operator working on V_{stat}

(calculated with a grid size equal to 1.25 mm) were resampled, using trilinear interpolation, to a grid with dimensions of 0.63 mm in the three directions. The part of V_{conv} that did not overlap with the approximation V_{margin}, was used as a measure of the accuracy of the approximation. This volume is equal to half the minimum of the cost function and was expressed relative to V_{conv} (denoted by M_{acc}).

D. Treatment techniques

Three-dimensional dose distributions were calculated using U-MPlan (University of Michigan, Ann Arbor, MI), using 8 MV x-ray beams for all cases. The calculation volume was chosen such that it enclosed the 95% isodose surface with a margin of at least 2 cm (three times the maximum value of the SD of the distribution of translations).

Using a water phantom (dimensions $X \times Y \times Z$ equal to 40 cm$\times$20 cm$\times$20 cm), three treatment techniques with rectangular fields were considered with the X-Z plane containing the beams' axes. First, a four-field box technique was studied with 10×10 cm^2 fields and equally weighted (at isocenter) beams. Second, a four-field technique with 10×5 cm^2 fields was considered (elongated box), leading to a 95% isodose surface that was elongated in the Y direction. Finally, a three-field technique was studied (with 10×10 cm^2 fields), with one beam in the Z direction (weight 1.0) and two opposed beams in the X direction (weights 0.6) with wedges (angles equal to 55°).

In addition, treatment plans for four prostate cases were examined. The patients were irradiated with an AP and a left and right lateral wedged field, with conformal blocks in each field. The calculation of the dose distribution was based on CT densities. For these cases, the coordinates X, Y, and Z corresponded to the left–right, caudal–cranial, and posterior–anterior directions, respectively. To study if rotations could have a large effect on the required margin, cases were selected with an "elongated" shape of the 95% isodose surface; for these cases the seminal vesicles were supposed to contain tumor cells and consequently belong to the CTV.

E. Applied standard deviations organ motion and setup deviations

For the three techniques with rectangular fields, the convolution was performed for an isotropic distribution of the translations and rotations. A range of SDs was taken, with values equal along/around the three axes and with the center of rotation coinciding with the isocenter. The static dose distribution was convolved with the SDs of the distribution of translations ranging from 0 to 7 mm, in steps of 0.5 mm, in the three directions. The effect of additional rotations was studied for three distributions (SDs equal to 0°, 3°, and 5° around the three axes). In addition, it was studied if an anisotropy in the distribution of translations and rotations and a shifted center of rotation had a large effect on the margins. The convolution was performed with the SD in the X direction ranging from 1.5 to 3.5 mm, combined with a SD in the two other directions, which was twice as large. Rotations were taken to be equal to zero in this case. Different distributions of rotations around the three main axes were considered (SD 5° around the X axis, no rotations around the other axes, SD translations equal to 2.5 mm in the three directions), with the isocenter as the center of rotation. Using these parameters, the convolution was also performed with the center of rotation shifted 3.5 cm with respect to the isocenter in the Y direction.

For the four prostate cases, the distribution of random deviations was estimated, using the results of two recent studies from our institution: an organ motion study of the prostate[10] and a portal imaging study, describing the setup accuracy of prostate treatments.[2] In the organ motion study,[10] the rotations were calculated around the center of gravity of the combined contours of the seminal vesicles and the prostate. From the correlation between rotations and translations, it was estimated, however, that the apex of the prostate was the actual center of rotation. Using this center of rotation, the SDs of the distribution of the translations were recalculated, yielding 0.7, 1.4, and 1.5 mm in the X, Y and Z directions, respectively. These SDs were smaller than reported by van Herk *et al.*,[10] since rotational deviations induce an overestimate of translational deviations when rotations are calculated around a center that is not the actual center of rotation. In the portal imaging study, we analyzed the distributions of translational setup deviations of patients treated for prostate cancer.[2] The SDs were equal to 2.0, 1.8, and 1.7 mm in the X, Y, and Z directions, respectively. The SDs of the distribution of random rotational deviations of the setup, were estimated to be 1° (1 SD) around the three main axes.

The variances of the distributions of random organ motion and setup deviations were added and these values were used for the convolution. The resulting SDs were equal to 2.1, 2.4, and 2.5 mm for the distribution of translations in the X, Y, and Z directions, respectively, and 4°, 2°, and 2° for the distribution of rotations around these axes, respectively.

III. RESULTS

A. Treatment techniques with rectangular fields

1. Isotropic distributions

The optimal size of the erosion operator (approximated margin) was calculated for the three treatment techniques with rectangular fields, for isotropic distributions of random deviations. For all these treatment techniques, this size was about equal in the X and Z directions. Therefore, the average over these two directions is presented (Fig. 2). The approximated margin was slightly smaller for the Y direction than for the other two directions. This was due to the less steep

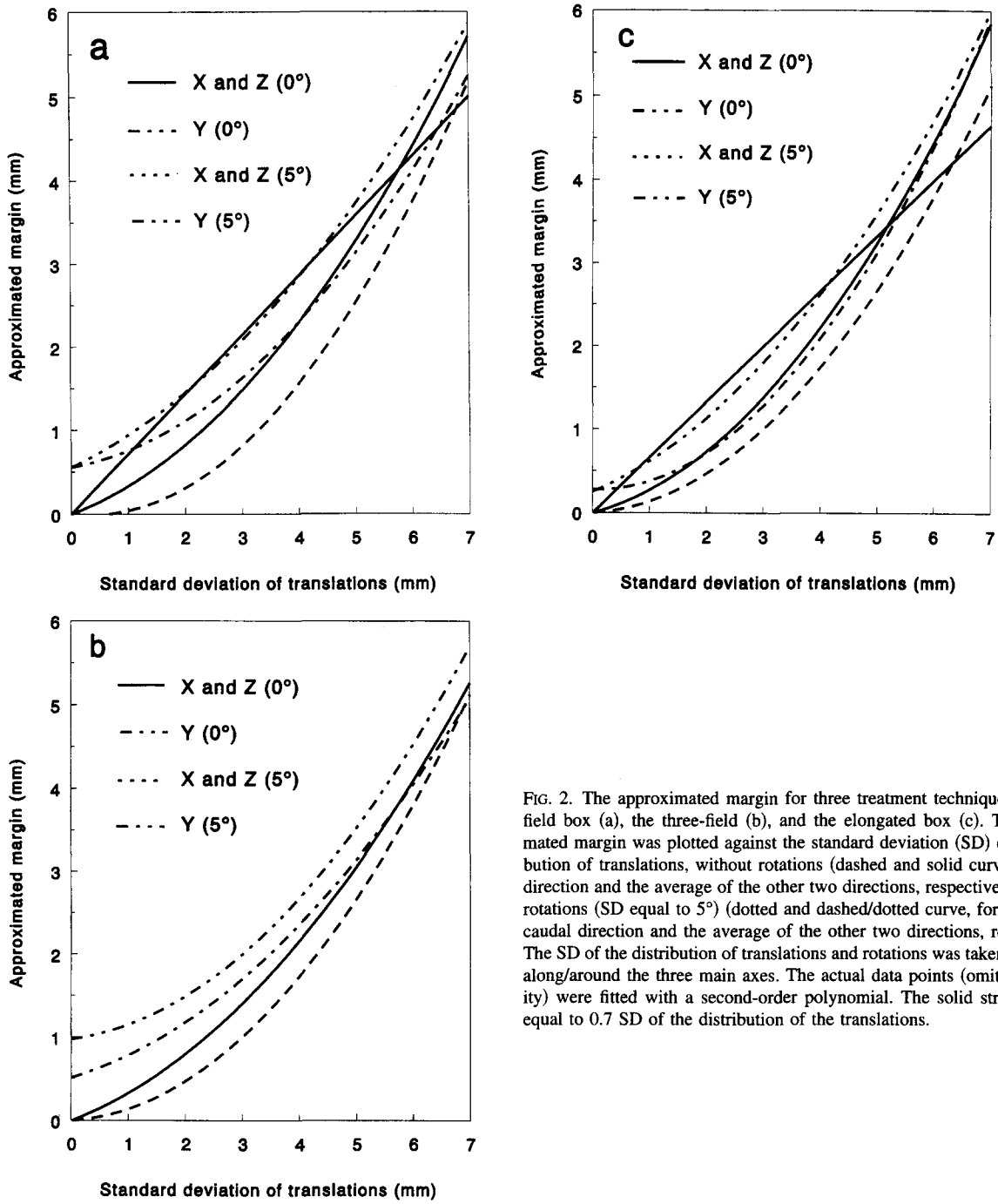

FIG. 2. The approximated margin for three treatment techniques: the four-field box (a), the three-field (b), and the elongated box (c). The approximated margin was plotted against the standard deviation (SD) of the distribution of translations, without rotations (dashed and solid curve, for the Y direction and the average of the other two directions, respectively) and with rotations (SD equal to 5°) (dotted and dashed/dotted curve, for the cranio–caudal direction and the average of the other two directions, respectively). The SD of the distribution of translations and rotations was taken to be equal along/around the three main axes. The actual data points (omitted for clarity) were fitted with a second-order polynomial. The solid straight line is equal to 0.7 SD of the distribution of the translations.

dose gradient around the 95% isodose surface in the Y direction, although the penumbra was smaller than in the other two directions.

Rotations had only a limited impact on the size of the approximated margins, since the center of rotation coincided with the center of the volume enclosed by the static 95% isodose surface, V_{stat}, (the isocenter), and this volume had round corners to start with. Even with a standard deviation (SD) of the distribution of rotations equal to 5°, there was only a slight increase in the approximated margin (Fig. 2).

The approximation of the margin by the erosion operator was good. For the three treatment techniques, for all values of the SDs, the mismatch between the convolved and approximated 95% isodose surface (M_{acc}) was smaller than 3%.

From these results, it is clear that the approximated margin did not strongly depend on the distribution of rotations, the treatment technique, or the penumbra in a particular direction. For instance, for the box technique with 10×10 cm^2 fields [Fig. 2(a)], the approximated margin without rotational deviations and with a SD of the distribution of translations of 4 mm, is equal to about 1.5 mm in the Y direction and 2 mm in the X and Z directions. With additional rotations (SD 5°), the approximated margin is equal to about 2 mm in the Y

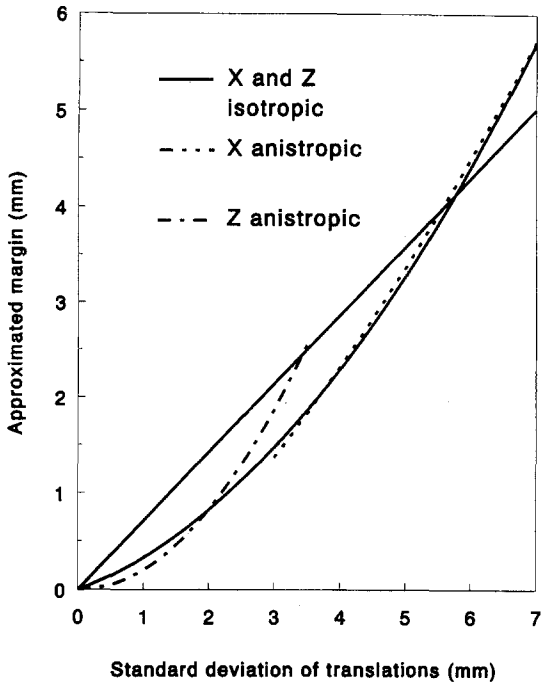

FIG. 3. The approximated margin for the four-field box technique for anisotropic distributions of the translations. The dotted curve represents the approximated margin in the X direction, with the standard deviation (SD) ranging from 1.5–3.5 mm. The dashed curve represents the approximated margin in the Z direction, with a SD that is twice as large as the corresponding SD in the X direction, thus ranging from 3–7 mm. The solid curve indicates the approximated margin in the isotropic case [the average of the X and Z directions; see Fig. 4(a)]. The points (omitted for clarity) were fitted with a second-order polynomial. The solid straight line is equal to 0.7 SD of the distribution of translations. The SD of the distribution of rotations was equal to zero in all cases.

direction and 2.5 mm in the X and Z directions. For larger values of the SD of the distribution of translations, the differences between the approximated margin in the main directions and the effect of additional rotations on the approximated margin are smaller. The results for the other treatment techniques are comparable [Figs. 2(b) and 2(c)]. In general, for a clinically relevant range of SDs of the distribution of translations, (2–5 mm), the approximated margin is about equal to or smaller than 0.7 SD of the distribution of the translations, independent of the treatment technique [Figs. 2(a)–2(c)].

2. Anisotropic distributions

The optimal size of the erosion operator was calculated for a convolution with anisotropic distributions of translations (SD in the X direction two times smaller than in the other two directions). For the box technique with four 10×10 cm^2 fields, the approximated margin in the X direction was slightly larger than the approximated margins that were estimated for the isotropic case (Fig. 3). For the other two directions, the approximated margin hardly changed with respect to the isotropic case. Similar results were obtained for the two other techniques (data not shown). The approximation of the margin by the erosion operator was

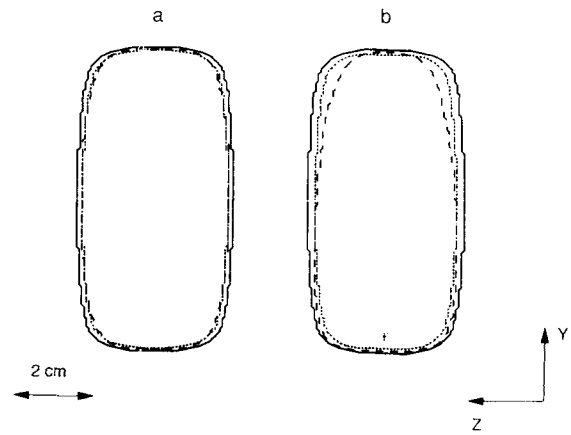

FIG. 4. Effect of a change of the center of rotation in the sagittal plane for the elongated box technique. The standard deviation (SD) of the distribution of rotations was equal to 5° around the X axis and 0° around the two other axes, and the SD of the distribution of translations was equal to 2.5 mm in the three directions. The static and convolved 95% isodose surface (enclosing V_{stat} and V_{conv}, respectively) are indicated by the solid and dashed line, respectively. V_{margin} (approximated V_{conv} after application of the erosion operator) is indicated by the dotted line. The center of rotation (indicated by the cross) was at the position of the isocenter (a) and shifted 3.5 cm with respect to that position (b).

good, with $M_{acc}\leqslant3\%$. In all cases, the approximated margin in each direction was still about equal to or smaller than 0.7 SD of the distribution of translations in that direction.

The margin hardly changed by an anisotropy in the rotations with respect to the isotropic case (only rotations around the Z axis, with SD 5°, and translations 2.5 mm in all directions) [Fig. 4(a)]. However, when the center of rotation did not coincide with the center of V_{stat}, the approximation of the margin by the erosion operator was rather poor. As an example, the result is shown for the elongated box [Fig. 4(b)]. There was clearly a mismatch between V_{conv} and its approximation V_{margin}, due to the place-dependent effect of the rotations on the change of the static 95% isodose surface by the convolution. In the Y-Z plane, the distance between the two surfaces in the main directions was about 2 mm near the center of rotation and 4 mm far from this center. M_{acc} was equal to 5% in this case. The results for the other treatment techniques (data not shown) were comparable.

B. Conformal technique: Prostate

The convolution of dose distributions was performed for four conformal prostate treatments, using the apex of the prostate as the center of rotation. For these cases, an equal size of the approximated margin was found in the X direction (Table II). In the other two directions, there was a slight variation from patient to patient. Because the center of rotation did not coincide with the center of V_{stat}, the approximation of V_{conv} by the erosion operator was rather poor. M_{acc} was in general larger than for the treatment techniques with rectangular fields (between 3% and 11%).

The value of M_{acc} was related to the shape of the static 95% isodose surface, V_{stat}. For case 1, with a relatively "round" shape of V_{stat}, M_{acc} was smaller than for case 4,

TABLE II. The approximated margins for the random uncertainties (i.e., size of the erosion operator) for the conformally treated prostate patients. M_{acc} indicates the accuracy of the approximation, and is defined of the percentage part of V_{conv} (volume enclosed by convolved 95% isodose) that did not overlap with the approximation by the erosion operator (V_{margin}).

	Approximated margin (mm)			
	X	Y	Z	M_{acc} (%)
Patient number				
1	1.3	1.3	3.2	3.2
2	1.3	1.9	2.6	5.0
3	1.3	1.3	1.9	6.7
4	1.3	1.9	2.6	11.0

with a relatively elongated shape of V_{stat} (Fig. 5). Due to the rotations, there was quite a large mismatch between V_{conv} and its approximation, V_{margin} for case 4. For both case 1 and case 4, the required margin was underestimated in the region far from the center of rotation (seminal vesicles). In the region near the center of rotation (apex), the size of the required margin was overestimated.

IV. DISCUSSION

The change of the 95% isodose surface due to random motion was approximated by an erosion operator. When the center of rotation is positioned at the isocenter the margin defined in this way is a good first approximation of the required margin for random deviations. The size of the erosion operator is about equal to 0.7 times the standard deviation (SD) of the distribution of translations in each direction. However, when the center of rotation did not coincide with the isocenter, the approximation becomes rather poor, because random rotations induce a strongly place-dependent change of the 95% isodose surface. The inaccuracy in the approximated margin, as defined by the erosion operator, is caused by the nature of such a morphologic filter, which can be direction dependent but which cannot describe place-dependent changes.

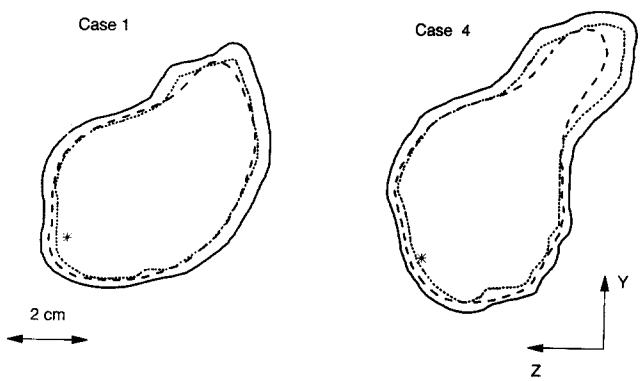

FIG. 5. Two examples of a sagittal view of 95% isodoses without and with the convolution for two prostate patients. The static and convolved 95% isodose surface (enclosing V_{stat} and V_{conv}, respectively) are indicated by the solid and dashed line, respectively. V_{margin} (approximated V_{conv} after application of the erosion operator) is indicated by the dotted line. The cross denotes the center of rotation.

When the margins are not place dependent, the erosion operator can be inverted to a morphological dilation operator. The dilation operator can be used to extend the clinical target volume (CTV) to the planning target volume (PTV). Similar operators for extending the CTV are rather commonly used in commercial planning systems.

For a margin that is strongly place dependent, a different approach is required. In this case, the convolution with the random deviations should be incorporated in the planning system to check if the applied margins are indeed appropriate. After defining the CTV and adding margins for systematic deviations, the CTV should be extended with a first guess of the margins for the random deviations (0.7 SD). The convolution should be performed to examine whether the treatment plan is acceptable. If this is not the case, the margins should be adapted locally and the dose distribution recalculated until the plan is satisfactory.

To find the approximated margin, a cost function was defined to minimize the difference between the volumes enclosed by the convolved 95% isodose surface (V_{conv}) and its approximation by the erosion operator (V_{margin}). This cost function was taken equal to the total nonoverlapping volume of V_{conv} and V_{margin}. Voxels inside and outside V_{conv} contributed equally to the cost function. However, other definitions of the cost function are possible by defining a different cost for voxels in a certain region. For instance, in a region without organs at risk, the cost for voxels inside V_{conv} can be taken equal to zero, resulting in a margin that is equal to the largest change of the static 95% isodose surface by the convolution. On the other hand, in a region where organs at risk are close to V_{conv}, the cost for a nonoverlapping volume can be given a higher value than for other regions.

Margins for systematic deviations were not considered in the present study. Further investigation is needed to find the required size of these margins. The total margin around the CTV can possibly be described by a dilation operator with a size equal to the sum of the margins for random and systematic deviations.

By applying a convolution of the dose with the distribution of random deviations, a shift of the CTV with respect to the beam positions was assumed to be equivalent to a shift of the dose distribution in the opposite direction, thereby neglecting effects of a different source–skin distance (SSD), irregularities of the outer contours, and inhomogeneities. Effects of variations in SSD can be estimated by applying a correction of the shifted dose with the inverse square law. For instance, for a relatively large shift of the CTV of 7.5 mm (about three SDs) parallel to a beam and with a SSD equal to 80 cm, the dose of a single beam is changed with about 1.8%. For the three-field techniques that were considered in this study, the change is about 0.8%, in the AP direction, since the AP beam contributes 45% to the total dose. The total dose for parallel opposing beams hardly changes (<0.1%). Thus, effects of a different SSD are small for the three-field techniques and completely negligible for the four-field techniques. There was only little curvature of the outer contours along the beam axes for this treatment technique. Finally, for the prostate cases, possible inhomogeneities

could occur, due to the vicinity of bony structures (pelvic) or air (rectum).

Recently, Viggars *et al.*[23] proposed a convolution method in which a shift of the dose distribution was corrected using the inverse square law. They[23] did not take rotations into account. Moreover, the effects of inhomogeneities and irregularities of the outer contours are possibly more important and a further study of these effects is needed.

Indications of the size of the margin were previously given by Lind *et al.*[20] and Urie *et al.*[21] Lind *et al.* used a one-dimensional biological model to find a margin for random deviations. They optimized the probability of uncomplicated tumor control. The size of the recommended margin was comparable to the present study, i.e. 0.5 SD–0.8 SD of the translations, depending on the vicinity of organs at risk. Urie *et al.*[21] suggested a margin, which was chosen in such a way that it encompassed the 85% (1.5 SD) level of confidence of the position of the CTV. Their results cannot be directly compared with our results since Urie *et al.*[21] did not separate random and systematic deviations. If no systematic deviations are present, the margin given by Urie *et al.*[21] was twice the size of the margin we found. On the other hand, for treatment sites with negligible random deviations, 15% of the patients would have a systematic deviation resulting in a CTV that is (partly) outside the region defined by the margin. It is clear that a margin, which is based on the combined distribution of random and systematic deviations and which does not take the actual dose distribution into account, might have unacceptable consequences.

V. CONCLUSION

Margins around the clinical target volume (CTV), varying in the three main directions, can be defined to ensure a sufficient dose to the CTV for random translational and rotational deviations when the center of rotation coincides with the center of the CTV. The margin is equal to about 0.7 times the standard deviation of the distribution of random translations in the corresponding direction. The margin can become strongly place dependent when the center of rotation does not coincide with the center of the CTV. In that case, a convolution of the dose distribution with the random deviations should be included in the planning system to check the adequacy of the applied margins.

ACKNOWLEDGMENTS

We would like to thank A. Blom for his assistance during the use of the planning system and Dr. J. de Munck and J. Stroom for interesting discussions about the convolution algorithm. Dr. B. Mijnheer and K. Gilhuijs are thanked for their useful criticism on the manuscript. This study was supported by the Dutch Cancer Society, NKB Grant No. NKI 91-01.

[a]Address for correspondence: A. Bel, Academic Hospital Free University Brussels, Laarbeeklaan 101, 1090 Brussels, Belgium. Fax: +32 2 477 6212; Telephone: +32 2 477 6131; Electronic mail: abel@minf.vub.ac.be

[1]ICRU, "Prescribing, recording, and reporting photon beam therapy," International Commission on Radiation Units and Measurements, Bethesda, MD, 1993.

[2]A. Bel, P. H. Vos, P. T. R. Rodrigus, C. L. Creutzberg, A. G. Visser, J. C. Stroom, and J. V. Lebesque, "High-precision prostate cancer irradiation by clinical application of an off-line patient setup verification procedure, using portal imaging," Int. J. Radiat. Oncol. Biol. Phys. **35**, 321–332 (1996).

[3]J. Bijhold, J. V. Lebesque, A. A. M. Hart, and R. E. Vijlbrief, "Maximizing setup accuracy using portal images as applied to a conformal boost technique for prostatic cancer," Radiother. Oncol. **24**, 261–271 (1992).

[4]I. Rabinowitz, J. Broomberg, M. Goitein, K. McCarthy, and J. Leong, "Accuracy of radiation field alignment in clinical practice," Int. J. Radiat. Oncol. Biol. Phys. **11**, 1857–1867 (1985).

[5]S. A. Rosenthal, J. M. Galvin, J. W. Goldwein, A. R. Smith, and P. H. Blitzer, "Improved methods for determination of variability in patient positioning for radiation therapy using simulation and serial portal film measurements," Int. J. Radiat. Oncol. Biol. Phys. **23**, 621–625 (1992).

[6]F. Van den Heuvel, W. De Neve, D. Verellen, M. Coghe, V. Coen, and G. Storme, "Clinical implementation of an objective computer-aided protocol for intervention in intra-treatment correction using electronic portal imaging," Radiother. Oncol. **35**, 232–239 (1995).

[7]W. De Neve, F. Van den Heuvel, M. De Beukeleer, M. Coghe, L. Thon, P. De Roover, M. Van Lancker, and G. Storme, "Routine clinical on-line portal imaging followed by immediate field adjustment using a telecontrolled patient couch," Radiother. Oncol. **24**, 45–54 (1992).

[8]A. Ezz, P. Munro, A. T. Porter, J. Battista, D. A. Jaffray, A. Fenster, and S. Osborne, "Daily monitoring and correction of radiation field placement using a video-based portal imaging system: A pilot study," Int. J. Radiat. Oncol. Biol. Phys. **22**, 159–165 (1992).

[9]J. Gildersleve, D. P. Dearnaley, P. M. Evans, M. Law, C. Rawlings, and W. Swindell, "A randomised trial of patient repositioning during radiotherapy using a megavoltage imaging system," Radiother. Oncol. **31**, 161–168 (1994).

[10]M. van Herk, A. Bruce, G. Kroes, T. Shouman, A. Touw, and J. V. Lebesque, "Quantification of organ motion during conformal radiotherapy of the prostate by three-dimensional image-registration," Int. J. Radiat. Oncol. Biol. Phys. **33**, 1311–1320 (1995).

[11]J. M. Balter, H. M. Sandler, K. H. Lam, R. L. Bree, A. S. Lichter, and R. K. Ten Haken, "Measurement of prostate motion over the course of routine radiotherapy using implanted markers," Int. J. Radiat. Oncol. Biol. Phys. **31**, 113–118 (1995).

[12]R. K. Ten Haken, J. D. Forman, D. K. Heimburger, A. Gerhardsson, D. L. McShan, C. Perez-Tamayo, S. L. Schoeppel, and A. S. Lichter, "Treatment planning issues related to prostate movement in response to differential filling of the rectum and bladder," Int. J. Radiat. Oncol. Biol. Phys. **20**, 1317–1324 (1991).

[13]E. Melian, G. J. Kutcher, S. A. Leibel, M. J. Zelefsky, B. Baldwin, and Z. Fuks, "Variation in prostate position: Quantitation and implications for three-dimensional conformal therapy," (abstract), Int. J. Radiat. Oncol. Biol. Phys. **27**, 137 (1993).

[14]C. J. Beard, M. R. Bussiere, M. E. Plunkett, C. N. Coleman, and P. K. Kijewski, "Analysis of prostate and seminal vesicle motion," (abstract). Int. J. Radiat. Oncol. Biol. Phys. **27**, 136 (1993).

[15]C. J. M Hoekstra, V. G. M. Althof, H. J. Te Loo, A. van 't Riet, and A. C. A. Mak, "Are set-up variations in bony structures equivalent with positional changes of the prostate in external radiotherapy?," (abstract), Radiother. Oncol. **24**, 45 (1992).

[16]G. J. Kutcher, G. S. Mageras, and S. A. Leibel, "Control, correction and modeling of setup errors and organ motion," Semn. Radiat. Oncol. **5**, 134–145 (1995).

[17]J. Leong, "Implementation of random positioning error in computerized radiation treatment planning as a result of fractionation," Phys. Med. Biol. **32**, 237–334 (1987).

[18]V. Rudat, M. Flentje, D. Oetzel, M. Menke, W. Schlegel, and M. Wannenmacher, "Influence of the positioning error on 3D conformal dose distributions during fractionated radiotherapy," Radiother. Oncol. **33**, 56–63 (1994).

[19]J. C. Stroom, A. G. Visser, J. C. J. de Boer, and H. Huizinga, "Use of coverage probability to quantify results of clinical positioning studies in

radiotherapy planning," (abstract), *Proceedings of the XIth International Conference on the use of Computers in Radiation Therapy*, 1994, pp. 264–265.

[20]B. K. Lind, P. Källman, B. Sundelin, and A. Brahme, "Optimal radiation beam profiles considering uncertainties in beam patient alignment," Acta Oncol. **32**, 331–342 (1993).

[21]M. M. Urie, M. Goitein, K. Doppke, J. G. Kutcher, T. LoSasso, R. Mohan, J. E. Munzenrider, M. Sontag, and J. W. Wong, "The role of uncertainty analysis in treatment planning," Int. J. Radiat. Oncol. Biol. Phys. **21**, 91–107 (1991).

[22]R. M. Haralick, S. R. Sternberg, and X. Zhuang, "Image analysis using mathematical morphology," IEEE Trans. Pattern Anal. Mach. Intell. **9**, 532–549 (1987).

[23]D. A. Viggars, C. W. Yu, J. S. Lewis, and S. Shalev, "An algorithm for the rapid calculation of the effects of localization uncertainties on radiotherapy dose distributions," (abstract), in Ref. 19, pp. 72–73.

BEAMSCAN® MR

STARCHECK*maxi*® MR

PRECISION MR-LINAC QA

New PTW technology delivers improved treatment success and patient safety in MR-guided radiotherapy. The **BEAMSCAN® MR*** motorized 3D water phantom – available in two models for Elekta Unity and ViewRay® MRIdian® – provides a dedicated, fully equipped solution for beam data commissioning and QA of MR-LINACs. The **STARCHECK*maxi*® MR** ionization chamber array provides comprehensive MR-LINAC QA with one single device and outstanding accuracy. One shot delivers all relevant beam data at 3 mm spatial resolution for radiation fields up to 40 x 40 cm^2.

Contact PTW today, and take a closer look at all the ways we can support your dosimetry needs for MR-guided radiotherapy.

(516) 827-3181 • www.MRdosimetry.com

PTW THE DOSIMETRY COMPANY

*Pending 510(k), not available for sale within the United States.

Exhibit G

IN THE UNITED STATES DISTRICT COURT

FOR THE DISTRICT OF DELAWARE

BEST MEDICAL INTERNATIONAL, INC.,	)	
	)	
Plaintiff,	)	
	)	
v.	)	C.A. No. 18-1599-MN
	)	
VARIAN MEDICAL SYSTEMS, INC. and VARIAN MEDICAL SYSTEMS INTERNATIONAL AG,	)	
	)	
Defendants.	)	

REQUEST FOR INTERNATIONAL JUDICIAL ASSISTANCE (LETTERS ROGATORY)

From: The Honorable Maryellen Noreika
United States District Court for the District of Delaware
J. Caleb Boggs Federal Building
844 N. King Street
Wilmington, DE 19801-3555
USA

To: The Appropriate Judicial Authority of Canada

The United States District Court for the District of Delaware presents its compliments to the appropriate judicial authority of Canada, and requests international judicial assistance to obtain evidence to be used in a civil proceeding before this Court in the above-captioned matter. A trial on this matter is scheduled at present for August 23, 2021, in Wilmington, Delaware.

The Court requests the assistance described herein as necessary in the interests of justice. Specifically, this matter is a patent case, and the Court requests that appropriate judicial authority of Canada compel the production of documentary evidence and deposition testimony from Nordion (Canada) Inc. ("Nordion"), 447 March Road, Ottawa, Ontario, Canada, K2K1X8, regarding a medical treatment system developed at Nordion (or one of its related companies) that may be prior art to one or more of the asserted patents. Nordion is outside this Court's subpoena

power, and therefore this Letter of Request is the only way that the requested information can be obtained.

Please return the executed request to this Court and defendants' counsel, with a requested return date of March 13, 2020:

Ryan K. Wong
KEKER, VAN NEST & PETERS LLP
633 Battery Street
San Francisco, CA 94111
USA

1. Summary of the Case

Plaintiff Best Medical, Inc. ("BMI") accuses defendants Varian Medical Systems, Inc. and Varian Medical Systems International AG ("Varian") of infringing four asserted patents: U.S. Patent Nos. 7,266,175, 7,015,490, 6,038,283, and 6,393,096. BMI amended its complaint on September 9, 2019, and Varian has moved to dismiss certain allegations in the amended complaint regarding indirect and willful infringement.

2. Evidence Requested

Varian seeks to obtain the following evidence, which it will use to develop its invalidity defenses for trial. The documents and testimony sought by these requests are directly relevant to the above-captioned litigation. These requests seek information regarding specific features of a medical treatment system developed at Nordion (or one of its related companies), which may be prior art to one or more of BMI's asserted patents under 35 U.S.C. § 102. If obtained, Varian

would use the documents and testimony to develop its invalidity defenses for trial, and may rely on the documents and testimony to seek invalidation of one or more asserted patents.

Nothing in this Letter of Request is intended to interfere with any rights of Nordion to assert privilege or refuse to give evidence under any applicable law of Canada or the United States of America.

a. Documents:

i. Documents sufficient to show the conception, design, and development of the following aspects of the intensity-modulated radiation therapy system developed at MDS Nordion AB, a version of which is described in the document located at https://www.accessdata.fda.gov/cdrh_docs/pdf/K993766.pdf (the "HELAX TMS IMRT System"), at MDS Nordion AB before the stated date:

(a) Before August 11, 2003:

cost function computation for determining, selecting, or optimizing a collimator angle of a multi-leaf collimator;

cost function minimization relating to the determination, selection, or optimization of a collimator angle (including, *inter alia*, use of simulated annealing, logic for accepting or rejecting a beam-weight set on a given iteration, and logic for stopping the iteration);

consideration of target conformity and/or treatment plan delivery efficiency as cost terms in a cost function to determine, select, or optimize a collimator angle; and

user interface(s) for receiving optimization input relating to the determination of a collimator angle.

(b) Before July 11, 2003:

cost function computation;

cost function minimization (including, *inter alia*, use of simulated annealing, logic for accepting or rejecting a beam-weight set on a given iteration, and logic for stopping the iteration);

use of treatment plan delivery efficiency;

treatment delivery time;

total beam segments and/or total monitor units as part of treatment plan optimization;

use of dosimetric fitness as part of treatment plan optimization; and

user interface(s) for receiving optimization inputs and/or controlling tradeoffs between treatment plan delivery efficiency and dosimetric fitness.

(c) Before May 27, 1998 and, if such documents exist, before October 24, 1996:

cost function computation;

cost function minimization (including, *inter alia*, use of simulated annealing, logic for accepting or rejecting a beam-weight set on a given iteration, and logic for stopping the iteration);

use of partial volume data or dose volume constraints;

use of dose volume histograms;

importance factors; and

user interface(s) for receiving optimization input.

ii. Documents sufficient to identify each version of the HELAX TMS IMRT System in use before August 11, 2003, the release date for each version, and differences between each version with respect to the aspects of the HELAX TMS IMRT System identified in Request No. i.

iii. Documents sufficient to show the design, operation, and functionality of the aspects of the HELAX TMS IMRT System identified in Request No. i for each version identified in response to Request No. ii.

iv. Documents sufficient to show that each version of the HELAX TMS IMRT System identified in response to Request No. ii was publicly available and/or in use anywhere in the world before August 11, 2003, and if such documents exist, before July 11, 2003, May 27, 1998, and October 24, 1996, such as academic journal articles, industry publications, press releases, product specifications, manuals, user guides, brochures, and/or web pages describing or identifying that version of the HELAX TMS IMRT System and its availability.

v. Documents sufficient to identify any apparatus, system, or device using the HELAX TMS IMRT System before August 11, 2003, and if such documents exist, before July 11, 2003, May 27, 1998, and October 24, 1996. This request includes linear accelerators, treatment planning programs, and multi-leaf collimators.

vi. Documents and communications sufficient to show the design, structure, function, operation, and availability of each apparatus, system, or device identified in response to Request No. v.

vii. Documents and communications sufficient to show the sale, offer for sale, or importation into the United States of each apparatus, system, or device identified in response to Request No. v before August 11, 2003, and if such documents exist, before July 11, 2003, May 27, 1998, and October 24, 1996.

b. Deposition Topics:

i. The conception, design, development, operation, and functionality of the aspects of the HELAX TMS IMRT System at MDS Nordion AB set forth in Document Request No. i before the date(s) specified in Document Request No. i.

ii. Each version of the HELAX TMS IMRT System in use before the date(s) specified in Document Request No. i, and the release date for each version.

iii. The date and circumstances of the first sale, offer for sale, and/or public use in the United States of the HELAX TMS IMRT System before the date(s) specified in Document Request No. i.

iv. The identity, design, operation, and functionality of any apparatus, system, or device using the aspects of the HELAX TMS IMRT System set forth in Document Request No. i before the date(s) specified in Document Request No. i.

v. The date and circumstances of the first sale, offer for sale, and/or public use in the United States of any apparatus, system, or device covered by Deposition Topic No. iv.

vi. The authenticity of documents produced in response to this Letter of Request, the public availability and publication dates of documents produced in response to this Letter of Request, the creation and authorship of documents produced in response to this Letter of Request, and whether and how the documents produced in response to this Letter of Request were created and/or stored in the ordinary course of business.

3. Requested Procedures for Deposition Testimony:

The Court requests that Nordion (Canada) Inc., 447 March Road, Ottawa, Ontario, Canada, K2K1X8, designate one or more witnesses who are knowledgeable about the subject matter identified in the deposition topics above. Because the testifying witnesses are outside this Court's subpoena power and cannot be compelled to attend trial, the Court requests that the witnesses' testimony be taken under oath in such manner as provided by the laws of Canada for the formal taking of evidence. The Court further requests that the testimony be taken by oral examination in such manner as provided by the laws of Canada for the formal taking of evidence. To the extent permitted by the laws of Canada, the Court requests that the testimony be recorded by a videographer and transcribed by a stenographer.

Please notify defendants' U.S. legal counsel of the time and place for execution of the requested deposition at the following address:

Ryan K. Wong
KEKER, VAN NEST & PETERS LLP
633 Battery Street
San Francisco, CA 94111
USA

4. Fees, Costs, and Reciprocity

If any reimbursable fees or costs are incurred in executing this Letter of Request, the Court requests that the appropriate judicial authorities of Canada submit a bill of fees and costs to the Court and defendants' U.S. legal counsel:

Ryan K. Wong
KEKER, VAN NEST & PETERS LLP
633 Battery Street
San Francisco, CA 94111
USA

The Court guarantees that defendants' counsel will reimburse the appropriate judicial authorities of Canada for all reimbursable fees and costs incurred in executing this Letter of Request.

This Court expresses its gratitude to the authorities of Canada for assisting with this Letter of Request, and will provide similar assistance to the judicial authorities of Canada when requested.

DATE OF REQUEST: _____

SIGNATURE AND SEAL OF THE REQUESTING AUTHORITY

_____
The Honorable Maryellen Noreika
United States District Judge
U.S. District Court for the District of Delaware
J. Caleb Boggs Federal Building
844 N. King Street
Wilmington, DE 19801-3555
USA